in *Wireless Communications over Rapidly Time-Varying Channels*
eds. Franz Hlawatsch and Gerald Matz
Amsterdam, The Netherlands: Academic Press
Chapter 1, pp. 1–63

1

Fundamentals of Time-Varying Communication Channels

Gerald Matz and Franz Hlawatsch

Vienna University of Technology

1.1 Introduction

Wireless communication systems, i.e., systems transmitting information via electromagnetic (radio) or acoustic (sound) waves, have become ubiquitous. In many of these systems, the transmitter or the receiver is mobile. Even if both link ends are static, scatterers — i.e., objects that reflect, scatter, or diffract the propagating waves — may move with significant velocities. These situations give rise to time variations of the wireless channel due to the Doppler effect. Non-ideal local oscillators are another source of temporal channel variations, even in the case of wireline channels. Because of their practical relevance, *linear time-varying (LTV) channels* have attracted considerable interest in the fields of signal processing, communications, propagation, information theory, and mathematics. In their most general form, LTV channels are also referred to as *time-frequency (TF) dispersive* or *doubly dispersive*, as well as *TF selective* or *doubly selective*.

In this chapter, we discuss the fundamentals of wireless channels from a signal processing and communications perspective. In contrast to existing textbooks (e.g., [Jak74, Par92, VB03, Mol05]), our focus will be on LTV channels. Many of the theoretical foundations of LTV channels were laid in the fifties and sixties of the twentieth century. In 1950, Zadeh proposed a "system function" that characterizes an LTV system in a joint TF domain [Zad50]. Driven by increasing interest in ionospheric channels, Kailath complemented Zadeh's work by introducing a dual system function, discussing sampling models, and addressing measurement issues [Kai59, Kai62]. A related discussion focusing on the concept of duality (an important notion in TF analysis) was provided by Gersho [Ger63]. In a seminal paper on random LTV channels [Bel63], Bello introduced the assumption of *wide-sense stationary uncorrelated scattering* (WSSUS), which has been used almost universally since. The estimation of channel statistics was addressed by Gallager [Gal64] and a few years later by Gaarder [Gaa68]. A fairly comprehensive coverage of the modeling of and communication over random LTV channels was pro-

vided by Kennedy in 1969 [Ken69]. Information-theoretic aspects of LTV channels were addressed in [Gal68, BPS98] (see also Chapter 2).

This chapter provides a review of this early work and a discussion of several more recent results. In Section 1.2, we summarize the most important physical aspects of LTV channels. Some basic tools for a deterministic description of LTV channels are discussed in Section 1.3, while the statistical description of random LTV channels is considered in Section 1.4. Section 1.5 is devoted to the important class of underspread channels and their properties. Parsimonious channel models are reviewed in Section 1.6. Finally, Section 1.7 discusses the measurement of LTV channels and of their statistics. Throughout this chapter, we will consider noise-free systems since our focus is on the signal distortions caused by LTV wireless channels and not on noise effects. The equivalent complex baseband representation of signals and systems (channels) will be used in most cases.

1.2 The physics of time-varying channels

In this section, we briefly describe some of the physical phenomena associated with wireless channels. We shall concentrate on radio channels, although much of our discussion is also relevant to acoustic channels. The term "wireless channel" will be understood as an abstraction of all effects on the transmit signal caused by the transmission. This typically includes the effects of antennas and radio-frequency front-ends in addition to the propagation environment affecting the electromagnetic waves.

1.2.1 Wave propagation

In wireless communications, information is transmitted by radiating a modulated electromagnetic wave at a certain carrier frequency by means of a transmit antenna and picking up energy of the radiated wave by means of a receive antenna. The behavior of the radio waves is determined by the propagation environment according to Maxwell's equations. For most scenarios of interest, solving Maxwell's equations is infeasible (even if the propagation environment is completely known, which rarely happens in practice). This is due to the fact that, except for free-space propagation, the wave interacts with dielectric or conducting objects. These interactions are usually classified as reflection, transmission, scattering, and diffraction. We will follow the prevailing terminology and refer to interacting objects simply as "scatterers," without distinguishing between the different types of interaction. While the behavior of radio waves strongly depends on the carrier frequency f_c (or, equivalently, wavelength λ_c), there are a number of common phenomena that lead to a high-level characterization valid for all wireless channels.

1.2.2 Multipath propagation and time dispersion

The presence of multiple scatterers (buildings, vehicles, hills, etc.) causes a transmitted radio wave to propagate along several different paths that terminate at the receiver. Hence, the receive antenna picks up a superposition of multiple attenuated copies of the transmit signal. This phenomenon is referred to as *multipath propagation*. Due to different lengths of the propagation paths, the individual multipath components experience different delays (time shifts). The receiver thus observes a temporally smeared-out version of the transmit signal. Even though the medium itself is not physically dispersive (in the sense that different frequencies propagate with different velocities), such channels are termed *time-dispersive*. The following example considers a simple idealized scenario.

Example 1.1 *Consider two propagation paths in a static environment. The receive signal in the equivalent complex baseband domain is given by*

$$r(t) = h_1\, s(t-\tau_1) + h_2\, s(t-\tau_2)\,.$$

Here, $h_p = |h_p| e^{j\varphi_p}$ and τ_p are, respectively, the complex attenuation factor and delay associated with the pth path. The magnitude of the Fourier transform $R(f) \triangleq \int_{-\infty}^{\infty} r(t)\, e^{-j2\pi f t} dt$ of the receive signal follows as

$$|R(f)| = |S(f)| \sqrt{|h_1|^2 + |h_2|^2 + 2|h_1||h_2| \cos\big(2\pi(\tau_1-\tau_2)f - (\varphi_1-\varphi_2)\big)}.$$

As can be seen from Example 1.1, a time-dispersive channel has a multiplicative effect on the transmit signal in the frequency domain (this, of course, is a basic equivalence in Fourier analysis). Therefore, time-dispersive channels are *frequency-selective* in the sense that different frequencies are attenuated differently; see Fig. 1.1 for illustration. These differences in attenuation become more severe when the difference of the path delays is large and the difference between the path attenuations is small.

Multipath propagation is not the only source of time dispersion. Further potential sources are transmitter and receiver imperfections, such as transmit/receive pulses not satisfying the Nyquist criterion, imperfect timing recovery, or sampling jitter. In the following example, we consider an equivalent discrete-time baseband representation that includes pulse amplitude modulation (PAM), analog-to-digital and digital-to-analog conversion, and demodulation.

Example 1.2 *Consider a single propagation path with complex attenuation factor h and delay* 0 *and a digital PAM system with symbol period T and transmit and receive pulses whose convolution yields a Nyquist pulse $p(t)$. Assuming a timing error ΔT, the received sequence in the equivalent discrete-time (symbol-rate) baseband domain equals*

$$r[k] = \sum_{l=-\infty}^{\infty} h_l\, a[k-l]\,, \qquad \textit{with} \quad h_k = h\, p(kT - \Delta T)\,,$$

where $a[k]$ denotes the sequence of transmit symbols. Note that in spite of a single propagation path, there is significant temporal dispersion unless $\Delta T = 0$ (in which case $h_k = 0$ for $k \neq 0$).

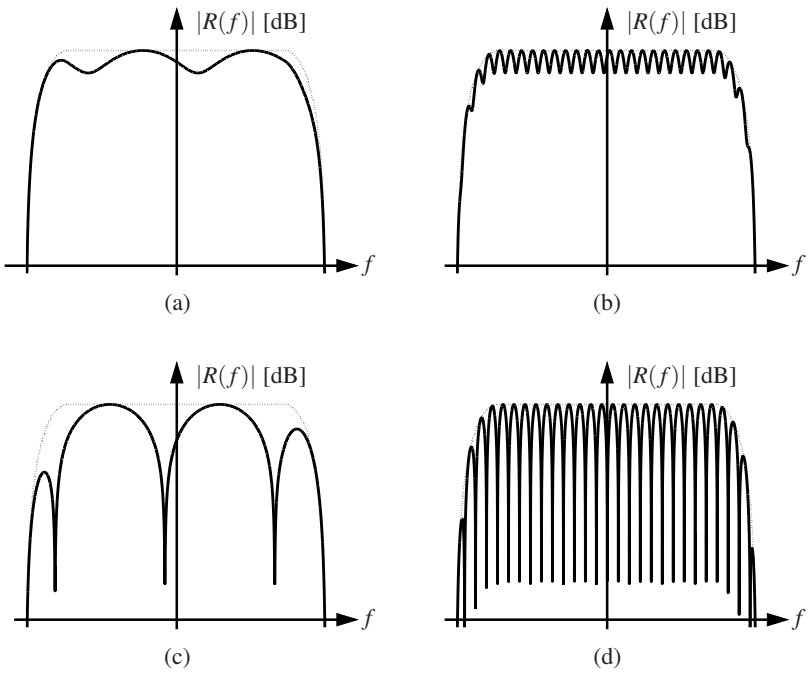

Figure 1.1 Illustration of frequency selectivity in a receive spectrum (thick solid line) for a two-path channel and a raised-cosine transmit spectrum (thin dotted line): (a) small $|\tau_1 - \tau_2|$ and $|h_1| \gg |h_2|$, (b) large $|\tau_1 - \tau_2|$ and $|h_1| \gg |h_2|$, (c) small $|\tau_1 - \tau_2|$ and $|h_1| \approx |h_2|$, (d) large $|\tau_1 - \tau_2|$ and $|h_1| \approx |h_2|$.

Although multipath propagation has traditionally been viewed as a transmission impairment, nowadays there is a tendency to consider it as beneficial since it provides additional degrees of freedom that are known as *delay diversity* or *frequency diversity*, and that can be exploited to realize diversity gains or, in the context of multiantenna systems, even multiplexing gains [TV05].

1.2.3 Doppler effect and frequency dispersion

In many wireless systems, the transmitter, receiver, and/or scatterers are moving. In such situations, the emitted wave is subject to the Doppler effect and hence experiences frequency shifts. We first restrict our discussion to a simple scenario with a static transmitter, no scatterers, and a receiver moving with velocity υ. In this case, a purely sinusoidal carrier wave of frequency f_c is observed by the receiver as a sinusoidal wave of frequency

$$\Big(1 - \frac{\upsilon \cos(\phi)}{c_0 + \upsilon \cos(\phi)}\Big) f_c \approx \Big(1 - \frac{\upsilon \cos(\phi)}{c_0}\Big) f_c \,, \tag{1.1}$$

where ϕ is the angle of arrival of the wave relative to the direction of motion of the receiver and c_0 is the speed of light. The above approximation on the right-hand side of

(1.1) holds for the practically predominant case $v \ll c_0$. For a general transmit signal $s(t)$ with Fourier transform $S(f)$, one can then show the following expressions of the receive signal (h is the complex attenuation factor):

$$R(f) = hS(\alpha f), \quad r(t) = \frac{h}{\alpha} s\Big(\frac{t}{\alpha}\Big), \qquad \text{with } \alpha = 1 - \frac{v\cos(\phi)}{c_0}. \tag{1.2}$$

This shows that the Doppler effect results in a temporal/spectral scaling (i.e., compression or dilation).

In many practical cases, the transmit signal is effectively band-limited around the carrier frequency f_c, i.e., $S(f)$ is effectively zero outside a band $[f_c - B/2, f_c + B/2]$, where $B \ll f_c$. The approximation $\alpha f = f - \frac{v\cos(\phi)}{c_0} f \approx f - \frac{v\cos(\phi)}{c_0} f_c$ (whose accuracy increases with decreasing normalized bandwidth B/f_c) then implies

$$R(f) \approx hS(f-\nu), \quad r(t) \approx h s(t) e^{j2\pi\nu t}, \qquad \text{with } \nu = \frac{v\cos(\phi)}{c_0} f_c. \tag{1.3}$$

Here, the Doppler effect essentially results in a frequency shift, with the Doppler shift frequency ν being proportional to both the velocity v and the carrier frequency f_c. The relations (1.2) and (1.3) are often referred to as wideband and narrowband Doppler effect, respectively, even though the "narrowband" approximation (1.3) holds true also for systems usually considered as wideband by communication engineers (e.g., for a WLAN at carrier frequency $f_c = 2.4\,\text{GHz}$ and with bandwidth $B = 20\,\text{MHz}$, there is $B/f_c = 8.3 \cdot 10^{-3}$).

In the general case of multipath propagation and moving transmitter, receiver, and/or scatterers, the received multipath components (echoes) experience different Doppler shifts since the angles of arrival/departure and the relative velocities associated with the individual multipath components are typically different. Hence, the transmit signal is spread out in the frequency domain — it experiences *frequency dispersion*.

Example 1.3 *Consider two propagation paths with equal delay τ_0 but different Doppler frequencies ν_1 and ν_2. Here, the Fourier transform of the receive signal is obtained as*

$$R(f) = \big[h_1 S(f-\nu_1) + h_2 S(f-\nu_2)\big] e^{-j2\pi\tau_0 f}, \tag{1.4}$$

where $h_p = |h_p| e^{j\varphi_p}$ denotes the complex attenuation factor of the pth path. The magnitude of the receive signal follows as

$$|r(t)| = |s(t-\tau_0)| \sqrt{|h_1|^2 + |h_2|^2 + 2|h_1||h_2| \cos\big(2\pi(\nu_1-\nu_2)(t-\tau_0) + (\varphi_1 - \varphi_2)\big)}. \tag{1.5}$$

While (1.4) illustrates the frequency dispersion, (1.5) shows that the Doppler effect leads to time-varying multiplicative modifications of the transmit signal in the time domain. Thus, channels involving Doppler shifts are also referred to as being *time-selective*. With the replacements $R(f) \to r(t)$, $f \to t$, $\tau_1 \to \nu_1$, and $\tau_2 \to \nu_2$, Fig. 1.1 can also be viewed as an illustration of time selectivity. Depending on the system architecture, time selectivity may be viewed as a transmission impairment or as a beneficial effect offering *Doppler diversity* (also termed *time diversity*).

Apart from the Doppler effect due to mobility, imperfect local oscillators are another cause of frequency dispersion because they result in carrier frequency offsets (i.e., different and possibly time-varying carrier frequencies at the transmitter and receiver), oscillator drift, and phase noise.

Example 1.4 *Consider a static scenario with line-of-sight propagation without multipath, i.e., the transmit and receive signals in the (complex) bandpass domain are related as* $r(t) = hs(t)$. *The transmitter uses a perfect local oscillator, i.e.,* $s(t) = s_{\mathrm{B}}(t)\, e^{j2\pi f_{\mathrm{c}} t}$ *(*$s_{\mathrm{B}}(t)$ *denotes the baseband signal). The local oscillator at the receiver is characterized by* $m(t) = p(t)\, e^{-j2\pi(f_{\mathrm{c}}+\Delta f)t}$, *where* Δf *is a carrier frequency offset and* $p(t)$ *models phase noise effects that broaden the oscillator's line spectrum. In this case, the received baseband signal* $r_{\mathrm{B}}(t) = r(t)\, m(t)$ *and its Fourier transform are given by*

$$r_{\mathrm{B}}(t) = h\, s_{\mathrm{B}}(t)\, p(t)\, e^{-j2\pi\Delta f t}, \qquad R_{\mathrm{B}}(f) = h \int_{-\infty}^{\infty} P(\nu - \Delta f)\, S_{\mathrm{B}}(f-\nu)\, d\nu\,.$$

Clearly, in spite of the static scenario (no Doppler effect), the transmit signal experiences temporal selectivity and frequency dispersion.

1.2.4 Path loss and fading

Wireless channels are characterized by severe fluctuations in the receive power, i.e., in the strength of the electromagnetic field at the receiver position. The receive power is usually modeled as a combination of three phenomena: path loss, large-scale fading, and small-scale fading.

The *path loss* describes the distance-dependent power decay of electromagnetic waves. Let us model the attenuation factor as $d^{-\beta}$, where d is the distance the wave has traveled and β denotes the path loss exponent, which is typically assumed to lie between 2 and 4. The path loss in decibels is then obtained as $P_{\mathrm{L}} = 10\,\beta \log_{10}(d)$.

Two receivers located at the same distance d from the transmitter may still experience significantly different receive powers if the radio waves have propagated through different environments. In particular, obstacles like buildings or dense vegetation can block or attenuate propagation paths and result in *shadowing* and *absorption loss*, respectively. This type of fading is referred to as *large-scale fading* since its effect on the receive power is constant within geographic regions whose dimensions are on the order of $10\lambda_{\mathrm{c}} \ldots 100\lambda_{\mathrm{c}}$, i.e., large relative to the wavelength λ_{c}. Experimental evidence indicates that for many systems, large-scale fading can be accurately modeled as a random variable with log-normal distribution [Mol05].

Finally, constructive and destructive interference of field components corresponding to different propagation paths causes receive power fluctuations within "small" regions whose dimensions are on the order of a few wavelengths. This *small-scale fading* can vary over several decades and is usually modeled stochastically by channel coefficients with Gaussian distribution. The magnitude of the channel coefficients is then Rayleigh distributed for zero-mean channel coefficients and Rice distributed for nonzero-mean channel coefficients. Rician fading is often assumed when there exists a line of sight.

Path loss and large-scale fading change only gradually and are relevant to the link budget and average receive signal-to-noise ratio (SNR); they are often combated by a feedback loop performing power control at the transmitter. In contrast, small-scale fading causes the receive power to fluctuate so rapidly that adjusting the transmit power is infeasible. Hence, small-scale fading has a direct impact on system performance (capacity, error probability, etc.). The main approach to mitigating small-scale fading is the use of diversity techniques (in time, frequency, or space).

1.2.5 Spatial characteristics

In a multipath scenario, the *angle of departure* (AoD) of a propagation path indicates the direction in which the planar wave corresponding to that path departs from the transmitter. Similarly, the *angle of arrival* (AoA) indicates from which direction the wave arrives at the receiver. AoA and AoD are spatial channel characteristics that can be measured using an antenna array at the respective link end. The angular resolution of an antenna array is determined by the number of individual antennas, their arrangement, and their distance. The transformation between the array signal vector and the angular domain is based on the array steering vector. In the case of a uniform linear array, this transformation is a discrete Fourier transform [TV05].

1.3 Deterministic description

We next discuss some basic deterministic[1] characterizations of LTV channels. We consider a wireless system operating at carrier frequency f_c. We will generally describe this system in the equivalent complex baseband domain for simplicity (an exception being the wideband system considered in Section 1.3.2). The LTV channel will be viewed and denoted as a linear operator [NS82] $\mathbf{H}$ that acts on the transmit signal $s(t)$ and yields the receive signal $r(t) = (\mathbf{H}s)(t)$.

1.3.1 Delay-Doppler domain — spreading function

As mentioned before, the physical effects underlying LTV channels are mainly multipath propagation and the Doppler effect. Hence, a physically meaningful and intuitive characterization of LTV channels is in terms of time delays and Doppler frequency shifts. Let us first assume an LTV channel $\mathbf{H}$ with P discrete propagation paths. The receive signal $r(t) = (\mathbf{H}s)(t)$ is here given by

$$r(t) = \sum_{p=1}^{P} h_p \, s(t-\tau_p) \, e^{j2\pi\nu_p t}, \tag{1.6}$$

[1] We call these characterizations "deterministic" because they do not assume a stochastic model of the channel; however, for a random channel, they are themselves random, i.e., nondeterministic — see Section 1.4.

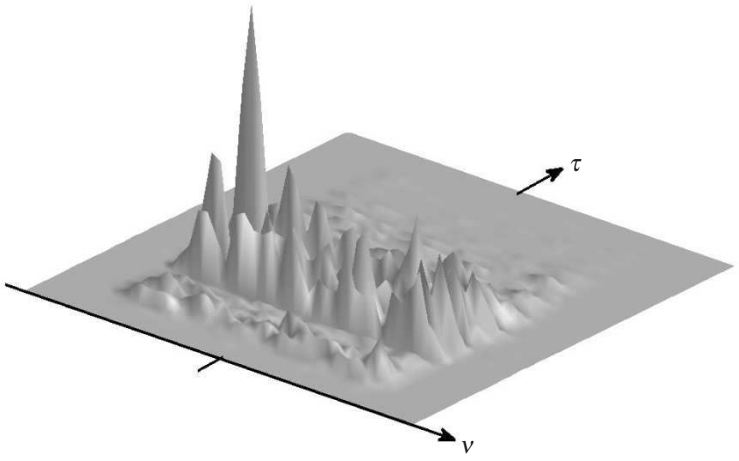

Figure 1.2 Example of a spreading function (magnitude).

where h_p, τ_p, and ν_p denote, respectively, the complex attenuation factor, time delay, and Doppler frequency associated with the pth path. Eq. (1.6) models the effect of P discrete specular scatterers (ideal point scatterers). This expression can be generalized to a continuum of scatterers as [Bel63, Pro95, Mol05]

$$r(t) = \int_{-\infty}^{\infty} \int_{-\infty}^{\infty} S_{\mathbf{H}}(\tau,\nu)\, s(t-\tau)\, e^{j2\pi\nu t}\, d\tau\, d\nu\,. \tag{1.7}$$

The weight function $S_{\mathbf{H}}(\tau,\nu)$ is termed the *(delay-Doppler) spreading function* of the LTV channel $\mathbf{H}$ since it describes the spreading of the transmit signal in time and frequency. The value of the spreading function $S_{\mathbf{H}}(\tau,\nu)$ at a given delay-Doppler point (τ,ν) characterizes the overall complex attenuation and scatterer reflectivity associated with all paths of delay τ and Doppler ν, and it describes how the delayed and Doppler-shifted version $s(t-\tau)\, e^{j2\pi\nu t}$ of the transmit signal $s(t)$ contributes to the receive signal $r(t)$. Thus, the spreading function expresses the channel's *TF dispersion characteristics*. As such, it is a generalization of the impulse response of time-invariant systems, which describes the time dispersion. An example is shown in Fig. 1.2. Note that (1.6) is reobtained as a special case of (1.7) for

$$S_{\mathbf{H}}(\tau,\nu) = \sum_{p=1}^{P} h_p\, \delta(\tau-\tau_p)\, \delta(\nu-\nu_p)\,. \tag{1.8}$$

A dual representation of the channel's TF dispersion in the frequency domain, again in terms of the spreading function $S_{\mathbf{H}}(\tau,\nu)$, is

$$R(f) = \int_{-\infty}^{\infty} \int_{-\infty}^{\infty} S_{\mathbf{H}}(\tau,\nu)\, S(f-\nu)\, e^{-j2\pi\tau(f-\nu)}\, d\tau\, d\nu.$$

We can also obtain a representation of the TF dispersion in a joint TF domain. We will use the *short-time Fourier transform* (STFT) of a signal $x(t)$, which is a linear TF signal

representation defined as $X^{(g)}(t,f) \triangleq \int_{-\infty}^{\infty} x(t')\, g^*(t'-t)\, e^{-j2\pi f t'}\, dt'$, where $g(t)$ denotes a normalized analysis window [NQ88, HBB92, Fla99]. The STFT of the receive signal in (1.7) can be expressed as

$$R^{(g)}(t,f) = \int_{-\infty}^{\infty}\int_{-\infty}^{\infty} S_{\mathbf{H}}(\tau,\nu)\, S^{(g)}(t-\tau, f-\nu)\, e^{-j2\pi\tau(f-\nu)}\, d\tau\, d\nu\,. \tag{1.9}$$

Apart from the phase factor, this is the two-dimensional (2-D) convolution of the STFT of the transmit signal with the spreading function of the channel. This again demonstrates that the spreading function describes the channel's TF dispersion.

Example 1.5 *For a two-path channel with delays τ_1, τ_2 and Doppler frequencies ν_1, ν_2, the spreading function is given by*

$$S_{\mathbf{H}}(\tau,\nu) = h_1\, \delta(\tau-\tau_1)\, \delta(\nu-\nu_1) + h_2\, \delta(\tau-\tau_2)\, \delta(\nu-\nu_2)\,.$$

Inserting this expression into (1.7) yields

$$r(t) = h_1\, s(t-\tau_1)\, e^{j2\pi\nu_1 t} + h_2\, s(t-\tau_2)\, e^{j2\pi\nu_2 t}.$$

We note that Examples 1.1 and 1.3 are essentially reobtained as special cases with $\nu_1 = \nu_2 = 0$ and $\tau_1 = \tau_2 = \tau_0$, respectively.

Writing (1.7) as $r(t) = \int_{-\infty}^{\infty} \big[\int_{-\infty}^{\infty} S_{\mathbf{H}}(\tau,\nu)\, s(t-\tau)\, d\tau\big]\, e^{j2\pi\nu t}\, d\nu = \int_{-\infty}^{\infty} r_\nu(t)\, d\nu$, we see that the LTV channel $\mathbf{H}$ can be viewed as a continuous (infinitesimal) parallel connection of systems parameterized by the Doppler frequency ν. The output signals of these systems are given by

$$r_\nu(t) = \tilde{r}_\nu(t)\, e^{j2\pi\nu t} \qquad \text{with} \quad \tilde{r}_\nu(t) = \big(S_{\mathbf{H}}(\cdot,\nu) * s\big)(t) = \int_{-\infty}^{\infty} S_{\mathbf{H}}(\tau,\nu)\, s(t-\tau)\, d\tau\,.$$

Thus, each system consists of a time-invariant filter with impulse response $S_{\mathbf{H}}(\tau,\nu)$, followed by a modulator (mixer) with frequency ν.

For a time-invariant channel with impulse response $h(\tau)$, the spreading function equals $S_{\mathbf{H}}(\tau,\nu) = h(\tau)\delta(\nu)$, so that (1.7) reduces to the convolution of $s(t)$ with $h(\tau)$. This correctly indicates the absence of Doppler shifts (frequency dispersion). In the dual case of a channel without frequency selectivity, i.e., $r(t) = \tilde{h}(t)\, s(t)$, there is $S_{\mathbf{H}}(\tau,\nu) = \widetilde{H}(\nu)\delta(\tau)$ with $\widetilde{H}(\nu) = \int_{-\infty}^{\infty} \tilde{h}(t)\, e^{-j2\pi\nu t}\, dt$, which correctly indicates the absence of time dispersion.

1.3.2 Delay-scale domain — delay-scale spreading function

Whereas for narrowband systems ($B/f_c \ll 1$) the Doppler effect can be represented as a frequency shift, it must be characterized by a time scaling (compression/dilation) in the case of *(ultra)wideband* systems. Relation (1.6) is here replaced by [Mol05]

$$r(t) = \sum_{p=1}^{P} a_p\, \frac{1}{\sqrt{\alpha_p}}\, s\Big(\frac{t-\tau_p}{\alpha_p}\Big), \qquad \text{with} \;\; \alpha_p = 1 - \frac{\upsilon\cos(\phi_p)}{c_0}\,.$$

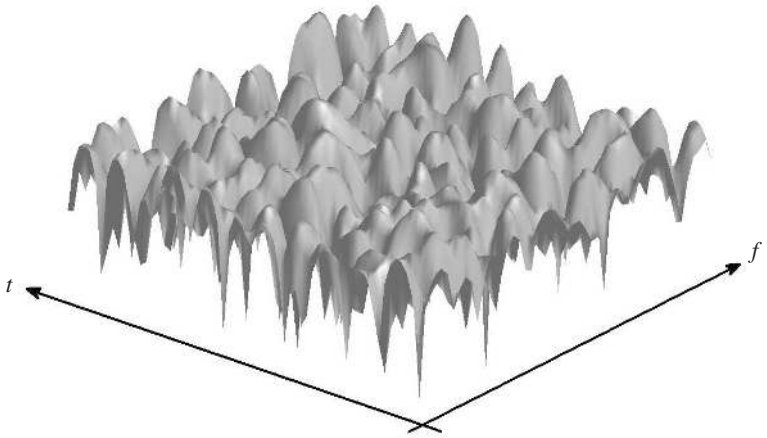

Figure 1.3 Example of a TF transfer function (magnitude, in dB).

Generalizing to a continuum of scatterers, we obtain

$$r(t) = \int_{-\infty}^{\infty}\int_{0}^{\infty} F_{\mathbf{H}}(\tau,\alpha)\,\frac{1}{\sqrt{\alpha}}\,s\Big(\frac{t-\tau}{\alpha}\Big)\,d\tau\,d\alpha\,. \tag{1.10}$$

Here, $F_{\mathbf{H}}(\tau,\alpha)$ denotes the *delay-scale spreading function* of the LTV channel $\mathbf{H}$ [YPS03, MSS07]. Like (1.7), expression (1.10) can represent any LTV channel, but it is most efficient (parsimonious) for wideband channels. The delay-scale description of LTV channels will be discussed in more detail in Chapter 9.

1.3.3 Time-frequency domain — time-varying transfer function

As explained in Section 1.2, time dispersiveness corresponds to frequency selectivity and frequency dispersiveness corresponds to time selectivity. The joint TF selectivity of an LTV channel is characterized by the *TF (or time-varying) transfer function* [Zad50, Bel63]

$$L_{\mathbf{H}}(t,f) \triangleq \int_{-\infty}^{\infty}\int_{-\infty}^{\infty} S_{\mathbf{H}}(\tau,\nu)\,e^{j2\pi(t\nu-f\tau)}\,d\tau\,d\nu\,. \tag{1.11}$$

This 2-D Fourier transform relation between shift (dispersion) domain and weight (selectivity) domain extends the 1-D Fourier transform relation $H(f) = \int_{-\infty}^{\infty} h(\tau)\,e^{-j2\pi f\tau}\,d\tau$ of time-invariant channels to the time-varying case. According to (1.11), the TF echoes described by $S_{\mathbf{H}}(\tau,\nu)$ correspond to TF fluctuations of $L_{\mathbf{H}}(t,f)$, which are a TF description of small-scale fading. For *underspread* channels (to be defined in Section 1.5), the TF transfer function $L_{\mathbf{H}}(t,f)$ can be interpreted as the channel's complex attenuation factor at time t and frequency f, and it inherits many properties of the transfer function (frequency response) defined in the time-invariant case. An example is shown in Fig. 1.3.

Example 1.6 *We reconsider the two-path channel from Example 1.5. Using (1.11), it can be shown that the squared magnitude of the channel's TF transfer function is given by*

$$|L_{\mathbf{H}}(t,f)|^2 = |h_1|^2 + |h_2|^2 + 2|h_1||h_2|\cos\bigl(2\pi[t(\nu_1-\nu_2) - f(\tau_1-\tau_2)] + \varphi_1 - \varphi_2\bigr)\,.$$

Clearly, this channel is TF selective in the sense that $L_{\mathbf{H}}(t,f)$ fluctuates with time and frequency. The rapidity of fluctuation with time is proportional to the "Doppler spread" $|\nu_1-\nu_2|$ whereas the rapidity of fluctuation with frequency is proportional to the "delay spread" $|\tau_1-\tau_2|$.

Inserting (1.11) into (1.7) and developing the integrals with respect to τ and ν leads to the channel input-output relation

$$r(t) = \int_{-\infty}^{\infty} L_{\mathbf{H}}(t,f)\,S(f)\,e^{j2\pi tf}\,df\,. \tag{1.12}$$

In spite of its apparent similarity to the relation $r(t) = \int_{-\infty}^{\infty} H(f)\,S(f)\,e^{j2\pi ft}\,df$ valid for time-invariant channels, (1.12) has to be interpreted with care. Specifically, (1.12) is not a simple inverse Fourier transform since $L_{\mathbf{H}}(t,f)\,S(f)$ also depends on t.

For the special case of a time-invariant channel (no frequency dispersion), the TF transfer function reduces to the frequency response, i.e., $L_{\mathbf{H}}(t,f) = H(f)$, and (1.12) corresponds to $R(f) = H(f)\,S(f)$. This correctly reflects the channel's pure frequency selectivity. In the dual case of a channel without time dispersion, the TF transfer function simplifies according to $L_{\mathbf{H}}(t,f) = \tilde{h}(t)$ and (1.12) thus reduces to the relation $r(t) = \tilde{h}(t)\,s(t)$, which describes the channel's pure time selectivity.

1.3.4 Time-delay domain — time-varying impulse response

While the spreading function was motivated by a specific physical model (multipath propagation, Doppler effect), it actually applies to any LTV system. To see this, we develop (1.7) as

$$r(t) = \int_{-\infty}^{\infty} \Bigl[\underbrace{\int_{-\infty}^{\infty} S_{\mathbf{H}}(\tau,\nu)\,e^{j2\pi t\nu}\,d\nu}_{h(t,\tau)}\Bigr]\,s(t-\tau)\,d\tau = \int_{-\infty}^{\infty} h(t,\tau)\,s(t-\tau)\,d\tau\,, \tag{1.13}$$

where $h(t,\tau) = \int_{-\infty}^{\infty} S_{\mathbf{H}}(\tau,\nu)\,e^{j2\pi t\nu}\,d\nu$ is the *(time-varying) impulse response* of the LTV channel $\mathbf{H}$. An example is depicted in Fig. 1.4. Defining the *kernel* of $\mathbf{H}$ as $k_{\mathbf{H}}(t,t') \triangleq h(t,t-t')$, (1.13) can be rewritten as

$$r(t) = \int_{-\infty}^{\infty} k_{\mathbf{H}}(t,t')\,s(t')\,dt', \tag{1.14}$$

which is the integral representation of a linear operator [NS82]. This shows that the input-output relation (1.7) is completely general, i.e., any LTV system (channel) can be

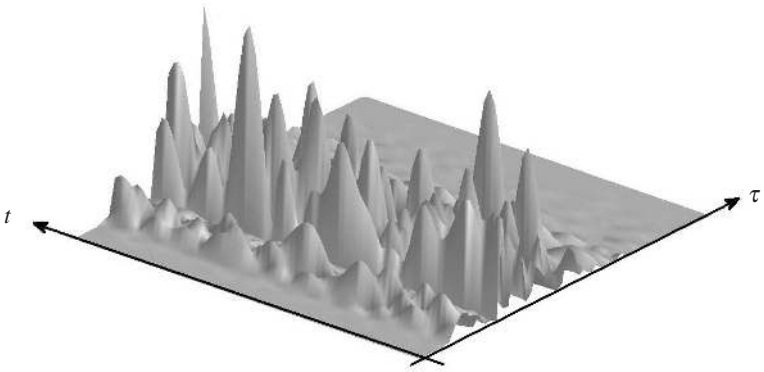

Figure 1.4 Example of a time-varying impulse response (magnitude).

characterized in terms of its spreading function. The spreading function and TF transfer function can be written in terms of the impulse response $h(t,\tau)$ as

$$S_{\mathbf{H}}(\tau,\nu) = \int_{-\infty}^{\infty} h(t,\tau)\, e^{-j2\pi\nu t}\, dt\,, \tag{1.15}$$

$$L_{\mathbf{H}}(t,f) = \int_{-\infty}^{\infty} h(t,\tau)\, e^{-j2\pi f\tau}\, d\tau\,. \tag{1.16}$$

From (1.13) and (1.14), it follows that for a transmit signal that is an impulse, $s(t) = \delta(t-t_0)$, the receive signal equals $r(t) = k(t,t_0) = h(t,t-t_0)$. The impulse response can also be interpreted in terms of a "continuous tapped delay line": for a fixed tap (delay) τ, $h(t,\tau)$ as a function of t describes the time-varying tap weight function that multiplies the delayed transmit signal $s(t-\tau)$. In the special case of a time-invariant channel, $h(t,\tau)$ simplifies to a function of τ only, and for a frequency-nonselective channel, it simplifies as $h(t,\tau) = \tilde{h}(t)\,\delta(\tau)$ with some $\tilde{h}(t)$.

Example 1.7 *A popular model of an LTV channel with specular scattering is specified in terms of the impulse response as*

$$h(t,\tau) = \sum_{p=1}^{P} h_p\, e^{j2\pi\nu_p t}\, \delta(\tau-\tau_p(t))\,. \tag{1.17}$$

Apart from the time dependence of the delays $\tau_p(t)$, this is just the inverse Fourier transform of (1.8) with respect to ν. The time-varying delays $\tau_p(t)$ account for a "delay drift" that is due to changing path lengths caused by the movement of the transmitter, receiver, and/or scatterers. However, these changes are much slower than the phase fluctuations resulting from small-scale fading (which are described by the exponential functions in (1.17)).

1.3.5 Extension to multiantenna systems

Consider a *multiple-input multiple-output* (MIMO) wireless system with M_{T} transmit antennas and M_{R} receive antennas [BGPvdV06, PNG03]. The signals emitted by the jth transmit antenna and captured by the ith receive antenna will be denoted by $s_j(t)$ and $r_i(t)$, respectively. Each receive signal $r_i(t)$ is a superposition of distorted versions of all transmit signals, i.e.,

$$r_i(t) = \sum_{j=1}^{M_{\mathrm{T}}} (\mathsf{H}_{ij}\, s_j)(t)\,, \quad i = 1,\ldots,M_{\mathrm{R}}\,, \tag{1.18}$$

where H_{ij} denotes the LTV channel between transmit antenna j and receive antenna i. (For a survey of MIMO channel modeling aspects, see [ABB+07] and references therein.) Defining the length-M_{T} transmit signal vector $\mathbf{s}(t) = (s_1(t)\cdots s_{M_{\mathrm{T}}}(t))^T$ and the length-M_{R} receive vector $\mathbf{r}(t) = (r_1(t)\cdots r_{M_{\mathrm{R}}}(t))^T$, all input-output relations (1.18) can be combined as

$$\mathbf{r}(t) = (\underline{\mathsf{H}}\mathbf{s})(t)\,, \qquad \text{with } \underline{\mathsf{H}} \triangleq \begin{pmatrix} \mathsf{H}_{11} & \cdots & \mathsf{H}_{1M_{\mathrm{T}}} \\ \vdots & \ddots & \vdots \\ \mathsf{H}_{M_{\mathrm{R}}1} & \cdots & \mathsf{H}_{M_{\mathrm{R}}M_{\mathrm{T}}} \end{pmatrix}. \tag{1.19}$$

The delay-Doppler, TF, and time-delay characterizations of single-antenna channels can be easily generalized to the MIMO case. Let us define the $M_{\mathrm{R}} \times M_{\mathrm{T}}$ matrices $\mathbf{S}_{\mathsf{H}}(\tau,\nu)$, $\mathbf{L}_{\mathsf{H}}(t,f)$, and $\mathbf{H}(t,\tau)$ whose (i,j)th elements equal the delay-Doppler spreading function, TF transfer function, and impulse response of H_{ij}, respectively. Then

$$\begin{aligned} \mathbf{r}(t) &= \int_{-\infty}^{\infty}\int_{-\infty}^{\infty} \mathbf{S}_{\mathsf{H}}(\tau,\nu)\,\mathbf{s}(t-\tau)\,e^{j2\pi\nu t}\,d\tau\,d\nu \\ &= \int_{-\infty}^{\infty} \mathbf{H}(t,\tau)\,\mathbf{s}(t-\tau)\,d\tau\,, \end{aligned} \tag{1.20}$$

with

$$\mathbf{S}_{\mathsf{H}}(\tau,\nu) = \int_{-\infty}^{\infty} \mathbf{H}(t,\tau)\,e^{-j2\pi\nu t}\,dt\,. \tag{1.21}$$

Furthermore,

$$\begin{aligned} \mathbf{L}_{\mathsf{H}}(t,f) &= \int_{-\infty}^{\infty}\int_{-\infty}^{\infty} \mathbf{S}_{\mathsf{H}}(\tau,\nu)\,e^{j2\pi(t\nu - f\tau)}\,d\tau\,d\nu \\ &= \int_{-\infty}^{\infty} \mathbf{H}(t,\tau)\,e^{-j2\pi f\tau}\,d\tau\,. \end{aligned} \tag{1.22}$$

The main difference between these relations and their single-antenna counterparts is the *spatial resolution* offered by the aperture of the antenna arrays. The transmit array and receive array make it possible to resolve to a certain extent the AoD and AoA, respectively, of the individual paths. This spatial or directional resolution is essentially determined by the array steering vectors that define a transformation to the angular domain [Say02, TV05].

Example 1.8 *Assuming uniform linear arrays at the transmitter and the receiver with antenna separation $\Delta_{\mathrm{T}}\lambda_c$ and $\Delta_{\mathrm{R}}\lambda_c$, respectively, the array steering vectors for given AoD ϕ and AoA ψ are [Mol05]*

$$\mathbf{a}_{\mathrm{T}}(\phi) = \frac{1}{\sqrt{M_{\mathrm{T}}}} \begin{pmatrix} 1 \\ e^{-j2\pi\Delta_{\mathrm{T}}\cos(\phi)} \\ \vdots \\ e^{-j2\pi(M_{\mathrm{T}}-1)\Delta_{\mathrm{T}}\cos(\phi)} \end{pmatrix}, \qquad \mathbf{a}_{\mathrm{R}}(\psi) = \frac{1}{\sqrt{M_{\mathrm{R}}}} \begin{pmatrix} 1 \\ e^{-j2\pi\Delta_{\mathrm{R}}\cos(\psi)} \\ \vdots \\ e^{-j2\pi(M_{\mathrm{R}}-1)\Delta_{\mathrm{R}}\cos(\psi)} \end{pmatrix}.$$

Further assuming purely specular scattering with P paths, where each path has its distinct AoD ϕ_p and AoA ψ_p, the matrix-valued spreading function is given by (cf. (1.8)*)*

$$\mathbf{S}_{\mathbf{H}}(\tau,\nu) = \sum_{p=1}^{P} \mathbf{H}_p\, \delta(\tau-\tau_p)\, \delta(\nu-\nu_p), \quad \text{with } \mathbf{H}_p = h_p\, \mathbf{a}_{\mathrm{R}}(\psi_p)\, \mathbf{a}_{\mathrm{T}}^T(\phi_p).$$

Note that here the MIMO matrices $\mathbf{H}_p = h_p\, \mathbf{a}_{\mathrm{R}}(\psi_p)\, \mathbf{a}_{\mathrm{T}}^T(\phi_p)$ describing the individual paths in the delay-Doppler domain (i.e., determining $\mathbf{S}_{\mathbf{H}}(\tau,\nu)$ at the corresponding delay-Doppler points (τ_p,ν_p)) all have rank equal to one. The TF transfer function is obtained as

$$\mathbf{L}_{\mathbf{H}}(t,f) = \sum_{p=1}^{P} \mathbf{H}_p\, e^{j2\pi(t\nu_p - f\tau_p)};$$

it involves a superposition of all matrices $\mathbf{H}_p$ at each TF point (t,f) and hence in general will have full rank everywhere, provided that more than $\min\{M_{\mathrm{T}},M_{\mathrm{R}}\}$ paths have sufficiently distinct AoA/AoD (rich scattering). We note that because of the finite aperture of the antenna arrays ($M_{\mathrm{T}}\Delta_{\mathrm{T}}$ and $M_{\mathrm{R}}\Delta_{\mathrm{R}}$), no more than, respectively, M_{T} and M_{R} orthogonal directions can be effectively resolved in the angular domain [Say02, TV05].

The spatial/angular dispersion of MIMO channels — i.e., the mixing of the signals emitted from all transmit antennas — can be viewed as an inconvenience necessitating spatial equalization. However, spatial dispersion actually provides additional degrees of freedom that can be exploited to realize *spatial diversity*. This diversity is analogous to the delay diversity due to time dispersion and the Doppler diversity due to frequency dispersion.

1.4 Stochastic description

A complete deterministic characterization of LTV channels (e.g., based on Maxwell's equations) is infeasible in virtually all scenarios of practical relevance. Even if such a characterization were possible, it would only apply to a specific environment, whereas wireless systems need to be designed for a wide variety of operating conditions. This motivates stochastic characterizations, which consider an LTV channel as a random quantity whose statistics describe common properties of an underlying *ensemble* of wireless channels.

We will restrict our discussion to the common case of Rayleigh fading, where the channel's system functions $S_{\mathbf{H}}(\tau,\nu)$, $L_{\mathbf{H}}(t,f)$, and $h(t,\tau)$ are 2-D complex Gaussian random processes with zero mean. For Rayleigh fading, the stochastic characterization of a channel reduces to the specification of its second-order statistics.

1.4.1 WSSUS channels

The WSS, US, and WSSUS properties

The second-order statistics of the 2-D system functions of an LTV channel (spreading function, TF transfer function, and impulse response) generally depend on four variables. In his seminal paper [Bel63], Bello provided a simplified description in terms of only two variables by introducing the assumption of *wide-sense stationary uncorrelated scattering* (WSSUS). The WSSUS property is also discussed, e.g., in [Pro95, Mol05, MH03].

A random LTV channel is said to feature *uncorrelated scattering* (US) [Bel63] if different channel taps (delay coefficients) are uncorrelated, i.e.,

$$\mathsf{E}\{h(t,\tau)\,h^*(t',\tau')\} = r'_h(t,t';\tau)\,\delta(\tau-\tau')\,,$$

with some correlation function $r'_h(t,t';\tau)$. Note that different taps can be interpreted as belonging to different scatterers. Furthermore, a channel is said to be *wide-sense stationary* (WSS) [Bel63] if the channel taps are jointly wide-sense stationary with respect to the time variable t, i.e.,

$$\mathsf{E}\{h(t,\tau)\,h^*(t',\tau')\} = \tilde{r}_h(t-t';\tau,\tau')\,,$$

with some correlation function $\tilde{r}_h(\Delta t;\tau,\tau')$. Combining the WSS and US properties, we obtain the WSSUS property

$$\mathsf{E}\{h(t,\tau)\,h^*(t',\tau')\} = r_h(t-t';\tau)\,\delta(\tau-\tau')\,. \tag{1.23}$$

This shows that the second-order statistics of a WSSUS channel are fully described by the 2-D function $r_h(\Delta t;\tau)$, which is a correlation function in the time-difference variable Δt.

Scattering function and TF correlation function

US channels have uncorrelated delay coefficients, and it can be shown that for WSS channels different Doppler frequency coefficients are uncorrelated. Taken together, this implies that the spreading function $S_{\mathbf{H}}(\tau,\nu)$ of a WSSUS channel is a 2-D *white* (but nonstationary) process, i.e.,

$$\mathsf{E}\big\{S_{\mathbf{H}}(\tau,\nu)\,S^*_{\mathbf{H}}(\tau',\nu')\big\} = C_{\mathbf{H}}(\tau,\nu)\,\delta(\tau-\tau')\,\delta(\nu-\nu')\,. \tag{1.24}$$

The rationale here is that each delay-Doppler pair (τ,ν) corresponds to a scatterer with reflectivity $S_{\mathbf{H}}(\tau,\nu)$, and the reflectivities of any two distinct scatterers (i.e., scatterers with different delay τ or different Doppler ν) are uncorrelated. The mean intensity of the 2-D white spreading function process, $C_{\mathbf{H}}(\tau,\nu) \geq 0$, is known as the channel's *scattering function* [Bel63, Mol05, MH03]. The scattering function characterizes the average

strength of scatterers with delay τ and Doppler frequency ν, and thus it provides a statistical characterization of the TF dispersion produced by a WSSUS channel. A *wideband scattering function* based on the delay-scale spreading function $F_{\mathbf{H}}(\tau,\alpha)$ in (1.10) can be defined in a similar manner (see [YPS03, MSS07, BPRV04] and Chapter 9).

By definition, WSS channels are stationary in time; furthermore, it can be shown that US channels are stationary in frequency. It follows that the statistics of a WSSUS channel do not change with time or frequency, and hence the TF transfer function $L_{\mathbf{H}}(t,f)$ is a 2-D *stationary* process, i.e.,

$$\mathsf{E}\{L_{\mathbf{H}}(t,f)\,L_{\mathbf{H}}^{*}(t',f')\} = R_{\mathbf{H}}(t-t',f-f')\,. \tag{1.25}$$

Here, $R_{\mathbf{H}}(\Delta t,\Delta f)$ denotes the channel's *TF correlation function*. The stationarity of $L_{\mathbf{H}}(t,f)$ as expressed by the above equation is consistent with the fact that the spreading function $S_{\mathbf{H}}(\tau,\nu)$, which is the 2-D Fourier transform of $L_{\mathbf{H}}(t,f)$, is a white process.

Using the inverse of the Fourier transform relation (1.11) in (1.24), we obtain a similar Fourier transform relation between the TF correlation function $R_{\mathbf{H}}(\Delta t,\Delta f)$ and the scattering function $C_{\mathbf{H}}(\tau,\nu)$:

$$C_{\mathbf{H}}(\tau,\nu) = \int_{-\infty}^{\infty}\int_{-\infty}^{\infty} R_{\mathbf{H}}(\Delta t,\Delta f)\,e^{-j2\pi(\nu\Delta t-\tau\Delta f)}\,d\Delta t\,d\Delta f. \tag{1.26}$$

By inspecting (1.25) and (1.26), it is seen that the scattering function is the 2-D *power spectral density* of the 2-D stationary process $L_{\mathbf{H}}(t,f)$. This observation suggests the use of spectrum estimation techniques to measure the scattering function [KD03] (see also Section 1.7.4).

Statistical input-output relations

The scattering function is a statistical characterization of the TF dispersion produced by a WSSUS channel. This interpretation can be made more explicit by considering the *Rihaczek spectra* [Fla99, MH06] of transmit signal $s(t)$ and receive signal $r(t)$. The Rihaczek spectrum of a (generally nonstationary) random process $x(t)$ with correlation function $R_x(t,t') = \mathsf{E}\{x(t)\,x^*(t')\}$ is defined as

$$\overline{\Gamma}_x(t,f) \triangleq \int_{-\infty}^{\infty} R_x(t,t-\Delta t)\,e^{-j2\pi f\Delta t}\,d\Delta t\,.$$

With some precautions, $\overline{\Gamma}_x(t,f)$ can be interpreted as a mean energy distribution of $x(t)$ over the TF plane. Thus, it generalizes the power spectral density of stationary processes.

Starting from (1.7), it can be shown that

$$\overline{\Gamma}_r(t,f) = \int_{-\infty}^{\infty}\int_{-\infty}^{\infty} C_{\mathbf{H}}(\tau,\nu)\,\overline{\Gamma}_s(t-\tau,f-\nu)\,d\tau\,d\nu\,. \tag{1.27}$$

This means that the TF energy spectrum of the receive signal is a superposition of TF translated versions of the TF energy spectrum of the transmit signal, weighted by the corresponding values of the scattering function. The "statistical input-output relation" (1.27) thus represents a second-order statistical analogue of the deterministic linear input-output relation (1.9).

Performing a 2-D Fourier transform of the convolution relation (1.27) yields

$$\bar{A}_r(\Delta t,\Delta f) = R_{\mathbf{H}}(\Delta t,\Delta f)\bar{A}_s(\Delta t,\Delta f)\,, \tag{1.28}$$

where $\bar{A}_x(\Delta t,\Delta f) \triangleq \int_{-\infty}^{\infty} R_x(t,t-\Delta t)\,e^{-j2\pi t\Delta f}\,dt$, the 2-D Fourier transform of $\overline{\Gamma}_x(t,f)$, is the *expected ambiguity function* of a random process $x(t)$. The simple multiplicative input-output relation (1.28) is the basis of certain methods for estimating the scattering function [Gaa68, AMH04]. Specifically, $\bar{A}_s(\Delta t,\Delta f)$ is known by design, and $\bar{A}_r(\Delta t,\Delta f)$ can be estimated from the receive signal. According to (1.28), an estimate of the TF correlation function $R_{\mathbf{H}}(\Delta t,\Delta f)$ can then be obtained by a (regularized) division of the estimate of $\bar{A}_r(\Delta t,\Delta f)$ by $\bar{A}_s(\Delta t,\Delta f)$, and an estimate of the scattering function $C_{\mathbf{H}}(\tau,\nu)$ is finally obtained by a 2-D Fourier transform according to (1.26). Further details of this approach are provided in Section 1.7.4.

Delay and Doppler profiles, time and frequency correlation functions

In some situations, only the delays or only the Doppler shifts of a WSSUS channel are of interest. An example is the exploitation of delay diversity in *orthogonal frequency division multiplexing* (OFDM) systems — see Chapter 7 — by (pre)coding across tones; here, the channel's Doppler characteristics are irrelevant. In such cases, the 2-D descriptions provided by the scattering function $C_{\mathbf{H}}(\tau,\nu)$ or TF correlation function $R_{\mathbf{H}}(\Delta t,\Delta f)$ may be too detailed, and it is sufficient to use one of the "marginals" of the scattering function. These marginals are defined as

$$c_{\mathbf{H}}^{(1)}(\tau) \triangleq \int_{-\infty}^{\infty} C_{\mathbf{H}}(\tau,\nu)\,d\nu\,, \qquad c_{\mathbf{H}}^{(2)}(\nu) \triangleq \int_{-\infty}^{\infty} C_{\mathbf{H}}(\tau,\nu)\,d\tau\,, \tag{1.29}$$

and termed *delay power profile* and *Doppler power profile*, respectively. The name "delay power profile" for $c_{\mathbf{H}}^{(1)}(\tau)$ is motivated by the relation $c_{\mathbf{H}}^{(1)}(\tau) = \mathsf{E}\{|h(t,\tau)|^2\}$, which shows that $c_{\mathbf{H}}^{(1)}(\tau)$ is the mean power of the channel tap with delay τ (this does not depend on t since WSSUS channels are stationary with respect to time). A similar relation and interpretation hold for $c_{\mathbf{H}}^{(2)}(\nu)$. Because of (1.26), the (1-D) Fourier transforms of the delay power profile $c_{\mathbf{H}}^{(1)}(\tau)$ and Doppler power profile $c_{\mathbf{H}}^{(2)}(\nu)$ are given by the *frequency correlation function* and *time correlation function* defined, respectively, as

$$r_{\mathbf{H}}^{(1)}(\Delta f) \triangleq R_{\mathbf{H}}(0,\Delta f) = \mathsf{E}\{L_{\mathbf{H}}(t,f)\,L_{\mathbf{H}}^{*}(t,f-\Delta f)\}\,,$$
$$r_{\mathbf{H}}^{(2)}(\Delta t) \triangleq R_{\mathbf{H}}(\Delta t,0) = \mathsf{E}\{L_{\mathbf{H}}(t,f)\,L_{\mathbf{H}}^{*}(t-\Delta t,f)\}\,.$$

The 1-D channel statistics discussed above can be used to formulate statistical input-output relations for stationary or white input (transmit) processes. For a stationary transmit signal with power spectral density $P_s(f)$, it can be shown that the receive signal produced by a WSSUS channel is stationary as well and its power spectral density and correlation function are respectively given by

$$P_r(f) = \int_{-\infty}^{\infty} c_{\mathbf{H}}^{(2)}(\nu)\,P_s(f-\nu)\,d\nu\,, \qquad r_r(\Delta t) = r_{\mathbf{H}}^{(2)}(\Delta t)\,r_s(\Delta t)\,.$$

Dual relations involving $c_{\mathbf{H}}^{(1)}(\tau)$ and $r_{\mathbf{H}}^{(1)}(\Delta f)$ hold for white transmit signals. Furthermore, similar relations exist for cyclostationary processes [MH03].

Global channel parameters

For many design and analysis tasks in wireless communications, only global channel parameters are relevant. These parameters summarize important properties of the scattering function and TF correlation function such as overall strength, position, extension (spread), etc.

As discussed in Section 1.2.4, the path loss (average power attenuation) is important, e.g., for link budget considerations. In the case of WSSUS channels, the path loss is equal to the volume of the scattering function or, equivalently, the maximum amplitude of the TF correlation function. That is, we have $P_{\mathrm{L}} = -10\log_{10}(\rho_{\mathbf{H}}^2)$ with

$$\begin{aligned}\rho_{\mathbf{H}}^2 &= \int_{-\infty}^{\infty}\int_{-\infty}^{\infty} C_{\mathbf{H}}(\tau,\nu)\,d\tau\,d\nu \\ &= \int_{-\infty}^{\infty} c_{\mathbf{H}}^{(1)}(\tau)\,d\tau = \int_{-\infty}^{\infty} c_{\mathbf{H}}^{(2)}(\nu)\,d\nu \\ &= R_{\mathbf{H}}(0,0) = \mathsf{E}\{|L_{\mathbf{H}}(t,f)|^2\}\,.\end{aligned}$$

Note that the last expression, $\mathsf{E}\{|L_{\mathbf{H}}(t,f)|^2\}$, does not depend on (t,f) due to the TF stationarity of WSSUS channels.

Further useful parameter are the *mean delay* and *mean Doppler* of a WSSUS channel, which are defined by the first moments (centers of gravity)

$$\bar{\tau} \triangleq \frac{1}{\rho_{\mathbf{H}}^2}\int_{-\infty}^{\infty}\int_{-\infty}^{\infty} \tau\, C_{\mathbf{H}}(\tau,\nu)\,d\tau\,d\nu = \frac{1}{\rho_{\mathbf{H}}^2}\int_{-\infty}^{\infty} \tau\, c_{\mathbf{H}}^{(1)}(\tau)\,d\tau\,, \tag{1.30a}$$

$$\bar{\nu} \triangleq \frac{1}{\rho_{\mathbf{H}}^2}\int_{-\infty}^{\infty}\int_{-\infty}^{\infty} \nu\, C_{\mathbf{H}}(\tau,\nu)\,d\tau\,d\nu = \frac{1}{\rho_{\mathbf{H}}^2}\int_{-\infty}^{\infty} \nu\, c_{\mathbf{H}}^{(2)}(\nu)\,d\nu\,. \tag{1.30b}$$

In particular, $\bar{\tau}$ describes the distance-dependent mean propagation delay. For physical channels, causality implies that $C_{\mathbf{H}}(\tau,\nu) = 0$ for $\tau < 0$ and consequently $\bar{\tau} \geq 0$. Assuming that the receiver's timing recovery unit locks to the center of gravity of the delay power profile, the subsequent receiver stages will see an equivalent channel $\tilde{\mathbf{H}}$ where the mean delay $\bar{\tau}$ is split off. That is, $\mathbf{H} = \tilde{\mathbf{H}}\mathbf{D}_{\bar{\tau}}$ where $\mathbf{D}_{\bar{\tau}}$ is a pure time delay operator acting as $(\mathbf{D}_{\tau}s)(t) = s(t-\bar{\tau})$ and $\tilde{\mathbf{H}}$ is an equivalent channel whose mean delay is zero. In many treatments, the equivalent channel $\tilde{\mathbf{H}}$ is considered even though this is not stated explicitly. Similar considerations apply to the mean Doppler shift $\bar{\nu}$, which can also be split off by frequency offset compensation techniques, resulting in an equivalent channel with mean Doppler equal to zero.

The mean delay $\bar{\tau}$ and mean Doppler $\bar{\nu}$ describe the overall location of the scattering function $C_{\mathbf{H}}(\tau,\nu)$ in the (τ,ν) plane. The extension of $C_{\mathbf{H}}(\tau,\nu)$ about $(\bar{\tau},\bar{\nu})$ can be measured by the *delay spread* and *Doppler spread*, which are defined as the root-mean-square (RMS) widths of delay power profile $c_{\mathbf{H}}^{(1)}(\tau)$ and Doppler power profile $c_{\mathbf{H}}^{(2)}(\nu)$,

respectively:

$$\sigma_\tau \triangleq \frac{1}{\rho_{\mathbf{H}}}\sqrt{\int_{-\infty}^{\infty}\int_{-\infty}^{\infty}(\tau-\bar{\tau})^2 C_{\mathbf{H}}(\tau,\nu)\,d\tau\,d\nu} = \frac{1}{\rho_{\mathbf{H}}}\sqrt{\int_{-\infty}^{\infty}(\tau-\bar{\tau})^2 c_{\mathbf{H}}^{(1)}(\tau)\,d\tau}\,, \quad (1.31a)$$

$$\sigma_\nu \triangleq \frac{1}{\rho_{\mathbf{H}}}\sqrt{\int_{-\infty}^{\infty}\int_{-\infty}^{\infty}(\nu-\bar{\nu})^2 C_{\mathbf{H}}(\tau,\nu)\,d\tau\,d\nu} = \frac{1}{\rho_{\mathbf{H}}}\sqrt{\int_{-\infty}^{\infty}(\nu-\bar{\nu})^2 c_{\mathbf{H}}^{(2)}(\nu)\,d\nu}\,. \quad (1.31b)$$

Sometimes it is more convenient to work with the reciprocals of Doppler spread and delay spread,

$$T_{\mathrm{c}} \triangleq \frac{1}{\sigma_\nu}\,, \qquad F_{\mathrm{c}} \triangleq \frac{1}{\sigma_\tau}\,, \quad (1.32)$$

which are known as the *coherence time* and *coherence bandwidth*, respectively. These two parameters can be used to quantify the duration and bandwidth within which the channel is approximately constant (or, at least, strongly correlated). This interpretation is supported by two arguments. First, it can be shown that the curvatures in the Δt and Δf directions of the squared magnitude of the TF correlation function $R_{\mathbf{H}}(\Delta t,\Delta f)$ at the origin are inversely proportional to the squared coherence bandwidth and coherence time, respectively. This corresponds to the following second-order Taylor series approximation of $|R_{\mathbf{H}}(\Delta t,\Delta f)|^2$ about the origin:

$$|R_{\mathbf{H}}(\Delta t,\Delta f)|^2 \approx \rho_{\mathbf{H}}^4\left[1-\left(\frac{2\pi\Delta t}{T_{\mathrm{c}}}\right)^2-\left(\frac{2\pi\Delta f}{F_{\mathrm{c}}}\right)^2\right].$$

(The first-order terms vanish since $|R_{\mathbf{H}}(\Delta t,\Delta f)|^2 \leq |R_{\mathbf{H}}(0,0)|^2 = \rho_{\mathbf{H}}^4$, i.e., $|R_{\mathbf{H}}(\Delta t,\Delta f)|^2$ assumes its maximum at the origin.) Thus, within durations $|\Delta t|$ smaller than T_{c} and bandwidths $|\Delta f|$ smaller than F_{c}, the channel will be strongly correlated. In addition, it can be shown that

$$\frac{1}{\rho_{\mathbf{H}}^2}\,\mathsf{E}\left\{|L_{\mathbf{H}}(t+\Delta t,f+\Delta f)-L_{\mathbf{H}}(t,f)|^2\right\} \leq 2\pi\left[\left(\frac{\Delta t}{T_{\mathrm{c}}}\right)^2+\left(\frac{\Delta f}{F_{\mathrm{c}}}\right)^2\right]. \quad (1.33)$$

This implies that within TF regions of duration $|\Delta t|$ smaller than T_{c} and bandwidth $|\Delta f|$ smaller than F_{c}, the channel is approximately constant (in the mean-square sense). More specifically, within the local *ε-coherence region* $\mathscr{B}_{\mathrm{c}}^{\varepsilon}(t,f) \triangleq [t,t+\varepsilon T_{\mathrm{c}}]\times[f,f+\varepsilon F_{\mathrm{c}}]$, the RMS error of the approximation $L_{\mathbf{H}}(t+\Delta t,f+\Delta f)\approx L_{\mathbf{H}}(t,f)$ is of order ε. An illustration of this coherence region will be provided by Fig. 1.8 on page 37.

We finally illustrate the characterization of WSSUS channels with a simple example.

Example 1.9 *A popular WSSUS channel model uses a separable scattering function $C_{\mathbf{H}}(\tau,\nu) = \frac{1}{\rho_{\mathbf{H}}^2}c_{\mathbf{H}}^{(1)}(\tau)c_{\mathbf{H}}^{(2)}(\nu)$ with an exponential delay power profile and a so-called Jakes Doppler power profile [Pro95, Mol05]:*

$$c_{\mathbf{H}}^{(1)}(\tau) = \begin{cases}\frac{\rho_{\mathbf{H}}^2}{\tau_0}e^{-\tau/\tau_0}, & \tau\geq 0\,,\\ 0, & \tau<0\,,\end{cases} \qquad c_{\mathbf{H}}^{(2)}(\nu) = \begin{cases}\frac{\rho_{\mathbf{H}}^2}{\pi\sqrt{\nu_{\max}^2-\nu^2}}, & |\nu|<\nu_{\max}\,,\\ 0, & |\nu|>\nu_{\max}\,.\end{cases}$$

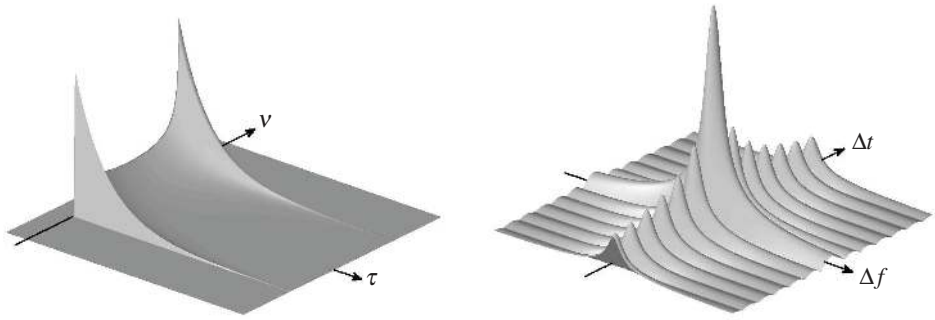

Figure 1.5 WSSUS channel following the Jakes-exponential model: scattering function (left) and magnitude of TF correlation function (right).

Here, τ_0 is a delay parameter and $\nu_{\max}$ is the maximum Doppler shift. The exponential delay profile is motivated by the exponential decay of receive power with path length (which is proportional to delay), and the Jakes Doppler profile results from the assumption of uniformly distributed AoA [Jak74]. Note that $c_{\mathbf{H}}^{(1)}(\tau)$ ignores the fundamental propagation delay of the first (and, in this case, also strongest) multipath component. The corresponding TF correlation function is separable as well, i.e., $R_{\mathbf{H}}(\Delta t,\Delta f) = \frac{1}{\rho_{\mathbf{H}}^2} r_{\mathbf{H}}^{(2)}(\Delta t) r_{\mathbf{H}}^{(1)}(\Delta f)$, with time correlation function and frequency correlation function given by

$$r_{\mathbf{H}}^{(2)}(\Delta t) = \rho_{\mathbf{H}}^2 J_0(2\pi\nu_{\max}\Delta t)\,, \qquad r_{\mathbf{H}}^{(1)}(\Delta f) = \frac{\rho_{\mathbf{H}}^2}{1+j2\pi\tau_0\Delta f}\,.$$

Here, $J_0(\cdot)$ denotes the zeroth-order Bessel function of the first kind. The scattering function and TF correlation function for this WSSUS channel are depicted in Fig. 1.5.

Assuming a delay parameter $\tau_0 = 10\,\mu$s and maximum Doppler $\nu_{\max} = 100\,$Hz, we obtain the mean delay $\bar{\tau} = \tau_0 = 10\,\mu$s and mean Doppler $\bar{\nu} = 0\,$Hz. Furthermore, the delay spread and Doppler spread follow as

$$\sigma_\tau = \tau_0 = 10\,\mu\text{s}\,, \qquad \sigma_\nu = \frac{\nu_{\max}}{\sqrt{2}} = 70.71\,\text{Hz}\,,$$

and the corresponding coherence time and coherence bandwidth are

$$T_{\text{c}} = \frac{\sqrt{2}}{\nu_{\max}} = 14.14\,\text{ms}\,, \qquad F_{\text{c}} = \frac{1}{\tau_0} = 100\,\text{kHz}\,.$$

For a narrowband system with bandwidth 10 kHz and frame duration 1 ms, the bound (1.33) *implies that the mean-square difference between any two values of $L_{\mathbf{H}}(t,f)$ within the frame duration and transmit band is at most roughly 1.5%. Thus, the TF transfer function can be assumed constant, i.e., $L_{\mathbf{H}}(t,f) \approx h$. Within one frame, the input-output relation* (1.12) *then simplifies to $r(t) \approx h\,s(t)$, a model known as block (slow) fading.*

1.4.2 Extension to multiantenna systems

We next outline the extension of the WSSUS property to multiple-antenna (MIMO) channels, mostly following [Mat06]. The main difference from the single-antenna case is the need for joint statistics of the individual links.

Scattering function matrix and space-time-frequency correlation function matrix

Extending [Bel63] (see also Section 1.4.1), we call a MIMO channel WSSUS if all $M_{\mathrm{T}}M_{\mathrm{R}}$ elements of the TF transfer function matrix $\mathbf{L}_{\mathbf{H}}(t,f)$ in (1.22) are *jointly* (wide-sense) stationary. Defining the length-$M_{\mathrm{T}}M_{\mathrm{R}}$ vector $\mathbf{l}_{\mathbf{H}}(t,f) \triangleq \mathrm{vec}\{\mathbf{L}_{\mathbf{H}}(t,f)\}$, this condition can be written as (cf. (1.25))

$$\mathsf{E}\{\mathbf{l}_{\mathbf{H}}(t,f)\,\mathbf{l}_{\mathbf{H}}^{H}(t',f')\} = \mathbf{R}_{\mathbf{H}}(t-t',f-f')\,. \tag{1.34}$$

Here, the $M_{\mathrm{T}}M_{\mathrm{R}} \times M_{\mathrm{T}}M_{\mathrm{R}}$ matrix $\mathbf{R}_{\mathbf{H}}(\Delta t,\Delta f)$ is referred to as the *space-time-frequency correlation function matrix* of the channel. This matrix-valued function describes the correlation of the transfer functions $L_{\mathbf{H}_{ij}}(t,f)$ and $L_{\mathbf{H}_{i'j'}}(t',f')$ of any two component channels $\mathbf{H}_{ij}$ and $\mathbf{H}_{i'j'}$ at time lag $t-t'=\Delta t$ and frequency lag $f-f'=\Delta f$.

Equivalently, the MIMO-WSSUS property expresses the fact that the elements of the spreading function matrix $\mathbf{S}_{\mathbf{H}}(\tau,\nu)$ in (1.21) are *jointly* white (cf. (1.24)), i.e.,

$$\mathsf{E}\{\mathbf{s}_{\mathbf{H}}(\tau,\nu)\,\mathbf{s}_{\mathbf{H}}^{H}(\tau',\nu')\} = \mathbf{C}_{\mathbf{H}}(\tau,\nu)\,\delta(\tau-\tau')\,\delta(\nu-\nu')\,,$$

with $\mathbf{s}_{\mathbf{H}}(\tau,\nu) \triangleq \mathrm{vec}\{\mathbf{S}_{\mathbf{H}}(\tau,\nu)\}$. The $M_{\mathrm{T}}M_{\mathrm{R}} \times M_{\mathrm{T}}M_{\mathrm{R}}$ matrix $\mathbf{C}_{\mathbf{H}}(\tau,\nu)$ will be referred to as the *scattering function matrix* (SFM). The SFM is nonnegative definite for all (τ,ν). It summarizes the mean spatial characteristics and strength of all scatterers with delay τ and Doppler ν. The SFM and the space-time-frequency correlation function matrix are related via a 2-D Fourier transform (cf. (1.26)):

$$\mathbf{C}_{\mathbf{H}}(\tau,\nu) = \int_{-\infty}^{\infty}\int_{-\infty}^{\infty} \mathbf{R}_{\mathbf{H}}(\Delta t,\Delta f)\,e^{-j2\pi(\nu\Delta t-\tau\Delta f)}\,d\Delta t\,d\Delta f\,.$$

Thus, recalling (1.34), the SFM $\mathbf{C}_{\mathbf{H}}(\tau,\nu)$ can be interpreted as the 2-D power spectral density matrix of the 2-D stationary multivariate random process $\mathbf{l}_{\mathbf{H}}(t,f)$.

Canonical decomposition

While the SFM provides a decorrelated representation with respect to delay and Doppler, it still features spatial correlations. For a spatially decorrelated representation, consider the (τ,ν)-dependent eigendecomposition of the SFM,

$$\mathbf{C}_{\mathbf{H}}(\tau,\nu) = \sum_{i=1}^{M_{\mathrm{R}}}\sum_{j=1}^{M_{\mathrm{T}}} \lambda_{ij}(\tau,\nu)\,\mathbf{u}_{ij}(\tau,\nu)\,\mathbf{u}_{ij}^{H}(\tau,\nu)\,.$$

Here, $\lambda_{ij}(\tau,\nu) \geq 0$ and $\mathbf{u}_{ij}(\tau,\nu)$ denote the eigenvalues and eigenvectors of $\mathbf{C}_{\mathbf{H}}(\tau,\nu)$, respectively (we use 2-D indexing for later convenience). For each (τ,ν), the $M_{\mathrm{T}}M_{\mathrm{R}}$ vectors $\mathbf{u}_{i,j}(\tau,\nu)$ form an orthonormal basis of $\mathbb{C}^{M_{\mathrm{T}}M_{\mathrm{R}}}$. Using the $M_{\mathrm{R}} \times M_{\mathrm{T}}$ matrix form of

this basis, $\mathbf{U}_{ij}(\tau,\nu) \triangleq \mathrm{unvec}\{\mathbf{u}_{ij}(\tau,\nu)\}$, the channel's spreading function can be expanded as

$$\mathbf{S}_{\mathbf{H}}(\tau,\nu) = \sum_{i=1}^{M_{\mathrm{R}}} \sum_{j=1}^{M_{\mathrm{T}}} \alpha_{ij}(\tau,\nu)\, \mathbf{U}_{ij}(\tau,\nu), \tag{1.35}$$

with the random coefficients $\alpha_{ij}(\tau,\nu) \triangleq \mathbf{u}_{ij}^H(\tau,\nu)\,\mathbf{s}_{\mathbf{H}}(\tau,\nu)$. It can be shown that these coefficients are orthogonal with respect to delay, Doppler, and space, i.e.,

$$\mathsf{E}\{\alpha_{ij}(\tau,\nu)\,\alpha^*_{i'j'}(\tau',\nu')\} = \lambda_{ij}(\tau,\nu)\,\delta_{i,i'}\,\delta_{j,j'}\,\delta(\tau-\tau')\,\delta(\nu-\nu').$$

The expansion (1.35) entails the following representation of the MIMO channel (see (1.19) and (1.20)):

$$\mathbf{r}(t) = (\underline{\mathbf{H}}\mathbf{s})(t) = \int_{-\infty}^{\infty}\int_{-\infty}^{\infty} \sum_{i=1}^{M_{\mathrm{R}}} \sum_{j=1}^{M_{\mathrm{T}}} \alpha_{ij}(\tau,\nu)\, \mathbf{U}_{ij}(\tau,\nu)\, \mathbf{s}(t-\tau)\, e^{j2\pi\nu t}\, d\tau\, d\nu. \tag{1.36}$$

It is seen that the eigenvector matrices $\mathbf{U}_{ij}(\tau,\nu)$ describe the spatial characteristics of deterministic atomic MIMO channels associated with delay τ and Doppler frequency ν. The expansion (1.36) is "doubly orthogonal" since for any (τ,ν), the matrices $\mathbf{U}_{ij}(\tau,\nu)$ are (deterministically) orthonormal and the coefficients $\alpha_{ij}(\tau,\nu)$ are stochastically orthogonal. Thus, (1.36) represents any MIMO-WSSUS channel as a superposition of deterministic atomic MIMO channels weighted by uncorrelated scalar random coefficients. In this representation, the channel transfer effects (space-time-frequency dispersion/selectivity) are separated from the channel stochastics.

Example 1.10 *For spatially i.i.d. MIMO-WSSUS channels, the SFM is given by* $\mathbf{C}_{\mathbf{H}}(\tau,\nu) = C(\tau,\nu)\,\mathbf{I}$*, i.e., all component channels* $\mathbf{H}_{ij}$ *are independent WSSUS channels with identical scattering function* $C(\tau,\nu)$*. In this case,* $\lambda_{ij}(\tau,\nu) = C(\tau,\nu)$ *and* $\mathbf{U}_{ij}(\tau,\nu) = \mathbf{e}_i\,\mathbf{e}_j^H$*, with* $\mathbf{e}_i$ *denoting the ith unit vector. Here, the action of the atomic channels is* $\mathbf{U}_{ij}(\tau,\nu)\mathbf{s}(t) = s_j(t)\,\mathbf{e}_i$*, which means that for the atomic channels, the ith receive antenna observes the signal emitted by the jth transmit antenna. Since due to the i.i.d. assumption the individual spatial links are independent, there is* $\alpha_{ij}(\tau,\nu) = \mathbf{u}_{ij}^H(\tau,\nu)\,\mathbf{s}_{\mathbf{H}}(\tau,\nu) = S_{\mathbf{H}_{ij}}(\tau,\nu)$ *and* (1.36) *simplifies to*

$$\mathbf{r}(t) = \int_{-\infty}^{\infty}\int_{-\infty}^{\infty} \sum_{i=1}^{M_{\mathrm{R}}} \sum_{j=1}^{M_{\mathrm{T}}} S_{\mathbf{H}_{ij}}(\tau,\nu)\; s_j(t-\tau)\, e^{j2\pi\nu t}\, \mathbf{e}_i\, d\tau\, d\nu\,.$$

The i.i.d. MIMO-WSSUS model is an extremely simple model in that it is already completely decorrelated in all domains. Slightly more complex—but more realistic—MIMO-WSSUS models are discussed in the next example.

Example 1.11 *An extension of the flat-fading MIMO model of Weichselberger et al. [WHOB06] assumes that the spatial eigenmodes (but not necessarily the associated powers* $\lambda_{ij}(\tau,\nu)$*) are separable, i.e.,* $\mathbf{U}_{ij}(\tau,\nu) = \mathbf{v}_i(\tau,\nu)\,\mathbf{w}_j^H(\tau,\nu)$*. Here, the spatial modes* $\mathbf{v}_i(\tau,\nu)$ *and* $\mathbf{w}_j(\tau,\nu)$ *can be interpreted as transmit and receive beamforming vectors, respectively. The resulting simplified version of* (1.35) *can be written as*

$$\mathbf{S}_{\mathbf{H}}(\tau,\nu) = \mathbf{V}(\tau,\nu)\,\mathbf{\Sigma}(\tau,\nu)\,\mathbf{W}^H(\tau,\nu), \tag{1.37}$$

with the deterministic matrices $\mathbf{V}(\tau,\nu) = [\mathbf{v}_1(\tau,\nu)\cdots\mathbf{v}_{M_\mathrm{R}}(\tau,\nu)]$ *(dimension* $M_\mathrm{R}\times M_\mathrm{R}$*) and* $\mathbf{W}(\tau,\nu) = [\mathbf{w}_1(\tau,\nu)\cdots\mathbf{w}_{M_\mathrm{T}}(\tau,\nu)]$ *(dimension* $M_\mathrm{T}\times M_\mathrm{T}$*) and the random matrix* $\mathbf{\Sigma}$ *(dimension* $M_\mathrm{R}\times M_\mathrm{T}$*) given by* $[\mathbf{\Sigma}(\tau,\nu)]_{ij} = \alpha_{ij}(\tau,\nu)$*. In this context, the average powers* $\lambda_{ij}(\tau,\nu)$ *are referred to as* coupling coefficients *since they describe how strongly the spatial transmit modes* $\mathbf{w}_j(\tau,\nu)$ *and spatial receive modes* $\mathbf{v}_i(\tau,\nu)$ *are coupled on average.*

A special case of the above model for uniform linear arrays is obtained by assuming that the spatial modes equal the array steering vectors, i.e., $\mathbf{V}(\tau,\nu) = \mathbf{F}_{M_\mathrm{R}}$ *and* $\mathbf{W}(\tau,\nu) = \mathbf{F}_{M_\mathrm{T}}$*, where* $\mathbf{F}_N$ *denotes the* $N\times N$ *DFT matrix. This model is known in the literature as the* virtual MIMO model *[Say02].*

Another simplification of (1.37) *is obtained by assuming that also the SFM eigenvalues are spatially separable, i.e.,* $\lambda_{ij}(\tau,\nu) = \kappa_i(\tau,\nu)\,\mu_j(\tau,\nu)$*. This corresponds to a WSSUS extension of the so-called* Kronecker model *[KSP+02].*

An analysis of channel measurements in [Mat06] revealed that for a channel having a dominant scatterer with delay τ_0 and Doppler frequency ν_0, the SFM at $(\tau,\nu) = (\tau_0,\nu_0)$, $\mathbf{C}_\mathbf{H}(\tau_0,\nu_0)$, has a single dominant eigenvalue (i.e., effective rank one), and the same holds true for the associated atomic MIMO channel matrix $\mathbf{U}_{11}(\tau_0,\nu_0)$. That is, $\mathbf{U}_{11}(\tau_0,\nu_0) = \mathbf{v}_1(\tau_0,\nu_0)\,\mathbf{w}_1^H(\tau_0,\nu_0)$, where the spatial signatures $\mathbf{v}_1(\tau_0,\nu_0)$ and $\mathbf{w}_1(\tau_0,\nu_0)$ essentially capture the AoA and AoD, respectively, associated with that dominant scatterer. It follows that in the delay-Doppler domain, a rank-one Kronecker model sufficiently characterizes the channel, i.e., $\mathbf{S}_\mathbf{H}(\tau_0,\nu_0) = \alpha_{11}(\tau_0,\nu_0)\,\mathbf{v}_1(\tau_0,\nu_0)\,\mathbf{w}_1^H(\tau_0,\nu_0)$. Note, however, that the Kronecker model is not necessarily applicable to the TF transfer function matrix $\mathbf{L}_\mathbf{H}(t,f)$. This is because the spatial averaging effected by the Fourier transform (1.22) will generally build up full-rank matrices.

1.4.3 Non-WSSUS channels

The WSSUS assumption greatly simplifies the statistical characterization of LTV channels. However, it is satisfied by practical wireless channels only approximately within certain time intervals and frequency bands. A similarly simple and intuitive framework for *non-WSSUS* channels is provided next, following to a large extent [Mat05]. This framework includes WSSUS channels as a special case.

A fundamental property of WSSUS channels is the fact that different scatterers (delay-Doppler components) are uncorrelated, i.e., the spreading function $S_\mathbf{H}(\tau,\nu)$ is a white process. In practice, this property will not be satisfied because channel components that are close to each other in the delay-Doppler domain often result from the same physical scatterer and will hence be correlated. In addition, filters, antennas, and windowing operations at the transmit and/or receive side are often viewed as part of the channel; they cause some extra time and frequency dispersion that results in correlations of the spreading function of the overall channel.

Example 1.12 *Consider a channel with a single specular scatterer with delay* τ_0*, Doppler shift* ν_0*, and random reflectivity h. The transmitter uses a filter with impulse response* $g(\tau)$*, and the receiver multiplies the receive signal by a window* $\gamma(t)$*. It can be shown*

that the spreading function of the effective channel (including transmit filter and receiver window) is given by

$$S_{\mathbf{H}}(\tau,\nu) = h\, g(\tau-\tau_0)\Gamma(\nu-\nu_0)\,,$$

where $\Gamma(\nu)$ *is the Fourier transform of* $\gamma(t)$*. Clearly, the spreading function exhibits correlations in a neighborhood of* (τ_0,ν_0) *that is determined by the effective duration of* $g(\tau)$ *and the effective bandwidth of* $\gamma(t)$*.*

An alternative view of non-WSSUS channels builds on the TF transfer function, which is no longer TF stationary. The physical mechanisms causing $L_{\mathbf{H}}(t,f)$ to be nonstationary include shadowing, delay and Doppler drift due to mobility, and changes in the propagation environment. These effects occur at a much larger scale than small-scale fading.

Example 1.13 *Consider a receiver approaching the transmitter with changing speed* $\upsilon(t)$ *so that their distance decreases according to* $d(t) = d_0 - \int_0^t \upsilon(t')\,dt'$*. In this case, the transmit signal is delayed by* $\tau_1(t) = d(t)/c_0$ *and Doppler-shifted by* $\nu_1(t) = f_c\upsilon(t)/c_0$*. The impulse response and TF transfer function are here given by* $h(t,\tau) = h\,e^{j2\pi\nu_1(t)t}\delta(\tau-\tau_1(t))$ *and* $L_{\mathbf{H}}(t,f) = h\,e^{j2\pi(\nu_1(t)t-\tau_1(t)f)}$*, respectively. The correlation function of* $L_{\mathbf{H}}(t,f)$ *can be shown to depend explicitly on time. Hence, the channel is temporally nonstationary.*

Local scattering function and channel correlation function

In [Mat05], the *local scattering function* (LSF) was introduced as a physically meaningful second-order statistic that extends the scattering function $C_{\mathbf{H}}(\tau,\nu)$ of WSSUS channels to the case of non-WSSUS channels. The LSF is defined as a 2-D Fourier transform of the 4-D correlation function of TF transfer function $L_{\mathbf{H}}(t,f)$ or spreading function $S_{\mathbf{H}}(\tau,\nu)$ with respect to the lag variables, i.e.,

$$\begin{aligned}\mathscr{C}_{\mathbf{H}}(t,f;\tau,\nu) &\triangleq \int_{-\infty}^{\infty}\int_{-\infty}^{\infty} \mathsf{E}\big\{L_{\mathbf{H}}(t,f+\Delta f)L_{\mathbf{H}}^*(t-\Delta t,f)\big\}\, e^{-j2\pi(\nu\Delta t-\tau\Delta f)}\,d\Delta t\,d\Delta f\\ &= \int_{-\infty}^{\infty}\int_{-\infty}^{\infty} \mathsf{E}\big\{S_{\mathbf{H}}(\tau,\nu+\Delta\nu)S_{\mathbf{H}}^*(\tau-\Delta\tau,\nu)\big\}\, e^{j2\pi(t\Delta\nu-f\Delta\tau)}\,d\Delta\tau\,d\Delta\nu\,.\end{aligned}$$

For WSSUS channels, $\mathscr{C}_{\mathbf{H}}(t,f;\tau,\nu) = C_{\mathbf{H}}(\tau,\nu)$ (cf. (1.26)). It was shown in [Mat05] that the LSF describes the power of multipath components with delay τ and Doppler shift ν occurring at time t and frequency f. This interpretation can be supported by the following channel input-output relation extending (1.27):

$$\overline{\Gamma}_r(t,f) = \int_{-\infty}^{\infty}\int_{-\infty}^{\infty} \mathscr{C}_{\mathbf{H}}(t,f-\nu;\tau,\nu)\,\overline{\Gamma}_s(t-\tau,f-\nu)\,d\tau\,d\nu\,,$$

where, as before, $\overline{\Gamma}_x(t,f)$ denotes the Rihaczek spectrum of a random process $x(t)$. This relation shows that the LSF $\mathscr{C}_{\mathbf{H}}(t,f;\tau,\nu)$ describes the TF energy shifts from $(t-\tau,f)$ to $(t,f+\nu)$.

The LSF is a channel statistic that reveals the nonstationarities (in time and frequency) of a channel via its dependence on t and f. A dual second-order channel statistic that is

better suited for describing the channel's delay-Doppler correlations (in addition to TF correlations) is provided by the *channel correlation function* (CCF) defined as

$$\begin{aligned}\mathscr{R}_{\mathbf{H}}(\Delta t,\Delta f;\Delta\tau,\Delta\nu) &\triangleq \int_{-\infty}^{\infty}\int_{-\infty}^{\infty}\mathsf{E}\big\{L_{\mathbf{H}}(t,f+\Delta f)L_{\mathbf{H}}^{*}(t-\Delta t,f)\big\}\,e^{-j2\pi(t\Delta\nu-f\Delta\tau)}\,dt\,df\\ &= \int_{-\infty}^{\infty}\int_{-\infty}^{\infty}\mathsf{E}\big\{S_{\mathbf{H}}(\tau,\nu+\Delta\nu)S_{\mathbf{H}}^{*}(\tau-\Delta\tau,\nu)\big\}\,e^{j2\pi(\nu\Delta t-\tau\Delta f)}\,d\tau\,d\nu.\end{aligned}$$

The CCF can be shown to characterize the correlation of multipath components separated by Δt in time, by Δf in frequency, by $\Delta\tau$ in delay, and by $\Delta\nu$ in Doppler. It generalizes the TF correlation function $R_{\mathbf{H}}(\Delta t,\Delta f)$ of WSSUS channels to the non-WSSUS case: for WSSUS channels, $\mathscr{R}_{\mathbf{H}}(\Delta t,\Delta f;\Delta\tau,\Delta\nu) = R_{\mathbf{H}}(\Delta t,\Delta f)\,\delta(\Delta\tau)\,\delta(\Delta\nu)$, which correctly indicates the absence of delay and Doppler correlations. The CCF is symmetric and assumes its maximum at the origin. It is related to the LSF via a 4-D Fourier transform,

$$\begin{aligned}\mathscr{C}_{\mathbf{H}}(t,f;\tau,\nu) = \int_{-\infty}^{\infty}\int_{-\infty}^{\infty}\int_{-\infty}^{\infty}\int_{-\infty}^{\infty}\mathscr{R}_{\mathbf{H}}(\Delta t,\Delta f;\Delta\tau,\Delta\nu)\,e^{-j2\pi(\nu\Delta t-\tau\Delta f-t\Delta\nu+f\Delta\tau)}\\ \times\,d\Delta t\,d\Delta f\,d\Delta\tau\,d\Delta\nu\,,\end{aligned}$$

in which time t and Doppler lag $\Delta\nu$ are Fourier dual variables, and so are frequency f and delay lag $\Delta\tau$. Once again, this indicates that delay-Doppler correlations manifest themselves as TF nonstationarities (and vice versa).

Reduced-detail channel descriptions

Several less detailed channel statistics for non-WSSUS channels can be obtained as marginals of the LSF or as cross-sections of the CCF. Of specific interest are the *average scattering function*,

$$\bar{C}_{\mathbf{H}}(\tau,\nu) \triangleq \int_{-\infty}^{\infty}\int_{-\infty}^{\infty}\mathscr{C}_{\mathbf{H}}(t,f;\tau,\nu)\,dt\,df = \mathsf{E}\{|S_{\mathbf{H}}(\tau,\nu)|^2\}$$

and its Fourier dual,

$$\mathscr{R}_{\mathbf{H}}(\Delta t,\Delta f;0,0) = \int_{-\infty}^{\infty}\int_{-\infty}^{\infty}\bar{C}_{\mathbf{H}}(\tau,\nu)\,e^{j2\pi(\nu\Delta t-\tau\Delta f)}\,d\tau\,d\nu\,,$$

which characterize the global delay-Doppler dispersion and TF correlations much in the same way as the scattering function $C_{\mathbf{H}}(\tau,\nu)$ and TF correlation function $R_{\mathbf{H}}(\Delta t,\Delta f)$ of WSSUS channels. Dual channel statistics describing particularly the nonstationarities and delay-Doppler correlations of non-WSSUS channels are given by the *TF dependent path loss*

$$\rho^2_{\mathbf{H}}(t,f) \triangleq \int_{-\infty}^{\infty}\int_{-\infty}^{\infty}\mathscr{C}_{\mathbf{H}}(t,f;\tau,\nu)\,d\tau\,d\nu = \mathsf{E}\{|L_{\mathbf{H}}(t,f)|^2\}$$

and its Fourier dual

$$\mathscr{R}_{\mathbf{H}}(0,0;\Delta\tau,\Delta\nu) = \int_{-\infty}^{\infty}\int_{-\infty}^{\infty}\rho^2_{\mathbf{H}}(t,f)\,e^{-j2\pi(t\Delta\nu-f\Delta\tau)}\,dt\,df\,.$$

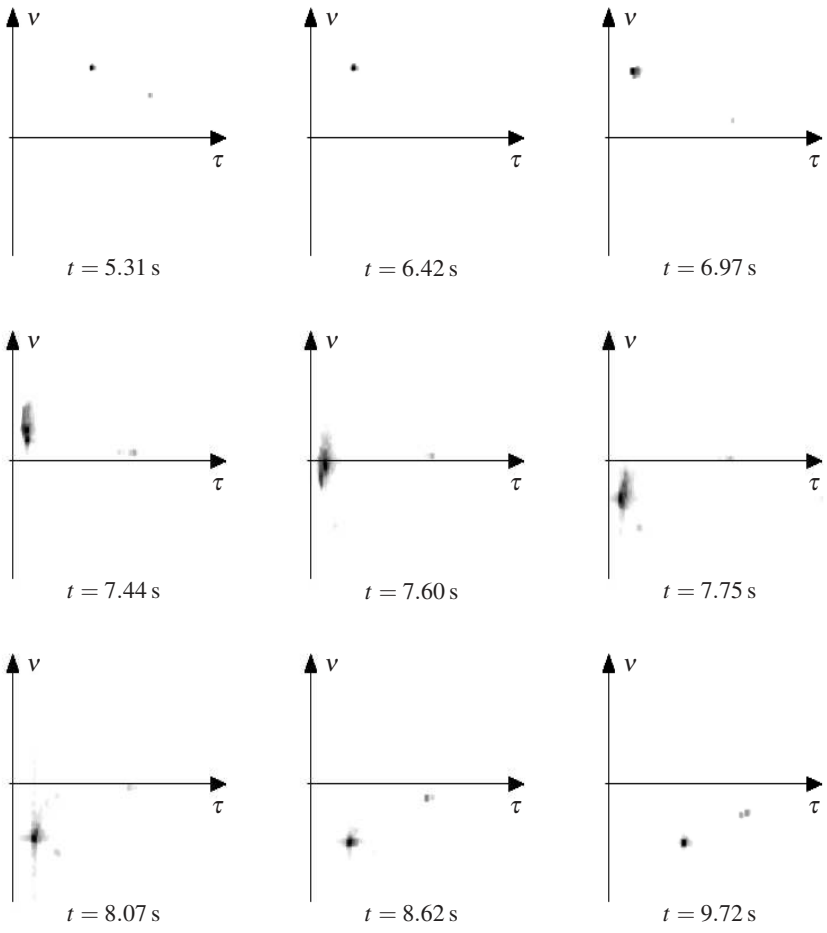

Figure 1.6 Temporal snapshots of the LSF estimate $\hat{\mathscr{C}}_{\mathbf{H}}(t, f_c; \tau, \nu)$ for a car-to-car channel.

In addition, it is possible to define TF dependent delay and Doppler power profiles,

$$c_{\mathbf{H}}^{(1)}(t, f; \tau) \triangleq \int_{-\infty}^{\infty} \mathscr{C}_{\mathbf{H}}(t, f; \tau, \nu)\, d\nu\,, \qquad c_{\mathbf{H}}^{(2)}(t, f; \nu) \triangleq \int_{-\infty}^{\infty} \mathscr{C}_{\mathbf{H}}(t, f; \tau, \nu)\, d\tau\,,$$

whose usefulness straightforwardly generalizes from the WSSUS case (see (1.29)).

Example 1.14 *We consider measurement data of a mobile radio channel for car-to-car communications. The channel measurements were recorded during* 10 s *at* $f_c = 5.2\,\text{GHz}$ *with the transmitter and receiver located in two cars that moved in opposite directions on a highway. (We note that channel sounding is addressed in Section 1.7.) Details of the measurement campaign are described in [PKC+09], and the measurement data are available at http://measurements.ftw.at. Fig. 1.6 shows nine snapshots of the estimated*

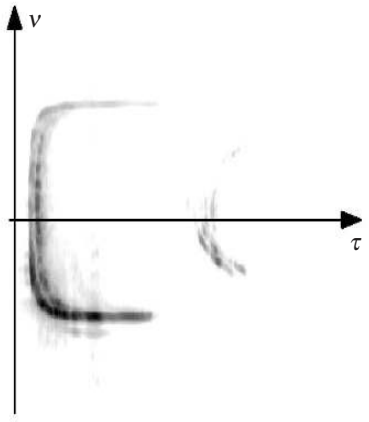

Figure 1.7 Estimate of the average LSF $\bar{C}_{\mathbf{H}}(\tau, \nu)$ for the car-to-car channel.

LSF $\hat{\mathscr{C}}_{\boldsymbol{H}}(t, f; \tau, \nu)$ at different time instants t and with frequency f fixed to f_c (see Section 1.7.4 for an estimator of the LSF). The figure depicts three successive phases: during phase I (top row), the cars approach each other; during phase II (middle row), they drive by each other; and during phase III (bottom row), they move away from each other. At each time instant, the LSF is seen to consist of only a small number of dominant components. These components correspond to i) the direct path between the two cars, ii) a path involving a reflection by a building located sideways of the highway, and iii) further paths corresponding to reflections by other vehicles on the highway. The direct path has a large delay and large positive Doppler frequency during phase I, a small delay and near-zero Doppler frequency during phase II, and a large delay and large negative Doppler frequency during phase III. Similar observations apply to the other multipath components.

Fig. 1.7 shows an estimate of the average LSF $\bar{C}_{\mathbf{H}}(\tau, \nu)$. While this representation indicates the maximum delay and Doppler frequency, it suggests a continuum of scatterers, and thus fails to indicate that at each time instant there are only a few dominant multipath components.

Global channel parameters

As in the WSSUS case, it is desirable to be able to characterize non-WSSUS channels in terms of a few global scalar parameters. In particular, the *transmission loss* is given by

$$\begin{aligned}\mathscr{E}_{\mathbf{H}}^2 &\triangleq \int_{-\infty}^{\infty}\int_{-\infty}^{\infty}\int_{-\infty}^{\infty}\int_{-\infty}^{\infty} \mathscr{C}_{\mathbf{H}}(t,f;\tau,\nu)\,dt\,df\,d\tau\,d\nu \\ &= \int_{-\infty}^{\infty}\int_{-\infty}^{\infty} \bar{C}_{\mathbf{H}}(\tau,\nu)\,d\tau\,d\nu \\ &= \int_{-\infty}^{\infty}\int_{-\infty}^{\infty} \rho_{\mathbf{H}}^2(t,f)\,dt\,df \\ &= \mathsf{E}\{\|\mathbf{H}\|^2\},\end{aligned}$$

where $\|\mathbf{H}\|^2 \triangleq \int_{-\infty}^{\infty}\int_{-\infty}^{\infty} |k_{\mathbf{H}}(t,t')|^2\,dt\,dt'$. The transmission loss quantifies the mean received energy for a normalized stationary and white transmit signal. Furthermore, non-WSSUS versions of the mean delay $\bar{\tau}$, mean Doppler $\bar{\nu}$, delay spread σ_τ, and Doppler spread σ_ν can be defined by replacing the scattering function $C_{\mathbf{H}}(\tau,\nu)$ and path loss $\rho_{\mathbf{H}}^2$ in the respective WSSUS-case definitions (1.30), (1.31) with the average scattering function $\bar{C}_{\mathbf{H}}(\tau,\nu)$ and transmission loss $\mathscr{E}_{\mathbf{H}}^2$, respectively. Time-dependent or frequency-dependent versions of these parameters can also be defined. As an example, we mention the time-dependent delay spread given by

$$\sigma_\tau(t) \triangleq \frac{1}{\rho_{\mathbf{H}}(t)}\sqrt{\int_{-\infty}^{\infty}\int_{-\infty}^{\infty}\int_{-\infty}^{\infty}[\tau-\bar{\tau}(t)]^2\,\mathscr{C}_{\mathbf{H}}(t,f;\tau,\nu)\,df\,d\tau\,d\nu}$$

with

$$\rho_{\mathbf{H}}^2(t) \triangleq \int_{-\infty}^{\infty} \rho_{\mathbf{H}}^2(t,f)\,df\,, \qquad \bar{\tau}(t) \triangleq \frac{1}{\rho_{\mathbf{H}}^2(t)}\int_{-\infty}^{\infty}\int_{-\infty}^{\infty}\int_{-\infty}^{\infty}\tau\,\mathscr{C}_{\mathbf{H}}(t,f;\tau,\nu)\,df\,d\tau\,d\nu\,.$$

As in the case of WSSUS channels, a coherence time T_{c} and a coherence bandwidth F_{c} can be defined as the reciprocal of Doppler spread σ_ν and delay spread σ_τ, respectively [Mat05]. These coherence parameters can be combined into a local ε-*coherence region* $\mathscr{B}_{\mathrm{c}}^{\varepsilon}(t,f) \triangleq [t,t+\varepsilon T_{\mathrm{c}}]\times[f,f+\varepsilon F_{\mathrm{c}}]$. It can then be shown that the TF transfer function is approximately constant within $\mathscr{B}_{\mathrm{c}}^{\varepsilon}(t,f)$ in the sense that the normalized RMS error of the approximation $L_{\mathbf{H}}(t',f') \approx L_{\mathbf{H}}(t,f)$ is maximally of order ε for all $(t',f') \in \mathscr{B}_{\mathrm{c}}^{\varepsilon}(t,f)$.

While much of the above discussion involved concepts familiar from WSSUS channels, delay-Doppler correlations and channel nonstationarity are phenomena specific to non-WSSUS channels. The amount of delay correlation and Doppler correlation can be measured by the following moments of the CCF:

$$\overline{\Delta\tau} \triangleq \frac{1}{\|\mathscr{R}_{\mathbf{H}}\|_1}\int_{-\infty}^{\infty}\int_{-\infty}^{\infty}\int_{-\infty}^{\infty}\int_{-\infty}^{\infty}|\Delta\tau|\,|\mathscr{R}_{\mathbf{H}}(\Delta t,\Delta f;\Delta\tau,\Delta\nu)|\,d\Delta t\,d\Delta f\,d\Delta\tau\,d\Delta\nu\,, \quad (1.38a)$$

$$\overline{\Delta\nu} \triangleq \frac{1}{\|\mathscr{R}_{\mathbf{H}}\|_1}\int_{-\infty}^{\infty}\int_{-\infty}^{\infty}\int_{-\infty}^{\infty}\int_{-\infty}^{\infty}|\Delta\nu|\,|\mathscr{R}_{\mathbf{H}}(\Delta t,\Delta f;\Delta\tau,\Delta\nu)|\,d\Delta t\,d\Delta f\,d\Delta\tau\,d\Delta\nu\,. \quad (1.38b)$$

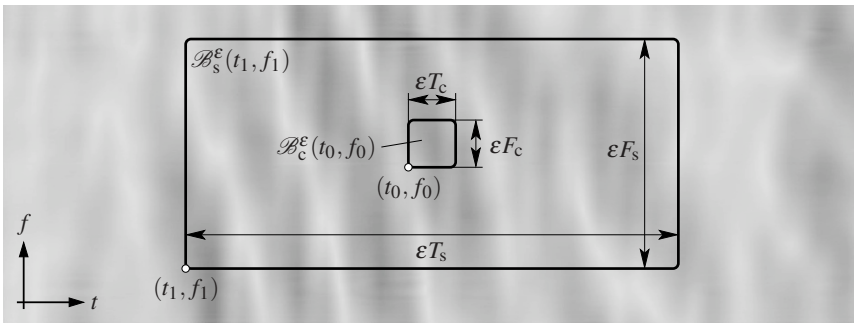

Figure 1.8 Illustration of coherence region $\mathscr{B}_{\mathrm{c}}^{\varepsilon}(t_0,f_0)$ and stationarity region $\mathscr{B}_{\mathrm{s}}^{\varepsilon}(t_1,f_1)$; the gray-shaded background corresponds to the magnitude of the channel's TF transfer function.

These parameters quantify the delay lag and Doppler lag spans within which there are significant correlations. Delay-Doppler correlations correspond to channel nonstationarity in the (dual) TF domain. The amount of (non-)stationarity can be measured in terms of a *stationarity time* and a *stationarity bandwidth* that are respectively defined as

$$T_{\mathrm{s}} \triangleq \frac{1}{\Delta\nu}, \qquad F_{\mathrm{s}} \triangleq \frac{1}{\Delta\tau}. \tag{1.39}$$

These two stationarity parameters can be combined into a local ε-*stationarity region* $\mathscr{B}_{\mathrm{s}}^{\varepsilon}(t,f) \triangleq [t,t+\varepsilon T_{\mathrm{s}}] \times [f,f+\varepsilon F_{\mathrm{s}}]$. It can be shown that the LSF is approximately constant within $\mathscr{B}_{\mathrm{s}}^{\varepsilon}(t,f)$ in the sense that the normalized error magnitude of the approximation $\mathscr{C}_{\mathsf{H}}(t',f';\tau,\nu) \approx \mathscr{C}_{\mathsf{H}}(t,f;\tau,\nu)$ is maximally of order ε for all $(t',f') \in \mathscr{B}_{\mathrm{s}}^{\varepsilon}(t,f)$. The stationarity region essentially quantifies the duration and bandwidth within which the channel can be approximated with good accuracy by a WSSUS channel. The relevance of the stationarity region to wireless system design was discussed in [Mat05]. For example, the ratio of the size of the stationarity region and the size of the coherence region, $T_{\mathrm{s}}F_{\mathrm{s}}/(T_{\mathrm{c}}F_{\mathrm{c}})$, is crucial for the operational meaning of ergodic capacity. An illustration of the stationarity region and the coherence region is provided in Fig. 1.8.

1.5 Underspread channels

So far, some of the system functions (e.g., TF transfer function and LSF) have been defined only formally without addressing their theoretical justification or practical applications.

Example 1.15 *If a pure carrier signal $s(t) = e^{j2\pi f_{\mathrm{c}}t}$ is transmitted over a linear time-invariant (purely time-dispersive/frequency-selective) channel with impulse response $h(\tau)$, the receive signal is given by the transmit signal multiplied by a complex factor, i.e.,*

$$r(t) = H(f_{\mathrm{c}})\, e^{j2\pi f_{\mathrm{c}}t}, \tag{1.40}$$

where $H(f) = \int_{-\infty}^{\infty} h(\tau)\, e^{-j2\pi f\tau}\, d\tau$ is the conventional channel transfer function. In mathematical language, complex exponentials are eigenfunctions of time-invariant channels.

For an LTV channel with spreading function $S_{\mathbf{H}}(\tau,\nu)$, we have

$$r(t) = L_{\mathbf{H}}(t, f_c)\, e^{j2\pi f_c t}\,, \tag{1.41}$$

where $L_{\mathbf{H}}(t,f) = \int_{-\infty}^{\infty}\int_{-\infty}^{\infty} S_{\mathbf{H}}(\tau,\nu)\, e^{j2\pi(t\nu - f\tau)}\, d\tau\, d\nu$ is the channel's TF transfer function. In spite of the formal similarity to (1.40)*, the receive signal in* (1.41) *is not a complex exponential in general; the time-dependence of the complex factor $L_{\mathbf{H}}(t,f_c)$ may result in strong amplitude and frequency modulation.*

Thus, the interpretation of the TF transfer function $L_{\mathbf{H}}(t,f)$ as a "transfer function" appears to be a doubtful matter. In this section, we will argue that this problem and related ones can be resolved using the concept of *underspread* channels. We will introduce two different underspread notions: one is based on the *dispersion spread* and is applicable to any LTV channel, while the other builds upon the *correlation spread* and is only relevant to non-WSSUS channels.

1.5.1 Dispersion-underspread property

A difficulty with general LTV channels is the fact that they can cause arbitrarily large joint TF spreads, i.e., arbitrarily severe TF dispersion. The amount of TF dispersion can be quantified by measuring the spread (extension, effective support) of a suitable delay-Doppler representation of the channel (the spreading function for a given channel realization, the scattering function for WSSUS channels, the LSF for non-WSSUS channels). In the following, we will focus on WSSUS channels and, thus, the scattering function. For a discussion of the formulation and implications of the dispersion-underspread property for individual channel realizations and non-WSSUS channels, we refer to [MH98] and [Mat05], respectively.

The spread of the scattering function $C_{\mathbf{H}}(\tau,\nu)$ of a WSSUS channel can be measured in different ways. If $C_{\mathbf{H}}(\tau,\nu)$ has a compact support $\mathscr{S}_{\mathbf{H}}$, i.e., $C_{\mathbf{H}}(\tau,\nu) = 0$ for $(\tau,\nu) \neq \mathscr{S}_{\mathbf{H}}$, a simple measure of its spread is given by the area of its support region, $|\mathscr{S}_{\mathbf{H}}|$. An even simpler — but also less accurate — measure of dispersion spread in the compact-support case is given by the area of the smallest rectangle circumscribing $\mathscr{S}_{\mathbf{H}}$, i.e.,

$$d_{\mathbf{H}} \triangleq 4\tau_{\max}\nu_{\max}\,, \tag{1.42}$$

where $\tau_{\max} \triangleq \max\{|\tau| :\ (\tau,\nu) \in \mathscr{S}_{\mathbf{H}}\}$ and $\nu_{\max} \triangleq \max\{|\nu| :\ (\tau,\nu) \in \mathscr{S}_{\mathbf{H}}\}$ are the channel's maximum delay and maximum Doppler, respectively.

A limitation of support-based measures of dispersion spread is the fact that the scattering function of most channels is not compactly supported. We could then use the notion of an "effective support," but this notion presents some arbitrariness. An alternative is provided by moments or, more generally, weighted integrals of the scattering function. The quantities most commonly used in this context are the delay spread σ_τ and Doppler

spread σ_ν defined in (1.31), whose product

$$\sigma_{\mathbf{H}} \triangleq \sigma_\tau \sigma_\nu$$

quantifies the dispersion spread without requiring a compact support of $C_{\mathbf{H}}(\tau, \nu)$.

The *dispersion-underspread* property expresses the fact that the channel's dispersion spread is "small." Usually, this constraint is formulated as [Pro95, Mol05, MH03]

$$d_{\mathbf{H}} \leq 1 \quad \text{or} \quad \sigma_{\mathbf{H}} \leq 1\,, \tag{1.43}$$

depending on which measure of dispersion spread is being used. A channel that does not satisfy (1.43) is termed *overspread*. Sometimes, the stronger condition $d_{\mathbf{H}} \ll 1$ or $\sigma_{\mathbf{H}} \ll 1$ is imposed. The underspread conditions (1.43) imply that the channel does not cause *both* strong time dispersion and strong frequency dispersion. An alternative formulation is in terms of the channel's coherence parameters (see (1.32)):

$$T_{\mathrm{c}} F_{\mathrm{c}} \geq 1, \qquad T_{\mathrm{c}} \geq \sigma_\tau, \qquad F_{\mathrm{c}} \geq \sigma_\nu.$$

Each of these three inequalities is strictly equivalent to the second inequality in (1.43). The first inequality says that (the TF transfer function of) an underspread channel has to remain constant within a TF region of area (much) larger than 1; thus, the channel cannot be *both* strongly time-selective and strongly frequency-selective. The second inequality states that the channel stays approximately constant over a time period that is larger than its delay spread, and the third inequality states that the channel stays approximately constant over a frequency band that is larger than its Doppler spread. Note that none of the above conditions requires the channel to be "slowly time-varying." In fact, the time variation (Doppler spread) can be arbitrarily large — i.e., the coherence time can be arbitrarily small — as long as the impulse response is sufficiently short.

Real-world wireless (radio) channels are virtually always underspread. This is because the delay and Doppler of any propagation path are both inversely proportional to the speed of light c_0, i.e., $\tau_{\max} = d_{\max}/c_0$ and $\nu_{\max} = \upsilon_{\max} f_{\mathrm{c}}/c_0$, where $d_{\max}$ and $\upsilon_{\max}$ denote the maximum path length and maximum relative velocity, respectively. It then follows from (1.42) that $d_{\mathbf{H}} = 4 d_{\max} \upsilon_{\max} f_{\mathrm{c}}/c_0^2$. Since $1/c_0^2 \approx 10^{-17}\mathrm{s}^2/\mathrm{m}^2$, violation of (1.43) would require that the product $4 d_{\max} \upsilon_{\max} f_{\mathrm{c}}$ is on the order of $10^{17}\mathrm{m}^2/\mathrm{s}^2$, which is practically impossible for wireless (radio) communications. However, the situation can be different for underwater acoustic channels (see Chapter 9).

Example 1.16 *Reconsider the WSSUS channel with exponential power profile and Jakes Doppler profile from Example 1.9. Here,* $\sigma_\tau = 10\,\mu\mathrm{s}$ *and* $\sigma_\nu = 70.71\,\mathrm{Hz}$ *or equivalently* $T_{\mathrm{c}} = 14.14\,\mathrm{ms}$ *and* $F_{\mathrm{c}} = 100\,\mathrm{kHz}$. *It follows that* $\sigma_{\mathbf{H}} = 7.1 \cdot 10^{-4}$ *and* $T_{\mathrm{c}} F_{\mathrm{c}} = 1.4 \cdot 10^3$, *which shows that this channel is strongly underspread. Indeed, the channel stays approximately constant over several milliseconds, which is much larger than the effective impulse response duration of some tens of microseconds.*

For an underspread channel, it follows from (1.11) that the TF transfer function $L_{\mathbf{H}}(t, f)$ is a *smooth* function. Indeed, its Fourier transform — the spreading function — has a

small "delay-Doppler bandwidth." This interpretation is furthermore supported by (1.33), which can be shown to imply

$$\frac{1}{\rho_{\mathbf{H}}^2}\,\mathsf{E}\big\{\big|L_{\mathbf{H}}(t+\Delta t, f+\Delta f) - L_{\mathbf{H}}(t,f)\big|^2\big\} \;\leq\; 4\pi\,|\Delta t|\,|\Delta f|\,\sigma_{\mathbf{H}}\,.$$

This means that the normalized TF transfer function varies very little within TF regions of area $|\Delta t|\,|\Delta f| \ll 1/\sigma_{\mathbf{H}}$. For a channel that is more underspread (smaller $\sigma_{\mathbf{H}}$), the TF region within which $L_{\mathbf{H}}(t,f)$ stays approximately constant is larger.

An alternative view of the channel's TF variation is obtained by studying the TF correlation function $R_{\mathbf{H}}(\Delta t, \Delta f)$. By working out the square on the left-hand side of (1.33), one can show that

$$\frac{|R_{\mathbf{H}}(\Delta t, \Delta f)|}{\rho_{\mathbf{H}}^2} \geq 1 - \pi\big[\sigma_\nu^2 (\Delta t)^2 + \sigma_\tau^2 (\Delta f)^2\big].$$

Thus, $R_{\mathbf{H}}(\Delta t, \Delta f)$ has a slow decay, which means that $L_{\mathbf{H}}(t,f)$ features significant correlations over TF regions whose area is on the order of $1/(\sigma_\tau^2\sigma_\nu^2)$.

In addition to the smoothness and correlation of the TF transfer function, the underspread property has several other useful consequences, some of which are discussed in Sections 1.5.3–1.5.5. Further results in a similar spirit can be found in [MH98, MH03, Mat05].

1.5.2 Correlation-underspread property

For WSSUS channels, the TF transfer function $L_{\mathbf{H}}(t,f)$ is a 2-D stationary process whose (delay-Doppler) power spectrum is given by the scattering function $C_{\mathbf{H}}(\tau,\nu)$. Even though this no longer holds true for non-WSSUS channels, one would intuitively expect, e.g., that the LSF $\mathscr{C}_{\mathbf{H}}(t,f;\tau,\nu)$ of a non-WSSUS channel is a TF dependent (delay-Doppler) power spectrum. While such an interpretation does not hold in general, it holds in an approximate sense for the practically important class of correlation-underspread channels.

We will first introduce a global measure of the amount of correlation of a non-WSSUS channel via the extension (effective support) of the CCF $\mathscr{R}_{\mathbf{H}}(\Delta t, \Delta f; \Delta\tau, \Delta\nu)$. Specifically, the amount of correlation in time and frequency is measured by the coherence time T_{c} and coherence bandwidth F_{c} defined in (1.32), respectively, and the amount of correlation in delay and Doppler is measured by the moments $\overline{\Delta\tau}$ and $\overline{\Delta\nu}$ defined in (1.38), respectively. Based on these parameters, we define the *correlation spread* as

$$c_{\mathbf{H}} \;\triangleq\; T_{\mathrm{c}}\,F_{\mathrm{c}}\,\overline{\Delta\tau}\,\overline{\Delta\nu}\,.$$

The correlation spread characterizes the effective support of the CCF. Note that for a WSSUS channel, $\overline{\Delta\tau} = \overline{\Delta\nu} = 0$ and hence $c_{\mathbf{H}} = 0$.

An LTV channel is called *correlation-underspread* if its correlation spread is (much) less than one, i.e., if

$$c_{\mathbf{H}} \leq 1\,. \tag{1.44}$$

This condition requires that the channel does not exhibit both strong TF correlations and strong delay-Doppler correlations. It is a 2-D extension of the underspread notion for 1-D nonstationary processes as described, e.g., in [MH06]. The correlation-underspread property for non-WSSUS channels is satisfied by most practical wireless (radio) channels.

Using $T_c = 1/\sigma_\nu$ and $F_c = 1/\sigma_\tau$, the correlation-underspread property (1.44) can be alternatively written as

$$\overline{\Delta\tau}\,\overline{\Delta\nu} \leq \sigma_\tau \sigma_\nu = \sigma_{\mathbf{H}}\,.$$

That is, the amount of delay-Doppler correlation has to be smaller than the amount of delay-Doppler dispersion. This requires that only delay-Doppler components that are close to each other in the delay-Doppler plane are correlated. Yet another interpretation is obtained by using (1.39), which gives

$$T_c F_c \leq T_s F_s\,.$$

This means that the channel's stationarity region (whose area is measured by $T_s F_s$) is larger than the channel's coherence region (whose area is measured by $T_c F_c$). The equivalent requirement that the channel statistics change at a much slower rate than the channel's transfer characteristics is fundamental and indispensable for any transceiver technique that is based on channel statistics (in fact, it is tacitly assumed in most of the relevant publications).

Example 1.17 *Consider a mobile WiMAX system operating at carrier frequency* $f_c = 3.5\,\text{GHz}$. *We assume that the user's speed is around* $\upsilon = 30\,\text{m/s}$ *and the path length between base station and user is around* $d = 6\,\text{km}$. *This corresponds to a Doppler spread of* $\sigma_\nu = \upsilon f_c/c_0 = 350\,\text{Hz}$ *and a delay spread of* $\sigma_\tau = d/c_0 = 20\,\mu\text{s}$. *The dispersion spread is thus obtained as* $\sigma_{\mathbf{H}} = 7 \cdot 10^{-3}$, *which shows that the channel is dispersion-underspread. The coherence parameters are* $T_c = 2.9\,\text{ms}$ *and* $F_c = 50\,\text{kHz}$.

Reflections from the same physical object (e.g., a building) are an important source of correlated delay-Doppler components. Assuming objects of width $w = 30\,\text{m}$ *and maximum angular spread (viewed from the user's position) of* $\delta = 2^\circ$ *yields the moments* $\overline{\Delta\tau} = w/c_0 = 0.1\,\mu\text{s}$ *and* $\overline{\Delta\nu} = 2\sigma_\nu \sin(\delta/2) = 12.2\,\text{Hz}$.

Thus, for this scenario, we obtain a correlation spread of $c_{\mathbf{H}} = 1.7 \cdot 10^{-4}$, *and hence the channel is strongly correlation-underspread. This can also be concluded from the relation* $\overline{\Delta\tau}\,\overline{\Delta\nu} = 1.2 \cdot 10^{-6} \ll \sigma_{\mathbf{H}} = 7 \cdot 10^{-3}$. *The stationarity parameters are* $T_s = 82\,\text{ms}$ *and* $F_s = 10\,\text{MHz}$. *Comparing with the coherence parameters* T_c, F_c *given above, we also have* $T_c F_c = 1.4 \cdot 10^2 \ll T_s F_s = 8.3 \cdot 10^5$.

1.5.3 Approximate eigenrelation

The eigendecomposition of a linear system (channel) $\mathbf{H}$ is of fundamental importance. The *eigenfunctions* $u_k(t)$ and *eigenvalues* λ_k are defined by the eigenequation[2]

$$(\mathbf{H}u_k)(t) \equiv \int_{-\infty}^{\infty} k_{\mathbf{H}}(t,t')\,u_k(t')\,dt' = \lambda_k\,u_k(t)\,. \tag{1.45}$$

[2]We do not consider singular value decompositions since underspread channels can be shown [MH98] to be approximately normal, and for normal systems, the singular value decomposition is equivalent to the eigendecomposition [NS82].

For normal channels ($\mathbf{H}\mathbf{H}^* = \mathbf{H}^*\mathbf{H}$, where $\mathbf{H}^*$ denotes the adjoint of $\mathbf{H}$ [NS82]), the (normalized) eigenfunctions $u_k(t)$ constitute an orthonormal basis, i.e., any square-integrable signal can be expanded into the $u_k(t)$ and $\langle u_k, u_l \rangle = \delta_{kl}$. Together with (1.45), this implies the operator diagonalization [NS82]

$$\langle \mathbf{H}u_k, u_l \rangle = \langle \lambda_k u_k, u_l \rangle = \lambda_k \langle u_k, u_l \rangle = \lambda_k \delta_{kl}$$

and, also, the following decomposition of the channel $\mathbf{H}$ or its kernel $k_{\mathbf{H}}(t,t')$:

$$\mathbf{H} = \sum_k \lambda_k u_k \otimes u_k^*, \qquad k_{\mathbf{H}}(t,t') = \sum_k \lambda_k u_k(t) u_k^*(t') .$$

Here, $u_k \otimes u_k^*$ denotes the rank-1 projection operator with kernel $u_k(t) u_k^*(t')$.

In the context of digital communications, the channel eigendecomposition is useful for modulator design. Modulating the data symbols a_k onto the eigenfunctions $u_k(t)$, in the sense that the eigenfunctions constitute the "transmit pulses," yields the transmit signal $s(t) = \sum_k a_k u_k(t)$. The resulting receive signal (ignoring noise) is $r(t) = \sum_k a_k (\mathbf{H}u_k)(t) = \sum_k a_k \lambda_k u_k(t)$. Performing demodulation by correlating with the transmit pulses, i.e., projecting $r(t)$ onto the eigenfunctions, gives $\langle r, u_l \rangle = \lambda_l a_l$. Thus, all symbols are recovered free of mutual interference. Note that this scheme requires knowledge of the channel eigenfunctions at the transmitter.

In the limiting case of a time-invariant channel, the index k becomes a frequency variable, the eigenfunctions are given by the complex exponentials, and the eigenvalues correspond to the channel's frequency response. The eigendecomposition here possesses an intuitive physical interpretation (in terms of the physically meaningful quantity "frequency") and a computationally attractive structure. With LTV channels, on the other hand, the set of eigenfunctions is no longer independent of $\mathbf{H}$, and it provides neither a physical interpretation nor a computationally attractive structure. However, following [MH98, MH03], we will now show that these problems can be resolved in an approximate manner for the class of dispersion-underspread WSSUS channels. (Similar results, not discussed here because of space restrictions, apply to non-WSSUS channels.)

Approximate eigenfunctions

We will first argue that at the output of an underspread WSSUS channel, a transmit signal that is well TF localized is received almost undistorted. Consider an underspread WSSUS channel $\mathbf{H}$ whose mean delay and mean Doppler are zero, i.e., $\bar{\tau} = \bar{\nu} = 0$ (the case of nonzero $\bar{\tau}$ and $\bar{\nu}$ will be discussed later). The transmit signal is constructed as a TF shifted version of a given unit-energy pulse $g(t)$, i.e., $s(t) = g(t - t_0) e^{j2\pi f_0 t}$, where $g(t)$ is well TF localized about time 0 and frequency 0 and t_0 and f_0 are arbitrary (thus, $s(t)$ is well TF localized about time t_0 and frequency f_0). It is then possible to show the approximations (see e.g. [MH98] and Chapter 2)

$$r(t) = (\mathbf{H}s)(t) \approx \langle \mathbf{H}s, s \rangle s(t) \approx L_{\mathbf{H}}(t_0, f_0) s(t) . \tag{1.46}$$

Hence, up to small errors, the effect of an underspread channel on a well TF localized transmit signal is merely a (complex-valued) amplitude scaling, with the scaling factor

being approximately equal to $L_{\mathbf{H}}(t_0, f_0)$, i.e., the value of the TF transfer function at the TF location of the transmit signal. The approximation error $r(t) - L_{\mathbf{H}}(t_0, f_0)\, s(t)$ in (1.46) can be bounded as

$$\begin{aligned} \|r - L_{\mathbf{H}}(t_0, f_0)\, s\| &\leq \|r - \langle \mathbf{H}s, s\rangle\, s\| + \|\langle \mathbf{H}s, s\rangle\, s - L_{\mathbf{H}}(t_0, f_0)\, s\| \\ &= \|r - \langle r, s\rangle\, s\| + \left|\langle \mathbf{H}s, s\rangle - L_{\mathbf{H}}(t_0, f_0)\right|, \end{aligned} \tag{1.47}$$

where we subtracted/added the term $\langle \mathbf{H}s, s\rangle\, s(t)$, applied the triangle inequality, and used $\|s\| = 1$. We will next quantify the two terms in this bound in the mean-square sense.

With regard to the first term, it can be shown that

$$\mathsf{E}\{\|r - \langle r, s\rangle\, s\|^2\} = \int_{-\infty}^{\infty}\int_{-\infty}^{\infty} C_{\mathbf{H}}(\tau, \nu)\left[1 - |A_g(\tau, \nu)|^2\right] d\tau\, d\nu\,, \tag{1.48}$$

with the *ambiguity function* [Fla03, HBB92, Woo53]

$$A_g(\tau, \nu) \triangleq \int_{-\infty}^{\infty} g(t)\, g^*(t - \tau)\, e^{-j2\pi\nu t}\, dt\,.$$

We note that the ambiguity function satisfies

$$|A_g(\tau, \nu)| \leq |A_g(0, 0)| = \|g\|^2 = 1. \tag{1.49}$$

In order for the right-hand side in (1.48) to be small, since both $C_{\mathbf{H}}(\tau, \nu)$ and $1 - |A_g(\tau, \nu)|^2$ are nonnegative, there must be $|A_g(\tau, \nu)|^2 \approx 1$ on the effective support of $C_{\mathbf{H}}(\tau, \nu)$. For a well TF localized pulse $g(t)$, consistent with (1.49), $|A_g(\tau, \nu)|^2$ decreases when moving away from the origin, and thus $|A_g(\tau, \nu)|^2 \approx 1$ only in a small region about the origin. Hence, the above requirement means that $C_{\mathbf{H}}(\tau, \nu) \approx 0$ outside this region. In other words, the effective support of $C_{\mathbf{H}}(\tau, \nu)$ has to be concentrated about the origin, i.e., $\mathbf{H}$ has to be an underspread channel.

This line of reasoning can be made more explicit by using the second-order Taylor series expansion of $|A_g(\tau, \nu)|^2$. To simplify the discussion, we assume $g(t)$ to be real-valued and even-symmetric. We then obtain

$$|A_g(\tau, \nu)|^2 \approx 1 - 2\pi^2\left(B_g^2\tau^2 + D_g^2\nu^2\right). \tag{1.50}$$

Here, we have used the facts that the first-order and mixed second-order terms are zero because of the even symmetry of $|A_g(\tau, \nu)|^2$ (i.e., $|A_g(-\tau, -\nu)|^2 = |A_g(\tau, \nu)|^2$), and that the curvatures of $|A_g(\tau, \nu)|^2$ at the origin are determined by the RMS bandwidth B_g and RMS duration D_g of $g(t)$:

$$\begin{aligned} -\frac{1}{4\pi^2}\frac{\partial^2 |A_g(\tau, \nu)|^2}{\partial \tau^2}\bigg|_{(0,0)} &= B_g^2 \triangleq \int_{-\infty}^{\infty} f^2\, |G(f)|^2\, df, \\ -\frac{1}{4\pi^2}\frac{\partial^2 |A_g(\tau, \nu)|^2}{\partial \nu^2}\bigg|_{(0,0)} &= D_g^2 \triangleq \int_{-\infty}^{\infty} t^2\, |g(t)|^2\, dt\,. \end{aligned}$$

Inserting (1.50) into (1.48) gives

$$\mathsf{E}\{\|r - \langle r, s\rangle\, s\|^2\} \approx 2\pi^2\rho_{\mathbf{H}}^2\left(\sigma_\tau^2 B_g^2 + \sigma_\nu^2 D_g^2\right). \tag{1.51}$$

This expression is minimized by temporally scaling $g(t)$ such that its duration and bandwidth are balanced according to

$$\frac{D_g}{B_g} = \frac{\sigma_\tau}{\sigma_\nu}, \tag{1.52}$$

in which case

$$\mathsf{E}\{\|r - \langle r,s\rangle s\|^2\} \approx 4\pi^2 \rho_{\mathbf{H}}^2 \sigma_{\mathbf{H}} B_g D_g . \tag{1.53}$$

We conclude from this final expression that $r(t) \approx \langle r,s\rangle s(t)$ in the mean-square sense if $g(t)$ is well TF localized (i.e., $B_g D_g$ is small) and $\mathbf{H}$ is underspread (i.e., $\sigma_{\mathbf{H}}$ is small). Hence, under these conditions, $s(t) = g(t-t_0)e^{j2\pi f_0 t}$ is an *approximate eigenfunction* of a WSSUS channel. In contrast to the exact eigenfunctions of $\mathbf{H}$, the approximate eigenfunctions $g(t-t_0)e^{j2\pi f_0 t}$ are highly structured because they are TF translates of a single prototype function $g(t)$; they do not depend on the specific channel realization and their parameters t_0, f_0 have an immediate physical interpretation.

We note that the above results and interpretations remain valid even in the case $\bar{\tau} \neq 0$, $\bar{\nu} \neq 0$, provided that the eigenequation is relaxed as

$$(\mathbf{H}s)(t) = \lambda\, s(t-\bar{\tau})\, e^{j2\pi\bar{\nu}t}.$$

This still preserves the shape of the transmit signal but allows for a time delay and frequency shift.

Next, we consider the second term in the bound (1.47).

Approximate eigenvalues

The final approximation in (1.46), $r(t) = (\mathbf{H}s)(t) \approx L_{\mathbf{H}}(t_0,f_0)\, s(t)$, suggests that $L_{\mathbf{H}}(t_0,f_0)$, i.e., the TF transfer function evaluated at the TF location of $s(t)$, plays the role of an approximate eigenvalue. This extends a similar interpretation of the frequency response of time-invariant channels (see (1.40)).

A qualitative argument corroborating this interpretation is as follows. The above approximation implies $\langle r,s\rangle = \langle \mathbf{H}s,s\rangle \approx L_{\mathbf{H}}(t_0,f_0)$. Using $s(t) = g(t-t_0)e^{j2\pi f_0 t}$, one can show

$$\langle r,s\rangle = \langle \mathbf{H}s,s\rangle = \int_{-\infty}^{\infty}\int_{-\infty}^{\infty} L_{\mathbf{H}}(t,f)\,\Gamma_g^*(t-t_0,f-f_0)\,dt\,df, \tag{1.54}$$

where $\Gamma_g(t,f) \triangleq \int_{-\infty}^{\infty} g(t)\,g^*(t-\tau)\,e^{-j2\pi f\tau}\,d\tau$ is the *Rihaczek distribution* of the function $g(t)$ [Fla99, HBB92]. We note that $\int_{-\infty}^{\infty}\int_{-\infty}^{\infty}\Gamma_g(t,f)\,dt\,df = \|g\|^2 = 1$. Therefore, in order for the weighted integral in (1.54) to be approximately equal to $L_{\mathbf{H}}(t_0,f_0)$, $L_{\mathbf{H}}(t,f)$ has to be effectively constant in a neighborhood of (t_0,f_0) that is determined by the effective support of $\Gamma_g(t-t_0,f-f_0)$. We thus conclude that the approximation $\langle r,s\rangle \approx L_{\mathbf{H}}(t_0,f_0)$ will be better for a smaller support of $\Gamma_g(t-t_0,f-f_0)$ (better TF concentration of $g(t)$) and a smaller rate of variation of $L_{\mathbf{H}}(t,f)$ (smaller dispersion spread of $\mathbf{H}$).

To support this argument by a quantitative result, we consider the second term in the bound (1.47), $\big|\langle r,s\rangle - L_{\mathbf{H}}(t_0,f_0)\big|$, in the mean-square sense. Indeed, the mean-square difference between $\langle r,s\rangle$ and $L_{\mathbf{H}}(t_0,f_0)$ can be shown to equal

$$\mathsf{E}\{|\langle r,s\rangle - L_{\mathbf{H}}(t_0,f_0)|^2\} = \int_{-\infty}^{\infty}\int_{-\infty}^{\infty} C_{\mathbf{H}}(\tau,\nu)\,|1-A_g(\tau,\nu)|^2\,d\tau\,d\nu .$$

This expression is very similar to (1.48), and thus similar conclusions can be made. That is, in order for $\langle r,s\rangle - L_{\mathbf{H}}(t_0,f_0)$ to be small in the mean-square sense, it is necessary that $s(t)$ (and hence $g(t)$) is well TF localized and $\mathbf{H}$ is underspread. Similarly to the previous subsection, a second-order Taylor series expansion of $A_g(\tau,\nu)$ (analogous to (1.50)) can be used to make this conclusion more concrete. Specifically, the approximation $|1 - A_g(\tau,\nu)|^2 \approx 2\pi^2(B_g^2\tau^2 + D_g^2\nu^2)$ entails

$$\mathsf{E}\big\{|\langle r,s\rangle - L_{\mathbf{H}}(t_0,f_0)|^2\big\} \approx 2\pi^2\rho_{\mathbf{H}}^2(\sigma_\tau^2 B_g^2 + \sigma_\nu^2 D_g^2).$$

The interpretation of this latter approximation is analogous to that of (1.51).

Example 1.18 *For the WSSUS channel of Example 1.9, we found* $\sigma_\tau = 10\,\mu$s, $\sigma_\nu = 70.71\,$Hz, *and* $\sigma_{\mathbf{H}} = 7.1\cdot 10^{-4}$. *Consider the Gaussian pulse* $g(t) = \frac{1}{\sqrt{\sqrt{2\pi}D_g}}\exp\big(-(\frac{t}{2D_g})^2\big)$ *with RMS duration* D_g *and RMS bandwidth* $B_g = 1/(4\pi D_g)$. *The rule* (1.52) *requires that* $D_g/B_g = 4\pi D_g^2$ *is equal to* $\sigma_\tau/\sigma_\nu = \sqrt{2}\cdot 10^{-7}$, *which yields*

$$D_g = 106\,\mu\text{s}, \quad B_g = 750\,\text{Hz}.$$

With this choice, the mean-square error (normalized by $\rho_{\mathbf{H}}^2$*) of the approximate eigenrelation* $(\mathbf{H}s)(t) \approx L_{\mathbf{H}}(t_0,f_0)s(t)$ *with* $s(t) = g(t-t_0)e^{j2\pi f_0 t}$ *is on the order of (cf.* (1.53)*)*

$$4\pi^2\sigma_{\mathbf{H}}B_gD_g = 2.2\cdot 10^{-3}.$$

1.5.4 Time-frequency sampling

In many problems like transceiver design and performance evaluation, sampling models for WSSUS channels play an important role. In this section, we consider 2-D uniform sampling of the channel's TF transfer function $L_{\mathbf{H}}(t,f)$. This is particularly important for systems employing OFDM [Bin90], e.g., for OFDM-based channel sounding (see [STC07, dCK$^+$07] and Section 1.7.2). Without loss of generality, we assume $\bar\tau = \bar\nu = 0$ (note that a bulk delay and Doppler shift can be easily split off from $\mathbf{H}$).

Let us consider the representation of a WSSUS channel $\mathbf{H}$ by the samples of $L_{\mathbf{H}}(t,f)$ taken on the uniform rectangular sampling lattice (kT,lF) with $k,l\in\mathbb{Z}$. From the samples $L_{\mathbf{H}}(kT,lF)$, we may attempt to reconstruct $L_{\mathbf{H}}(t,f)$ by means of the following interpolation:

$$\hat L_{\mathbf{H}}(t,f) = \sum_{k=-\infty}^{\infty}\sum_{l=-\infty}^{\infty} L_{\mathbf{H}}(kT,lF)\,\mathrm{sinc}\Big(\frac{\pi}{T}(t-kT)\Big)\,\mathrm{sinc}\Big(\frac{\pi}{F}(f-lF)\Big). \tag{1.55}$$

This interpolation is consistent with the samples in that $\hat L_{\mathbf{H}}(kT,lF) = L_{\mathbf{H}}(kT,lF)$. In order to have perfect reconstruction, i.e., $\hat L_{\mathbf{H}}(t,f) = L_{\mathbf{H}}(t,f)$ for all t,f in the mean-square sense, the channel's scattering function $C_{\mathbf{H}}(\tau,\nu)$ must have a compact support contained within the rectangular area $[-\tau_{\max},\tau_{\max}]\times[-\nu_{\max},\nu_{\max}]$ with $\tau_{\max}\le 1/(2F)$ and $\nu_{\max}\le 1/(2T)$. (Using different sampling lattices and reconstruction kernels, it may

be possible to slightly relax these conditions.) Note that for decreasing dispersion spread $d_{\mathbf{H}} = 4\tau_{\max}\nu_{\max}$, the number of required transfer function samples per second per Hertz decreases.

If the above conditions are not satisfied (i.e., if the sampling lattice is too coarse or if the scattering function does not have compact support), the reconstructed TF transfer function $\hat{L}_{\mathbf{H}}(t,f)$ will differ from $L_{\mathbf{H}}(t,f)$ due to aliasing. However, it can be shown that the normalized mean-square reconstruction error is bounded as

$$\frac{1}{\rho_{\mathbf{H}}^2}\mathsf{E}\left\{\left|\hat{L}_{\mathbf{H}}(t,f)-L_{\mathbf{H}}(t,f)\right|^2\right\} \leq 2\left(\sigma_\tau^2 F^2+\sigma_\nu^2 T^2\right).$$

Even though this bound is sometimes rather loose, it yields some useful insights. First, it shows that the mean-square reconstruction error will be small if σ_τ and σ_ν are small relative to the reciprocals $1/F$ and $1/T$ of the sampling periods F and T, respectively, i.e., if the channel is underspread. Second, the bound is minimized by choosing the sampling lattice such that

$$\frac{T}{F}=\frac{\sigma_\tau}{\sigma_\nu}. \tag{1.56}$$

In this case, we obtain

$$\frac{1}{\rho_{\mathbf{H}}^2}\mathsf{E}\left\{\left|\hat{L}_{\mathbf{H}}(t,f)-L_{\mathbf{H}}(t,f)\right|^2\right\} \leq 4TF\sigma_{\mathbf{H}}, \tag{1.57}$$

which shows that good reconstruction is guaranteed for underspread channels (small $\sigma_{\mathbf{H}}$) and sufficiently dense sampling (small TF). Note, in particular, that $4TF\sigma_{\mathbf{H}} \ll 1$ or equivalently $4TF \ll 1/\sigma_{\mathbf{H}}$ ensures small aliasing errors: together with (1.56), $4TF \ll 1/\sigma_{\mathbf{H}}$ implies $2T \ll 1/\sigma_\nu$ and $2F \ll 1/\sigma_\tau$.

Example 1.19 *The example WSSUS channel considered previously has an exponential delay profile with* $\sigma_\tau = \tau_0 = 10\,\mu\text{s}$ *and a Jakes Doppler profile with* $\sigma_\nu = 70.71\,\text{Hz}$ *(*$\nu_{\max} = 100\,\text{Hz}$*), and thus a dispersion spread of* $\sigma_{\mathbf{H}} = 7.1\cdot 10^{-4}$*. For this channel, temporal aliasing is avoided if* $T \leq 1/(2\nu_{\max}) = 5\,\text{ms}$*. Let us choose* $T = 0.5\,\text{ms}$*. The optimum choice of* F *according to* (1.56) *is then* $F = 3.5\,\text{kHz}$*. With these parameters, our upper bound on the normalized mean-square reconstruction error in* (1.57) *is obtained as* $4TF\sigma_{\mathbf{H}} = 5\cdot 10^{-3}$.

1.5.5 Approximate Karhunen-Loève expansion

Non-WSSUS channels are complicated objects because they exhibit two kinds of TF variation:

1. their transfer characteristics, characterized by $L_{\mathbf{H}}(t,f)$, depend on time and frequency;
2. their second-order statistics, described by $\mathscr{C}_{\mathbf{H}}(t,f;\tau,\nu)$, are TF-dependent as well.

However, we have seen in Section 1.5.2 that for correlation-underspread channels, the rate of TF variation of $\mathscr{C}_{\mathbf{H}}(t,f;\tau,\nu)$ is much smaller than that of $L_{\mathbf{H}}(t,f)$.

To simplify the characterization of a non-WSSUS channel $\mathbf{H}$, it is desirable to decouple the channel's transfer characteristics (TF selectivity) and the channel's randomness. A canonical way of doing this is provided by the *Karhunen-Loève expansion* [Ken69, Tre92, CV74]

$$\mathbf{H} = \sum_k \eta_k \mathbf{G}_k \,. \tag{1.58}$$

Here, the $\mathbf{G}_k$ are "atomic" LTV channels that are deterministic and *orthonormal* in the sense that $\langle \mathbf{G}_k, \mathbf{G}_l \rangle \triangleq \int_{-\infty}^{\infty}\int_{-\infty}^{\infty} k_{\mathbf{G}_k}(t,t') k^*_{\mathbf{G}_l}(t,t')\, dt\, dt' = \delta_{kl}$, and the η_k are random coefficients that are *uncorrelated*. The uncorrelatedness of the η_k is due to an appropriate choice of the $\mathbf{G}_k$. Assuming $\mathbf{H}$ to be zero-mean for simplicity, the η_k are zero-mean as well and thus their uncorrelatedness is equivalent to statistical orthogonality, i.e., $\mathsf{E}\{\eta_k \eta_l^*\} = 0$ for $k \neq l$.

In spite of this remarkable double-orthogonality property (deterministic orthogonality of the $\mathbf{G}_k$ and statistical orthogonality of the η_k), the Karhunen-Loève expansion is difficult to use in practice since the atomic channels $\mathbf{G}_k$ are generally unstructured, not localized with respect to time and frequency or delay and Doppler, and dependent on the channel's second-order statistics. An important exception is given by WSSUS channels. For these, a continuous version of (1.58) reads

$$\mathbf{H} = \int_{-\infty}^{\infty}\int_{-\infty}^{\infty} S_{\mathbf{H}}(\tau,\nu)\, \mathbf{S}_{\tau,\nu}\, d\tau d\nu \,,$$

where $\mathbf{S}_{\tau,\nu}$ denotes the *TF shift operators* defined by $(\mathbf{S}_{\tau,\nu} s)(t) = s(t-\tau)\, e^{j2\pi\nu t}$. Here, the delay-Doppler integration variable (τ,ν) replaces the summation index k, the TF shift operators $\mathbf{S}_{\tau,\nu}$ play the role of the atomic channels $\mathbf{G}_k$, and the spreading function $S_{\mathbf{H}}(\tau,\nu)$ takes the place of the coefficients η_k. The atomic channels $\mathbf{S}_{\tau,\nu}$ are orthogonal and the coefficients $S_{\mathbf{H}}(\tau,\nu)$ are uncorrelated (because the spreading function of a WSSUS channel is white). In addition, the $\mathbf{S}_{\tau,\nu}$ are structured, physically meaningful, and perfectly localized with respect to delay and Doppler, and they do not depend on the channel's second-order channel statistics.

We will now develop an *approximate* Karhunen-Loève expansion for the broad class of correlation-underspread non-WSSUS channels. This expansion uses highly structured atomic channels that are well localized *both* in time and frequency and in delay and Doppler. Consider a deterministic underspread prototype channel $\mathbf{G}$ that is normalized such that $\|\mathbf{G}\|^2 = \int_{-\infty}^{\infty}\int_{-\infty}^{\infty} |k_{\mathbf{G}}(t,t')|^2\, dt\, dt' = 1$, and whose TF transfer function $L_{\mathbf{G}}(t,f)$ is localized about the origin and smooth so that also the spreading function $S_{\mathbf{G}}(\tau,\nu)$ is concentrated about the origin. This channel acts like a filter that passes only signal components localized about the origin of the TF plane. Based on $\mathbf{G}$, we define

$$\mathbf{G}^{\tau,\nu}_{t,f} \triangleq \mathbf{S}_{t,f+\nu}\, \mathbf{G}\, \mathbf{S}^{+}_{t-\tau,f} \,, \tag{1.59}$$

which is a continuously parameterized set of deterministic underspread channels that pick up transmit signal components localized about the TF point $(t-\tau, f)$ and shift them to the TF point $(t, f+\nu)$. That is, $\mathbf{G}^{\tau,\nu}_{t,f}$ performs a TF shift by the delay-Doppler pair (τ,ν) on signals localized about the TF point (t,f) and suppresses all other signals (see Fig. 1.9 for an illustration). However, rather than the continuous parameterization in

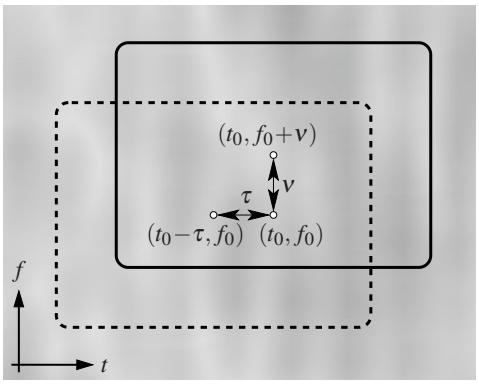

Figure 1.9 Action of the atomic channel $\mathbf{G}_{t_0,f_0}^{\tau,\nu}$: signal energy is picked up in the region centered about $(t_0-\tau, f_0)$ (dashed line) and shifted by (τ,ν) to the region centered about $(t_0, f_0+\nu)$ (solid line).

(1.59), our approximate Karhunen-Loève expansion uses the discrete parameterization $\tilde{\mathbf{G}}_{k,l}^{m,d} \triangleq \mathbf{G}_{kT_0,lF_0}^{m\tau_0,d\nu_0}$, where T_0, F_0, τ_0, and ν_0 are sampling periods chosen such that $\{\tilde{\mathbf{G}}_{k,l}^{m,d}\}$ is a *frame* [Grö01] for the space of square-integrable channels (this presupposes, in particular, that $T_0F_0\tau_0\nu_0 \leq 1$).

With these assumptions, any square-integrable channel $\mathbf{H}$ (i.e., $\|\mathbf{H}\| < \infty$) can be decomposed as

$$\mathbf{H} = \sum_k \sum_l \sum_m \sum_d \eta_{k,l}^{m,d}\, \tilde{\mathbf{G}}_{k,l}^{m,d}\,. \tag{1.60}$$

Here, the coefficients are given by $\eta_{k,l}^{m,d} = \langle \mathbf{H}, \mathbf{\Gamma}_{k,l}^{m,d} \rangle$, with $\mathbf{\Gamma}$ denoting a prototype channel that is *dual* to $\mathbf{G}$ [Grö01]. The expansion (1.60) constitutes a *Gabor expansion* [Grö01] of the channel $\mathbf{H}$. It is formally similar to the Karhunen-Loève expansion (1.58) but uses a different parameterization and a set of channels with a strong mathematical structure and an intuitive interpretation. Note that (1.60) indeed decouples the transfer characteristics and randomness of the channel $\mathbf{H}$: the atomic channels $\tilde{\mathbf{G}}_{k,l}^{m,d}$ are deterministic and capture the TF selectivity/dispersiveness of $\mathbf{H}$, whereas the coefficients $\eta_{k,l}^{m,d}$ are random and capture the (nonstationary) channel statistics.

In order for (1.60) to constitute an approximate Karhunen-Loève expansion, the coefficients $\eta_{k,l}^{m,d}$ need to be effectively uncorrelated. Indeed, it can be shown that if $\mathbf{H}$ is correlation-underspread and if $\mathbf{G}$ and T_0, F_0, τ_0, ν_0 are suitably chosen, then

$$\mathrm{E}\left\{ \eta_{k,l}^{m,d} \left(\eta_{k',l'}^{m',d'} \right)^* \right\} \approx \mathscr{C}_{\mathbf{H}}(kT_0, lF_0; m\tau_0, d\nu_0)\, \delta_{kk'}\, \delta_{ll'}\, \delta_{mm'}\, \delta_{dd'}\,.$$

This also reveals that the mean power of $\eta_{k,l}^{m,d}$ is approximately equal to the LSF evaluated at $t = kT_0$, $f = lF_0$, $\tau = m\tau_0$, and $\nu = d\nu_0$.

A bound showing that the coefficients $\eta_{k,l}^{m,d}$ are approximately uncorrelated for correlation-underspread channels is provided in [Mat05]. Here, we only consider the approxi-

mation $\mathsf{E}\{|\eta_{k,l}^{m,d}|^2\} \approx \mathscr{C}_{\mathbf{H}}(kT_0, lF_0; m\tau_0, d\nu_0)$, whose error can be bounded as

$$\begin{aligned}&\left|\mathsf{E}\{|\eta_{k,l}^{m,d}|^2\} - \mathscr{C}_{\mathbf{H}}(kT_0, lF_0; m\tau_0, d\nu_0)\right| \\ &\leq \int_{-\infty}^{\infty}\int_{-\infty}^{\infty}\int_{-\infty}^{\infty}\int_{-\infty}^{\infty} \left|\mathscr{R}_{\mathbf{H}}(\Delta t, \Delta f; \Delta\tau, \Delta\nu)\right| \left|1 - \mathscr{R}_{\mathbf{\Gamma}}(\Delta t, \Delta f; \Delta\tau, \Delta\nu)\right| d\Delta t\, d\Delta f\, d\Delta\tau\, d\Delta\nu\,.\end{aligned}$$

For this bound to be small, we require $\mathscr{R}_{\mathbf{\Gamma}}(\Delta t, \Delta f; \Delta\tau, \Delta\nu) \approx 1$ on the effective support of the channel's CCF $\mathscr{R}_{\mathbf{H}}(\Delta t, \Delta f; \Delta\tau, \Delta\nu)$. Since $\mathscr{R}_{\mathbf{\Gamma}}(\Delta t, \Delta f; \Delta\tau, \Delta\nu) \leq \mathscr{R}_{\mathbf{\Gamma}}(0,0;0,0) = 1$ and $\mathscr{R}_{\mathbf{\Gamma}}(\Delta t, \Delta f; \Delta\tau, \Delta\nu)$ tends to decrease when moving away from the origin, this requirement can only be satisfied if the effective support of $\mathscr{R}_{\mathbf{H}}(\Delta t, \Delta f; \Delta\tau, \Delta\nu)$ is small, i.e., if the channel $\mathbf{H}$ is correlation-underspread. This argument is largely analogous to the one we provided in the context of (1.48), and it can be made more precise in a similar manner, i.e., by means of a second-order Taylor expansion of $\mathscr{R}_{\mathbf{\Gamma}}(\Delta t, \Delta f; \Delta\tau, \Delta\nu)$.

We conclude that (1.60) provides a decomposition of correlation-underspread channels into simple, well-structured deterministic channels; these channels are weighted by effectively uncorrelated random coefficients whose mean power is approximately given by samples of the LSF.

1.6 Parsimonious channel models

The complete mathematical description of LTV channels is rather complex. Characterizing T seconds of a transmission—i.e., how T seconds of the receive signal depend on T seconds of the transmit signal—requires a $T \times T$ section of the channel's kernel $k_{\mathbf{H}}(t, t')$ (see (1.14)). Thus, the complexity of characterization grows quadratically with the duration of transmission. Fortunately, most practical channels feature some additional structure, such as the underspread property described in the previous section, which simplifies the description in the sense that a smaller number of parameters are sufficient to model the channel's behavior. Several such parsimonious (low-dimensional, low-rank) representations of LTV channels have been proposed and found to be useful in many applications like channel estimation and equalization (see Chapters 4–8).

For simplicity, we will discuss parsimonious channel representations in a discrete-time setting where the channel's input-output relation reads

$$r[n] = \sum_{m=0}^{M-1} h[n,m]\, s[n-m]\,. \tag{1.61}$$

Here, $s[n]$, $r[n]$, and $h[n,m]$ are sampled versions of, respectively, $s(t)$, $r(t)$, and $h(t,\tau)$ in (1.13) (the sampling frequency $f_{\mathrm{s}} = 1/T_{\mathrm{s}}$ is assumed to be larger than $B + \nu_{\max}$, where B is the transmit bandwidth); furthermore, $M = \lceil \tau_{\max}/T_{\mathrm{s}} \rceil$ is the number of discrete channel taps, i.e., the maximum discrete-time delay.

1.6.1 Basis expansion models

A popular class of low-rank channel models uses an expansion with respect to time n of each tap of the channel impulse response $h[n,m]$ into a basis $\{u_i[n]\}_{i=0,\ldots,I-1}$ [TG96, GT98], i.e.,

$$h[n,m] = \sum_{i=0}^{I-1} c_i[m]\, u_i[n]\,. \tag{1.62}$$

This *basis expansion model* (BEM) is motivated by the observation that the temporal (n) variation of $h[n,m]$ is usually rather smooth due to the channel's limited Doppler spread, and hence $\{u_i[n]\}_{i=0,\ldots,I-1}$ can be chosen as a small set of smooth functions. In most cases, the BEM (1.62) is considered only within a finite interval, hereafter assumed to be $[0,N-1]$ without loss of generality. The ith coefficient for the mth tap in (1.62) is given by

$$c_i[m] = \langle h[\,\cdot\,,m], \tilde{u}_i\rangle = \sum_{n=0}^{N-1} h[n,m]\, \tilde{u}_i^*[n]\,,$$

where $\{\tilde{u}_i[n]\}_{i=0,\ldots,I-1}$ is the bi-orthogonal basis for the span of $\{u_i[n]\}_{i=0,\ldots,I-1}$ (i.e., $\langle u_i, \tilde{u}_{i'}\rangle = \delta_{ii'}$ for all i,i'). In particular, choosing complex exponentials and polynomials for the $u_i[n]$ results in Fourier and Taylor series, respectively. These two BEMs were essentially proposed already in [Bel63]. The usefulness of (1.62) is due to the fact that the complexity of characterizing $h[n,m]$ on the interval $[0,N-1]$ is reduced from N^2 to $MI \ll N^2$ numbers. However, it is important to note that in most practical cases, an extension of the time interval will require a proportional increase in the BEM model order (i.e., $I \propto N$).

Inserting the basis expansion (1.62) into (1.61) results in

$$r[n] = \sum_{m=0}^{M-1}\sum_{i=0}^{I-1} c_i[m]\, u_i[n]\, s[n-m] = \sum_{i=0}^{I-1} u_i[n] \underbrace{\sum_{m=0}^{M-1} c_i[m]\, s[n-m]}_{\tilde{r}_i[n]}\,.$$

Hence, the channel can be viewed as a bank of I time-invariant filters (convolutions) with impulse responses $c_i[m]$ whose outputs $\tilde{r}_i[n]$ are multiplied by the basis functions $u_i[n]$ and added. This parallel connection of "convolution-multiplication" branches is depicted in Fig. 1.10.

By taking length-N discrete Fourier transforms (DFT) of (1.62) with respect to m or n, we obtain the following expressions for the discrete time-varying transfer function (cf. (1.16)) and the discrete spreading function (cf. (1.15)):

$$L_{\mathbf{H}}[n,l] \triangleq \sum_{m=0}^{N-1} h[n,m]\, e^{-j2\pi\frac{lm}{N}} = \sum_{i=0}^{I-1} C_i[l]\, u_i[n]\,, \tag{1.63}$$

$$S_{\mathbf{H}}[m,d] \triangleq \sum_{n=0}^{N-1} h[n,m]\, e^{-j2\pi\frac{dn}{N}} = \sum_{i=0}^{I-1} c_i[m]\, U_i[d]\,. \tag{1.64}$$

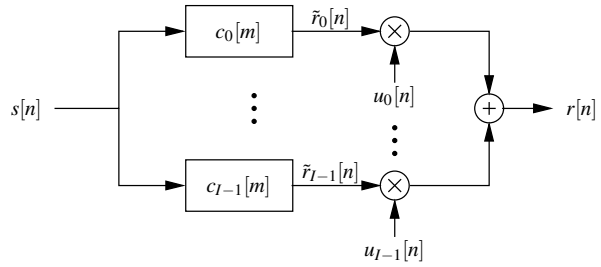

Figure 1.10 BEM-induced block diagram of an LTV channel.

Here, l and d denote discrete frequency and discrete Doppler, respectively, and $C_i[l]$ and $U_i[d]$ denote the DFT of $c_i[m]$ and $u_i[n]$, respectively. Since the spreading function of practical wireless channels is concentrated about the origin, (1.64) suggests that the functions $U_i[d]$ have to be concentrated about the origin as well and, hence, that the basis functions $u_i[n]$ have to be smooth.

The expressions (1.62), (1.63), and (1.64) imply that the $N \times N$ matrices $\mathbf{H}$, $\mathbf{L}$, and $\mathbf{S}$ with respective elements $[\mathbf{H}]_{n+1,m+1} = h[n,m]$, $[\mathbf{L}]_{n+1,l+1} = L_{\mathbf{H}}[n,l]$, and $[\mathbf{S}]_{m+1,d+1} = S_{\mathbf{H}}[m,d]$ are sums of I dyadic products and hence their rank is (at most) I. For a given channel matrix, the best low-rank approximation is given by the dominant modes of the singular value decomposition (SVD) of that matrix. Unfortunately, the singular vectors depend explicitly on the channel realization and lack a computationally convenient structure. BEMs can thus be viewed as low-rank approximations of the channel's SVD using a fixed and nicely structured set of functions.

Complex exponential (Fourier) basis

The BEM most often employed in practice uses a basis of complex exponentials [TG96, GT98]. This can be motivated by considering the inverse DFT of (1.64), i.e.,

$$h[n,m] = \frac{1}{N} \sum_{d=0}^{N-1} S_{\mathbf{H}}[m,d]\, e^{j2\pi \frac{nd}{N}}.$$

Assuming $S_{\mathbf{H}}[m,d] = 0$ for $|d| > D$, with D denoting the maximum discrete Doppler shift, results in the so-called (critically sampled) *complex exponential* (CE) BEM. Here, the model order equals $I = 2D+1$ and the basis functions and coefficients are given by $u_i[n] = e^{j2\pi \frac{(i-D)n}{N}}$ and $c_i[m] = \frac{1}{N} S_{\mathbf{H}}[m, i-D]$, respectively. Unfortunately, the assumption of a maximum discrete Doppler shift is poorly justified even if the underlying continuous channel has a compactly supported spreading function. This is because the multiplicative temporal windowing (i.e., time-limitation to the interval $[0, N-1]$) leading to (1.64) corresponds to a convolution in the Doppler domain. This causes Doppler leakage and thus requires a rather large D to achieve satisfactory modeling accuracy. An alternative interpretation is obtained by noting that the uniformly spaced discrete Doppler frequencies d/N (i.e., Doppler resolution $1/N$) usually do not coincide with the actual Doppler

frequencies of the continuous channel. In the time (n) domain, this problem manifests itself as a Gibbs (or ringing) phenomenon, which degrades the quality of the CE-BEM especially near the interval boundaries.

To mitigate this Doppler resolution/Gibbs phenomenon problem, oversampling has been proposed [TV00]. The basis functions are here given by $\left\{u_i[n] = e^{j2\pi\frac{(i-qD)n}{qN}}\right\}_{i=0,\ldots,I-1}$ where $I = 2qD+1$, with oversampling factor $q \in \mathbb{N}$. An even more general BEM based on complex exponentials reads

$$h[n,m] = \sum_{i=0}^{I-1} c_i[m]\, e^{j2\pi\xi_i n}, \tag{1.65}$$

where $\{\xi_i\}_{i=0,\ldots,I-1}$, with $\xi_i \in [-1/2, 1/2)$, is an arbitrary set of normalized Doppler frequencies. The critically sampled case and the oversampled case with uniform Doppler spacing are reobtained for $\xi_i = (i-D)/N$ and $\xi_i = (i-qD)/(qN)$, respectively. A BEM with nonuniform Doppler spacing is potentially able to achieve better modeling accuracy, provided that the "active" Doppler frequencies ξ_i are appropriately determined. Another modification of the CE-BEM that improves modeling accuracy uses windowing techniques [Leu04, Sch04].

Polynomial basis

Polynomial BEMs correspond to a Taylor series expansion [BH99, TGYL05]. More specifically, the continuous-time channel impulse response $h(t,\tau)$ can be approximated about any time instant t_0 as

$$h(t_0+t,\tau) \approx \sum_{i=0}^{I-1} c_i(t_0,\tau)\, t^i, \quad \text{with } c_i(t_0,\tau) = \frac{1}{i!}\frac{\partial^i h(t,\tau)}{\partial t^i}\bigg|_{t=t_0}.$$

For underspread channels that evolve smoothly with time, the magnitude of the Taylor series coefficients $c_i(t_0,\tau)$ quickly decreases for increasing i, so that a small order I is typically sufficient to approximate the channel within a short time (t) interval. The discrete-time (sampled) version of the polynomial basis expansion model on the interval $[0, N-1]$, using $t_0 = 0$, is then given by

$$h[n,m] = \sum_{i=0}^{I-1} c_i[m]\,(\tfrac{n}{N})^i, \tag{1.66}$$

where $c_i[m] = c_i(0, mT_s)\,(NT_s)^i$.

An alternative to the monomials t^i underlying (1.66) is given by Legendre polynomials. Here, $u_i[n] = P_i\big(\frac{2n}{N} - 1\big)$, where $P_i(t)$ is the continuous-time Legendre polynomial of degree i defined as [AS65]

$$P_i(t) = \frac{1}{2^i i!}\frac{d^i}{dt^i}(t^2-1)^i.$$

Even though all polynomial BEMs with identical model order I are mathematically equivalent in the sense that their basis functions span the same subspace, Legendre polynomials

are numerically more stable than monomials. In particular, they have the advantage of being orthogonal on the interval $(-1,1)$.

Because for a given model order I, polynomials tend to vary less with time than complex exponentials, a polynomial BEM is advantageous over a CE-BEM for low Doppler spreads.

Slepian basis

An approach to combating the Doppler leakage occurring in the CE-BEM, see [ZM05] and Chapter 8, is to replace the complex exponential basis functions by truncated versions of discrete prolate spheroidal sequences (DPSSs) [Sle78]. DPSSs are functions that are band-limited as well as maximally time-concentrated in the sense of having minimum energy outside a prescribed time interval $[0,N-1]$. For a given temporal blocklength N and a given maximum normalized Doppler frequency $\xi_{\max}$, they are the solutions $u_i[n]$ to the eigenvalue problem

$$\sum_{n'=0}^{N-1} \frac{\sin(2\pi\xi_{\max}(n-n'))}{\pi(n-n')}\, u_i[n'] \;=\; \lambda_i\, u_i[n]\,, \qquad n\in\mathbb{Z}\,.$$

The DPSSs $u_i[n]$ form an orthogonal basis on $[0,N-1]$ and an orthonormal basis on $\mathbb{Z}$. The eigenvalues λ_i indicate the percentage of energy of $u_i[n]$ within the interval $[0,N-1]$. In fact, for a BEM, only the samples in the interval $[0,N-1]$ are used; these finite-length sequences have been termed *Slepian sequences*. Although originally proposed in [ZM05] for the (flat fading) channel coefficients of individual OFDM subcarriers, the same idea is applicable in the time-delay domain on a per-tap basis in the sense of (1.62). Slepian sequences usually yield a better modeling accuracy than complex exponential sequences, provided the maximum Doppler frequency $\xi_{\max}$ is known with sufficient accuracy. Interestingly, as $\xi_{\max}$ approaches 0, the Slepian sequences asymptotically coincide with the Legendre polynomials.

1.6.2 Parsimonious WSSUS models

Parsimonious models for the second-order channel statistics are of practical interest, even though in the WSSUS case the statistics do not change with time. Applications of such models include linear minimum mean-square error methods for channel estimation (see Chapters 4, 5, and 7) and channel simulation.

AR, MA, and ARMA models

A flexible statistical channel model is the *autoregressive moving average* (ARMA) model [TG97, BB01, SMH01]. For a (discrete-time) WSSUS channel, the channel taps $h[n,m]$ are stationary processes with respect to time n and uncorrelated for different delays m. An

ARMA model with respect to n is then defined separately for each tap (m):

$$h[n,m] \;=\; -\sum_{\Delta n=1}^{N_{\mathrm{AR}}} a_m[\Delta n]\,h[n-\Delta n,m] \;+\; \sum_{\Delta n=0}^{N_{\mathrm{MA}}-1} b_m[\Delta n]\,e_m[n-\Delta n]\,, \qquad m=0,\ldots,M-1\,. \tag{1.67}$$

Here, the $e_m[n]$ are normalized, stationary, and white innovations processes that are mutually independent for different m, N_{AR} and N_{MA} denote the AR and MA model orders, respectively, and $\{a_m[\Delta n]\}_{\Delta n=1,\ldots,N_{\mathrm{AR}}}$ and $\{b_m[\Delta n]\}_{\Delta n=0,\ldots,N_{\mathrm{MA}}-1}$ are the (deterministic, time-invariant) parameters of the AR and MA part, respectively. For simplicity, we here assume identical ARMA model orders for all channel taps; the extension to m-dependent orders is straightforward.

The power spectral densities of the stationary tap processes constitute the scattering function according to

$$C_{\mathbf{H}}(m,\xi) = \left|\frac{B_m(\xi)}{A_m(\xi)}\right|^2. \tag{1.68}$$

Here, ξ is the normalized Doppler frequency and

$$A_m(\xi) \;\triangleq\; \sum_{\Delta n=0}^{N_{\mathrm{AR}}} a_m[\Delta n]\,e^{-j2\pi\xi\Delta n}, \qquad B_m(\xi) \;\triangleq\; \sum_{\Delta n=0}^{N_{\mathrm{MA}}-1} b_m[\Delta n]\,e^{-j2\pi\xi\Delta n},$$

with the convention that $a_m[0] \triangleq 1$. Hence, the second-order channel statistics are characterized by $M(N_{\mathrm{AR}}+N_{\mathrm{MA}})$ complex parameters. The *autoregressive* (AR) and *moving average* (MA) channel models are obtained as special cases of (1.67) for $N_{\mathrm{MA}}=1$ and $N_{\mathrm{AR}}=0$, respectively.

There is a rich literature on the properties of ARMA models and on methods for estimating the ARMA parameters $\{a_m[\Delta n], b_m[\Delta n]\}$ and model orders N_{AR}, N_{MA} [Kay88, SM97]. These results can be applied to ARMA channel models. However, a difficulty relates to the extremely small effective bandwidth (i.e., maximum normalized Doppler frequency $\xi_{\max}$) of the channel tap processes, which is due to the fact that the sampling frequency f_{s} is typically orders of magnitude larger than physical Doppler frequencies. Consider for example a mobile broadband transmission with terminal velocity 30 m/s (108 km/h), carrier frequency $f_{\mathrm{c}} = 5$ GHz, and bandwidth $B = 20$ MHz. The maximum Doppler frequency is obtained as $\nu_{\max} = 500$ Hz and, for critical sampling ($f_{\mathrm{s}} = B+\nu_{\max}$), the maximum normalized Doppler frequency is $\xi_{\max} = \nu_{\max}/f_{\mathrm{s}} = 2.5\cdot 10^{-4}$. This means that the tap processes are extremely narrowband, a fact causing difficulties with conventional ARMA design methods. This problem was tackled in [SMH01] via a multirate approach: a "subsampled" ARMA model designed for an intermediate sampling frequency that is close to the maximum Doppler frequency is followed by an optimum multistage interpolator in order to match the actual system sampling frequency.

Example 1.20 *A* first-order Gauss-Markov model *is often used for theoretical considerations and for Monte-Carlo simulations. This is a pure AR channel model with model order* $N_{\mathrm{AR}}=1$*, i.e.,*

$$h[n,m] \;=\; -a_m[1]\,h[n-1,m] + b_m[0]\,e_m[n]\,,$$

where $|a_m[1]| < 1$. *Setting* $a_m[1] = A_m e^{j\varphi_m}$ *with* $0 \le A_m < 1$ *and using* (1.68)*, we obtain for the scattering function*

$$C_{\mathbf{H}}(m,\xi) = \frac{|b_m[0]|^2}{|1+a_m[1]\,e^{-j2\pi\xi}|^2} = \frac{|b_m[0]|^2}{1+A_m^2+2A_m\cos(2\pi\xi-\varphi_m)}\,.$$

It is seen that $C_{\mathbf{H}}(m,\xi)$ *has peaks at the normalized Doppler frequencies* $\xi = \frac{\varphi_m}{2\pi} \pm \frac{1}{2}$. *These peaks are more pronounced when* A_m *is closer to 1.*

Other parametric WSSUS models

Besides ARMA models, there are several other parametric models for the second-order statistics of a WSSUS channel. A simple and frequently used model, previously considered in Example 1.9, is given by the following (continuous-time) scattering function that has a separable structure with exponential delay power profile and Jakes Doppler power profile [Pro95, Mol05]:

$$C_{\mathbf{H}}(\tau,\nu) = \begin{cases} \frac{\rho_{\mathbf{H}}^2}{\pi\tau_0}\, e^{-\tau/\tau_0}\, \frac{1}{\sqrt{\nu_{\max}^2-\nu^2}}\,, & |\nu| < \nu_{\max} \\ 0\,, & |\nu| > \nu_{\max}\,. \end{cases}$$

This model involves only three parameters: the path gain $\rho_{\mathbf{H}}^2$, the RMS delay spread $\sigma_\tau = \tau_0$, and the maximum Doppler $\nu_{\max}$. The Jakes Doppler profile results from the assumption of a uniform distribution of the azimuth (i.e., the AoA in the horizontal plane).

A very simple WSSUS channel model is given by the brick-shaped scattering function

$$C_{\mathbf{H}}(\tau,\nu) = \begin{cases} \frac{\rho_{\mathbf{H}}^2}{2\tau_{\max}\nu_{\max}}\,, & (\tau,\nu) \in [0,\tau_{\max}] \times [-\nu_{\max},\nu_{\max}] \\ 0\,, & \text{else}\,. \end{cases}$$

This model results in uniform delay and Doppler profiles. There are again three parameters: path gain $\rho_{\mathbf{H}}^2$, maximum delay $\tau_{\max}$, and maximum Doppler $\nu_{\max}$. A brick-shaped scattering function is convenient for theoretical calculations, and it often corresponds to the worst-case statistics for given $\tau_{\max}$ and $\nu_{\max}$ (see [LCS98] and Chapter 2, Section 2.3.4.4). We note that a uniform Doppler profile is obtained by assuming a jointly uniform distribution of azimuth and elevation (i.e., uniform AoA in all three dimensions) [Mol05].

1.6.3 Parsimonious non-WSSUS models

Due to their explicit dependence on time and frequency, the statistics of non-WSSUS channels are more difficult to characterize than those of WSSUS channels. In particular, the LSF and related statistical descriptions of non-WSSUS channels (see Section 1.4.3) are 4-D functions. However, the channel statistics change at a much lower rate than the channel itself. This fact can be exploited by parsimonious parametric models for non-WSSUS channels.

Non-WSSUS ARMA models

The ARMA channel model (1.67) can be extended to non-WSSUS channels. In order to obtain correlated and nonstationary tap processes, we consider the following joint vector ARMA model with time-varying ARMA parameter matrices:

$$\mathbf{h}[n] = -\sum_{\Delta n=1}^{N_{\mathrm{AR}}} \mathbf{A}[n,\Delta n]\,\mathbf{h}[n-\Delta n] + \sum_{\Delta n=0}^{N_{\mathrm{MA}}-1} \mathbf{B}[n,\Delta n]\,\mathbf{e}[n-\Delta n]\,. \tag{1.69}$$

Here, the vector $\mathbf{h}[n] \triangleq (h[n,0]\cdots h[n,M-1])^T$ contains the M channel taps at time n, $\mathbf{e}[n] \triangleq (e_0[n]\cdots e_{M-1}[n])^T$ is an innovations vector, and $\mathbf{A}[n,\Delta n]$ and $\mathbf{B}[n,\Delta n]$ denote the time-varying AR and MA parameter matrices, respectively. As before, the innovations processes $e_m[n]$ are normalized, stationary, and white as well as mutually independent for different m. A pure AR version of this model was previously considered in [JM05]. For (temporally) stationary channels, whose taps are still allowed to be correlated, the AR and MA parameter matrices do not depend on time n. This case was previously considered in [TGZ96]. If the tap processes are nonstationary but mutually uncorrelated, the AR and MA parameter matrices become diagonal.

In the general case, (1.69) involves $\mathcal{O}(N(N_{\mathrm{AR}}+N_{\mathrm{MA}})M^2)$ scalar parameters for a block of duration N. This is not really parsimonious, although more parsimonious than a general innovations representation, which would require $\mathcal{O}(N^2M^2)$ scalar parameters. To reduce the description complexity of (1.69), we can expand the ARMA parameter matrices into a low-dimensional basis, similarly to the BEM considered in Section 1.6.1 for the channel itself. Furthermore, exploiting the fact that only closely spaced channel taps are significantly correlated, we can impose a band structure on the ARMA parameter matrices. These two measures reduce the number of scalar parameters to $\mathcal{O}(I(N_{\mathrm{AR}}+N_{\mathrm{MA}})MD)$, where I and D denote the number of basis functions and the number of nonzero diagonals, respectively. We note that nonstationary vector AR processes and corresponding parameter and order estimation methods are discussed in more detail in [JMH09].

BEM statistics

Another parsimonious description of the channel statistics can be based on a channel BEM as given by (1.62). Since the basis $\{u_i[n]\}$ is deterministic, only the statistics of the MI BEM coefficients $c_i[m]$ need to be characterized. From (1.62), we obtain

$$\mathsf{E}\{h[n,m]h^*[n',m']\} = \sum_{i=0}^{I-1}\sum_{i'=0}^{I-1} \mathsf{E}\{c_i[m]c_{i'}^*[m']\}\,u_i[n]u_{i'}^*[n']\,.$$

This shows that the correlation function of $h[n,m]$ is completely characterized by the correlation function of $c_i[m]$. The description complexity is thus reduced from $(MN)^2$ to only $(MI)^2$.

For uncorrelated channel taps, $\mathsf{E}\{c_i[m]c_{i'}^*[m']\} = 0$ for $m \neq m'$, so that the channel statistics are described by only MI^2 parameters. In addition, it is often reasonable to assume that two BEM coefficients $c_i[m], c_{i'}[m]$ are uncorrelated even for the same m, so that

$$\mathsf{E}\{c_i[m]c_{i'}^*[m']\} = \mathsf{E}\{|c_i[m]|^2\}\,\delta_{mm'}\,\delta_{ii'}\,. \tag{1.70}$$

Here, only the *MI* powers $\mathsf{E}\{|c_i[m]|^2\}$ need to be specified. The channel statistics corresponding to (1.70) are still non-WSSUS in general. The only exception is a CE-BEM, i.e., $u_i[n] = \exp(j2\pi\xi_i n)$ as in (1.65). Here, (1.70) corresponds to a discrete-time version of a WSSUS channel (cf. (1.23)), i.e.,

$$\mathsf{E}\big\{h[n,m]h^*[n',m']\big\} = r_h[n-n';m]\,\delta_{mm'}\,, \tag{1.71}$$

with

$$r_h[\Delta n;m] = \sum_{i=0}^{I-1} \mathsf{E}\{|c_i[m]|^2\}\, e^{j2\pi\xi_i\Delta n}\,.$$

The associated (discrete-time) scattering function is given by

$$C_{\mathbf{H}}(m,\xi) = \sum_{i=0}^{I-1} \mathsf{E}\{|c_i[m]|^2\}\,\delta(\xi-\xi_i)\,.$$

1.7 Measurement

The measurement of wireless channels is vital for the design, simulation, and performance evaluation of broadband wireless systems. In this section, therefore, we review some of the techniques that can be used to obtain measurements of channel realizations (a task also known as *channel sounding*) and of channel statistics. We assume a transmission phase that is exclusively dedicated to channel measurement, without simultaneous data transmission. However, some of the insights gained apply also to training-based channel estimation during data transmission (see Chapters 4, 5, and 7). Throughout this section, we consider a noise-free scenario for simplicity; this can be justified by the fact that channel sounders usually operate in the high-SNR regime.

1.7.1 Spread-spectrum-like channel sounding

We first describe how the impulse response or transfer function of an LTV channel can be measured by means of wideband channel sounders using spreading sequences. Popular types of channel sounders are pseudo-noise sequence correlation sounders, swept time-delay cross-correlation sounders, and chirp sounders [PDT91, CFM93, FMSC91]. These sounders employ correlation/pulse-compression techniques that are motivated by the identification of time-invariant systems. As we will demonstrate, the application of such techniques to LTV systems or channels results in systematic measurement errors [MMH$^+$02]. These errors must be kept small by an appropriate choice of the sounder parameters.

Idealized impulse-train sounder

A conceptual basis for the above-mentioned correlation/pulse-compression techniques is provided by a very simple channel sounder [Kai62] that uses as the transmit (sounding)

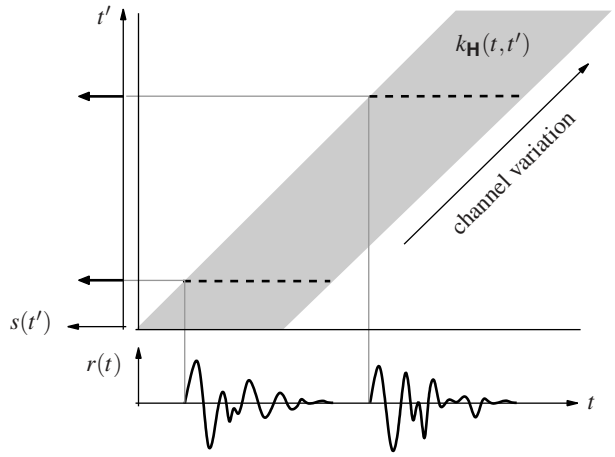

Figure 1.11 Schematic illustration of idealized impulse-train channel sounding.

signal an impulse train of period T:

$$s(t) = \Delta(t) \triangleq \sum_{k=-\infty}^{\infty} \delta(t-kT)\,. \tag{1.72}$$

The resulting channel output is a superposition of slices of the kernel $k_{\mathbf{H}}(t,t')$ in (1.14), i.e.,

$$r(t) = (\mathbf{H}\Delta)(t) = \int_{-\infty}^{\infty} k_{\mathbf{H}}(t,t')\,\Delta(t')\,dt' = \sum_{k=-\infty}^{\infty} k_{\mathbf{H}}(t,kT)\,. \tag{1.73}$$

This channel sounding principle is illustrated in Fig. 1.11. Let $p(\tau)$ denote a rectangular window of length T (i.e., $p(\tau)=1$ for $0 \le \tau < T$ and $p(\tau)=0$ otherwise), and assume that the channel's maximum delay satisfies $\tau_{\max} \le T$ (i.e., $k_{\mathbf{H}}(t,t')=0$ for $t-t' \notin [0,T)$). We then obtain with (1.73)

$$r(\tau+kT)\,p(\tau) = \sum_{k'=-\infty}^{\infty} k_{\mathbf{H}}(\tau+kT,k'T)\,p(\tau) = k_{\mathbf{H}}(\tau+kT,kT) = \tilde{h}(kT,\tau)\,, \tag{1.74}$$

where $\tilde{h}(t,\tau) \triangleq k_{\mathbf{H}}(t+\tau,t)$ is a channel impulse response that is dual to $h(t,\tau) = k_{\mathbf{H}}(t,t-\tau)$. Relation (1.74) shows that the kth block of the receive signal $r(t)$ (the kth "channel snapshot") is a slice of $\tilde{h}(t,\tau)$ at $t=kT$. Note, however, that it is *not* a slice of the usual channel impulse response $h(t,\tau)$. If the channel's maximum Doppler shift satisfies $\nu_{\max} \le 1/(2T)$, the complete dual impulse response can be recovered by interpolating between successive measurements [Kai62]:

$$\tilde{h}(t,\tau) = (\Upsilon r)(t,\tau) \triangleq \sum_{k=-\infty}^{\infty} r(\tau+kT)\,p(\tau)\,\mathrm{sinc}\Big(\frac{\pi}{T}(t-kT)\Big)\,. \tag{1.75}$$

From $\tilde{h}(t,\tau)$, the usual impulse response can then be obtained as $h(t,\tau) = \tilde{h}(t-\tau,\tau)$. Note that the two conditions for this sounding method to work are $\tau_{\max} \le T$ and $\nu_{\max} \le 1/(2T)$. Combining them gives the *underspread* condition $\tau_{\max}\nu_{\max} \le 1/2$ (see Section 1.5.1).

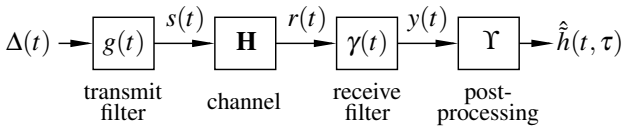

Figure 1.12 Correlative channel sounder model.

Generic correlative channel sounder model

While being conceptually simple, the idealized impulse-train sounder is impractical because the impulse-train sounding signal $\Delta(t)$ has a prohibitively large—theoretically infinite—crest factor (or peak-to-average power ratio). This disadvantage can be avoided by the use of correlation/pulse-compression techniques. Fig. 1.12 shows a generic *correlative channel sounder*. The sounding signal transmitted over the channel is given by

$$s(t) = (\Delta * g)(t) = \sum_{k=-\infty}^{\infty} g(t-kT)\,, \tag{1.76}$$

where T is the sounding period and $g(t)$ is a sounding pulse or, equivalently, the impulse response of a time-invariant transmit (pulse-shaping) filter. The receive signal $r(t) = (\mathbf{H}s)(t)$ is passed through a time-invariant receive filter with impulse response $\gamma(t)$, which yields the signal $y(t) = (r*\gamma)(t)$. Finally, an estimate $\hat{\tilde{h}}(t,\tau)$ of the channel's dual impulse response $\tilde{h}(t,\tau)$ is obtained by forming the snapshots $\hat{\tilde{h}}(kT,\tau) = y(\tau+kT)\,p(\tau)$ as in (1.74) and interpolating them (cf. (1.75)):

$$\hat{\tilde{h}}(t,\tau) \;=\; (\Upsilon y)(t,\tau)\,. \tag{1.77}$$

We note that the idealized impulse-train channel sounder is a special case of the generic correlative channel sounder with transmit and receive filters $g(t) = \gamma(t) = \delta(t)$.

Correlative channel sounding is based on the assumption that the order of the channel and the receive filter (see Fig. 1.12) can be approximately reversed (in the theoretical analysis), so that the signal $y(t)$ at the output of the receive filter $\gamma(t)$ can be approximately expressed as

$$y(t) \approx (\mathbf{H}\tilde{\Delta})(t)\,, \qquad \text{with } \tilde{\Delta}(t) \triangleq \sum_{k=-\infty}^{\infty} (g*\gamma)(t-kT)\,.$$

Hence, the overall scheme can be interpreted as if the channel were sounded using the *virtual sounding signal* $\tilde{\Delta}(t)$. The transmit and receive filters are designed such that[3] $(g*\gamma)(t) \approx \delta(t)$, since then the virtual sounding signal approximately equals an impulse train, i.e., $\tilde{\Delta}(t) \approx \Delta(t)$, and thus the sounder approximates the idealized impulse-train channel sounder, even though the actual sounding signal in (1.76) can have a small crest factor.

[3] Since only a band-limited part (with bandwidth B) of the channel is measured and since practical transmit and receive filters are causal, one should rather require $(g*\gamma)(t) \approx B\,\mathrm{sinc}(\pi B(t-t_0))$ with t_0 sufficiently large. However, here we use $t_0 = 0$ and $B \to \infty$ for simplicity.

For a time-invariant channel, the system with channel and receive filter interchanged is equivalent to the original system. For an LTV channel, however, this equivalence holds only approximately at best, and this fact entails a systematic error in the sounding result. This measurement error grows with the maximum Doppler frequency of the channel and with the duration of the impulse response of the receive filter [MMH+02].

Correlative channel sounding can also be represented in the TF domain. A definition of the frequency response of an LTV channel that is dual to the TF transfer function $L_{\mathbf{H}}(t,f)$ in (1.16) is given by the *frequency-dependent modulation function* [Bel63]

$$\tilde{L}_{\mathbf{H}}(t,f) \triangleq \int_{-\infty}^{\infty} \tilde{h}(t,\tau)\, e^{-j2\pi f\tau}\, d\tau\,.$$

An estimate of $\tilde{L}_{\mathbf{H}}(t,f)$ at time $t=kT$ can be obtained by Fourier transforming $\hat{\tilde{h}}(kT,\tau) = y(\tau+kT)\,p(\tau)$ with respect to τ:

$$\hat{\tilde{L}}_{\mathbf{H}}(kT,f) = \int_{-\infty}^{\infty} \hat{\tilde{h}}(kT,\tau)\, e^{-j2\pi f\tau} d\tau = \int_{-\infty}^{\infty} y(\tau+kT)\,p(\tau)\, e^{-j2\pi f\tau} d\tau\,. \tag{1.78}$$

Hence, $\hat{\tilde{L}}_{\mathbf{H}}(kT,f)$ can be viewed as the short-time Fourier transform [NQ88, HBB92, Fla99] of $y(t)$ using the analysis window $p(t)$, sampled at $t=kT$. An estimate of $\tilde{L}_{\mathbf{H}}(t,f)$ for arbitrary t can be obtained either by interpolating $\hat{\tilde{L}}_{\mathbf{H}}(kT,f)$ or by Fourier transforming the interpolated impulse response estimate $\hat{\tilde{h}}(t,\tau)$ in (1.77).

Sounder types

As mentioned above, the design of correlative channel sounders aims at achieving $(g * \gamma)(t) \approx \delta(t)$, since then the virtual sounding signal $\tilde{\Delta}(t)$ approximates an impulse train $\Delta(t)$. We next discuss two common designs.

- *PN-sequence sounder.* While all sounders within the correlative sounding model employ correlation techniques, the term "correlation sounder" usually refers to sounders whose transmit and receive filters are based on a binary pseudo-noise (PN) sequence $b_i \in \{-1,1\}$ according to

  $$g(t) = \sum_{i=1}^{N} b_i\, c(t-iT_c)\,, \qquad \gamma(t) = g(NT_c - t) = \sum_{i=i}^{N} b_{N-i+1}\, c(-(t-iT_c))\,.$$

  Here, $c(t)$ is a chip pulse and T_c is the chip duration; note that $NT_c \leq T$. For N sufficiently large, $g(t)$ and $\gamma(t)$ induce a virtual sounding signal $\tilde{\Delta}(t)$ that approximates an impulse train within the measurement bandwidth $1/(2T_c)$. We note that sounding sequences b_i other than PN sequences and receive filters that are not time-reversed replicas of the transmit filter have also been proposed (e.g., [SMS93, THR+00]). Furthermore, there exists a practical modification of the PN sequence sounder, termed *swept time-delay cross-correlator*, that trades delay resolution against channel tracking capability [Cox72, Rap96].

- *Chirp sounder.* As an alternative to PN sequences, chirp sounders use chirp signals, which have a similarly low crest factor. The transmit and receive filters are given by

[SNB98]

$$g(t) = e^{j2\pi B(t^2/T_g - t)}, \qquad \gamma(t) = g^*(T_g - t) = e^{-j2\pi B(t^2/T_g - t)}, \qquad \text{for } 0 \le t < T_g,$$

where $T_g \le T$. These filters again induce a virtual sounding signal $\tilde{\Delta}(t)$ that approximates an impulse train within the measurement band. This approximation can be improved by using nonrectangular (e.g., Gaussian) envelopes for $g(t)$ and $\gamma(t)$ [Sko84].

Measurement errors

For LTV channels, the correlative sounding techniques described above suffer from several types of systematic measurement errors [MMH+02], in addition to the random effects of measurement noise.

- As mentioned previously, the commutation argument underlying correlative channel sounding—i.e., obtaining a virtual sounding signal by swapping channel and receive filter—can hold true for LTV channels only in an approximate manner. The resulting *commutation error* increases with the Doppler spread of the channel and with the length of the receive filter.

- Practically realizable transmit and receive filters have imperfect pulse-compression (correlation) properties, i.e., $(g * \gamma)(t) \neq \delta(t)$ and hence $\tilde{\Delta}(t) \neq \Delta(t)$. This leads to a *pulse-compression error*, even in the case of a time-invariant channel. This error tends to be particularly pronounced for transmit and receive filters of small length. Usually, one attempts to reduce pulse-compression errors via back-to-back calibration, where transmitter and receiver are connected by a short cable and the response $(g * \gamma)(t)$ is recorded for later equalization of the channel measurements. However, back-to-back calibration tends to increase the measurement noise, and for the case of LTV channels it is also affected by systematic errors [MMS+99].

- For channels with maximum delay $\tau_{\max} > T$, successive channel snapshots will overlap (aliasing in the delay domain), and for channels with maximum Doppler shift $\nu_{\max} > 1/(2T)$, the channel snapshots do not track the channel variations sufficiently fast (aliasing in the Doppler domain). These two error mechanisms are combined in the *aliasing error*, which grows with the channel's dispersion spread and can be minimized by an appropriate choice of the sounding period T. The aliasing error vanishes if and only if [Kai62, MMH+02]

$$\tau_{\max} \le T \le \frac{1}{2\nu_{\max}}.$$

  As remarked previously, this in turn presupposes $\tau_{\max}\nu_{\max} \le 1/2$, i.e., a dispersion-underspread channel (see Section 1.5.1).

- Finally, the measured function $\hat{\tilde{h}}(t,\tau)$ is typically used as an estimate of the impulse response $h(t,\tau)$, even though it is actually an estimate of the dual impulse response $\tilde{h}(t,\tau)$. This *misinterpretation error* again grows with the channel's dispersion spread.

However, it can be easily avoided by converting $\hat{\tilde{h}}(t,\tau)$ to an estimate of $h(t,\tau)$ according to $\hat{h}(t,\tau) = \hat{\tilde{h}}(t-\tau,\tau)$.

A quantitative analysis of these systematic errors along with a corresponding optimization of relevant sounder parameters has been performed in [MMH+02].

1.7.2 Multicarrier channel sounding

The channel sounders described in the previous subsection resemble a spread spectrum communication system; the spreading is used to achieve favorable pulse compression/correlation properties. Next, we discuss channel sounding techniques that resemble multicarrier communication systems such as OFDM systems. Such sounders are described e.g. in [STC07, dCK+07].

Multicarrier basics

The basic principle of multicarrier systems—see Chapters 2 and 7 for details—is to split the transmit band (bandwidth B) into L subcarriers and transmit L symbol streams $a[k,l]$, $l = 0,\ldots,L-1$ in parallel over these subcarriers. This results in a transmit signal of the form

$$s(t) = \sum_k \sum_{l=0}^{L-1} a[k,l]\, g_{k,l}(t), \qquad \text{with } g_{k,l}(t) \triangleq g(t-kT)\, e^{j2\pi lFt},$$

where k and l denote the symbol (time) index and the subcarrier index, respectively; T is the symbol duration; $F = B/L$ is the frequency separation of the subcarriers; and $g(t)$ is a transmit pulse. From the channel output $r(t)$, the receiver calculates the following estimate of the transmit symbols $a[k,l]$:

$$y[k,l] = \langle r, \gamma_{k,l} \rangle = \int_{-\infty}^{\infty} r(t)\, \gamma_{k,l}^*(t)\, dt, \qquad \text{with } \gamma_{k,l}(t) \triangleq \gamma(t-kT)\, e^{j2\pi lFt},$$

where $\gamma(t)$ is a receive pulse. In the absence of noise and channel distortions, i.e., when $r(t) = s(t)$, there is $y[k,l] = a[k,l]$ if and only if the *biorthogonality condition* [Grö01] $\langle g_{k',l'}, \gamma_{k,l} \rangle = \delta_{kk'}\delta_{ll'}$ is satisfied. A necessary condition for biorthogonality is $TF \geq 1$. The most prominent example of a biorthogonal system is given by the rectangular pulses

$$g(t) = \begin{cases} \sqrt{F}, & 0 \leq t \leq T, \\ 0, & \text{else}, \end{cases} \qquad \gamma(t) = \begin{cases} \sqrt{F}, & 0 \leq t \leq 1/F, \\ 0, & \text{else}. \end{cases} \tag{1.79}$$

This corresponds to a classical OFDM system with a cyclic prefix (CP) of duration $T_{\text{cp}} = T - 1/F$.

Measurement principle

When using a multicarrier system for channel sounding, the symbols $a[k,l]$ are actually training symbols known by the receiver. The measurement principle of multicarrier channel sounders is motivated by the approximate eigenrelation discussed in Section 1.5.3 (see

(1.46)),

$$(\mathbf{H}g_{k,l})(t) \approx L_{\mathbf{H}}(kT,lF)\, g_{k,l}(t)\,. \tag{1.80}$$

This approximation is accurate if the transmit pulse $g(t)$ is well TF-localized and the channel is sufficiently dispersion-underspread. We note that for a time-invariant channel and CP-OFDM (see (1.79)), the approximation is exact, i.e., $(\mathbf{H}g_{k,l})(t) = H(lF)\, g_{k,l}(t)$, provided that the channel's maximum delay satisfies $\tau_{\max} \leq T_{\mathrm{cp}}$. Inserting the approximation (1.80) in $r(t) = (\mathbf{H}s)(t) = \sum_k \sum_{l=0}^{L-1} a[k,l]\,(\mathbf{H}g_{k,l})(t)$, we obtain for the demodulated symbols

$$y[k,l] = \langle r, \gamma_{k,l}\rangle \approx \sum_{k'} \sum_{l'=0}^{L-1} a[k',l']\, L_{\mathbf{H}}(k'T,l'F)\, \langle g_{k',l'}, \gamma_{k,l}\rangle = a[k,l]\, L_{\mathbf{H}}(kT,lF)\,, \tag{1.81}$$

where the biorthogonality property $\langle g_{k',l'}, \gamma_{k,l}\rangle = \delta_{kk'}\delta_{ll'}$ was used in the last step. Based on (1.81), an estimate of the channel transfer function at time kT and frequency lT ($l = 0,\ldots,L-1$) is obtained as

$$\hat{L}_{\mathbf{H}}(kT,lF) = \frac{y[k,l]}{a[k,l]}\,. \tag{1.82}$$

Still assuming a dispersion-underspread channel, it follows from our discussion in Section 1.5.4 that an estimate of the overall transfer function $\hat{L}_{\mathbf{H}}(t,f)$ can be calculated by lowpass interpolation of the estimate $\hat{L}_{\mathbf{H}}(kT,lF)$ according to (1.55). An estimate of the impulse response $h(t,\tau)$ can then be obtained from (1.82) via the Fourier series

$$\hat{h}(kT,\tau) = \sum_{l=0}^{L-1} \hat{L}_{\mathbf{H}}(kT,lF)\, e^{j2\pi lF\tau}, \qquad 0 \leq \tau \leq \frac{1}{F},$$

and subsequent interpolation with respect to t.

Measurement errors

The measurement principle described above hinges fundamentally on the approximation (1.80). This approximation becomes less accurate for a larger channel dispersion spread $\sigma_{\mathbf{H}}$ and for a larger time-bandwidth product of the transmit pulse $g(t)$ (we assume that the RMS duration and RMS bandwidth of $g(t)$ are chosen according to (1.52)). The approximation error in (1.80) manifests itself as *intersymbol interference* (ISI) and *intercarrier interference* (ICI), which are not described by (1.81). ISI and ICI represent the main limitations of multicarrier channel sounding. In CP-OFDM, ISI is avoided by an appropriate choice of the CP duration T_{cp}; however, the rectangular pulses used in CP-OFDM result in increased ICI, especially for fast time-varying channels (see, e.g., [MSG+07]).

Since (1.82) only provides estimates of samples of $L_{\mathbf{H}}(t,f)$ at $t = kT$ and $f = lF$, aliasing errors may arise (see Section 1.5.4). This is similar to spread-spectrum-like sounders. Assuming the optimum choice $T/F = \sigma_\tau/\sigma_\nu$ (see (1.56)), the aliasing errors can be bounded in terms of $\sigma_{\mathbf{H}}$ and TF according to (1.57).

1.7.3 Extension to multiantenna systems

The channel sounding techniques described above can be extended to multiantenna systems (i.e., MIMO systems) by means of a procedure known as *time-division multiplexed switching* (TDMS). Here, the individual spatial channels are measured successively by activating one antenna pair at a time. This can be done by physically moving the antennas of a single-antenna channel sounder (e.g., using a step motor), thereby creating a virtual multiantenna system. Alternatively, a single RF chain may be switched electronically between multiple antennas.

For time-invariant channels, theoretically, this measurement principle does not introduce any additional errors. In contrast, for LTV channels, the channel impulse response changes between successive measurements; thus, pretending that these measurements were taken simultaneously leads to errors. In practice, such errors arise even in static scenarios since oscillator drift and phase noise result in noticeable time variations of the effective channel (see Example 1.4). The resulting errors can be significant in the multiantenna setup [BB].

Example 1.21 *Consider a* 2×2 *MIMO system with a rank-one flat-fading time-invariant channel, i.e.,* $\mathbf{H} = h \left(\begin{smallmatrix} 1 \\ 1 \end{smallmatrix}\right) \left(\begin{smallmatrix} 1 \\ 1 \end{smallmatrix}\right)^T = h \left(\begin{smallmatrix} 1 & 1 \\ 1 & 1 \end{smallmatrix}\right)$. *Using a TDMS-based channel sounder with oscillator phase noise (but no other errors) results in the channel estimate* $\hat{\mathbf{H}} = h \left(\begin{smallmatrix} e^{j\phi_1} & e^{j\phi_2} \\ e^{j\phi_3} & e^{j\phi_4} \end{smallmatrix}\right)$, *where the matrix entries* $e^{j\phi_i}$ *describe phase rotations that are due to the oscillator phase noise in the four successive measurement periods. Clearly, the measured channel will be typically full-rank even though the actual channel has rank one.*

A detailed analysis of the sounding errors resulting from antenna switching or displacement is provided in [BB]. It is shown that the errors become larger for increasing temporal separation of successive spatial measurements. Furthermore, they typically lead to an increased rank of the measured MIMO channel matrix and, in turn, to over-estimation of the MIMO channel capacity.

Switching errors can be avoided by using a dedicated RF chain for each antenna and separating the spatial channels in the frequency domain rather than in the time domain (e.g., by dedicating each subcarrier in a multicarrier channel sounder to a single antenna pair).

1.7.4 Measurement of second-order statistics

Second-order channel statistics are important for many tasks in transceiver design and performance evaluation, such as the design of channel estimators, precoders and beamformers, as well as channel simulation. In the following, we summarize some nonparametric and parametric estimators of the second-order channel statistics. We will again consider a noise-free transmission for simplicity.

Nonparametric estimation

In the case of WSSUS channels, we are interested in estimating the scattering function $C_{\mathbf{H}}(\tau,\nu)$ or the TF correlation function $R_{\mathbf{H}}(\Delta t,\Delta f)$ (see (1.26)). An estimator of the scattering function that is based on the statistical input-output relation (1.28) was proposed in [Gaa68]. For a deterministic transmit signal $s(t)$, (1.28) becomes $\bar{A}_r(\Delta t,\Delta f) = R_{\mathbf{H}}(\Delta t,\Delta f)A_s(\Delta t,\Delta f)$, where $\bar{A}_r(\Delta t,\Delta f)$ is the expected ambiguity function of $r(t)$ as defined in Section 1.4.1 and $A_s(\Delta t,\Delta f) = \int_{-\infty}^{\infty} s(t)\,s^*(t-\Delta t)\,e^{-j2\pi t\Delta f}dt$ is the ambiguity function of $s(t)$ previously used in Section 1.5.3. Hence, the TF correlation function can be expressed as $R_{\mathbf{H}}(\Delta t,\Delta f) = \bar{A}_r(\Delta t,\Delta f)/A_s(\Delta t,\Delta f)$. An estimate of $R_{\mathbf{H}}(\Delta t,\Delta f)$ can then be calculated as

$$\hat{R}_{\mathbf{H}}(\Delta t,\Delta f) = \frac{\hat{A}_r(\Delta t,\Delta f)}{A_s(\Delta t,\Delta f)}, \tag{1.83}$$

where $\hat{A}_r(\Delta t,\Delta f)$ is an estimate of $\bar{A}_r(\Delta t,\Delta f)$. To obtain this latter estimate, a finite-duration sounding signal $s(t)$ is successively transmitted Q times, resulting in Q receive signals $r_q(t)$ (we assume that the different arrival times of these signals have been compensated so that all $r_q(t)$ are temporally aligned). The estimated expected ambiguity function $\hat{A}_r(\Delta t,\Delta f)$ is taken to be the average of the ambiguity functions of the $r_q(t)$:

$$\hat{A}_r(\Delta t,\Delta f) = \frac{1}{Q}\sum_{q=1}^{Q} A_{r_q}(\Delta t,\Delta f).$$

Finally, an estimate of the scattering function $C_{\mathbf{H}}(\tau,\nu)$ is derived from $\hat{R}_{\mathbf{H}}(\Delta t,\Delta f)$ according to (1.26), i.e.,

$$\hat{C}_{\mathbf{H}}(\tau,\nu) = \int_{-\infty}^{\infty}\int_{-\infty}^{\infty} \hat{R}_{\mathbf{H}}(\Delta t,\Delta f)\,e^{-j2\pi(\nu\Delta t-\tau\Delta f)}\,d\Delta t\,d\Delta f.$$

A problem of this simple estimator is due to the following facts. On the one hand, the area of the effective support of $A_s(\Delta t,\Delta f)$ equals one (this follows from the identity $\int_{-\infty}^{\infty}\int_{-\infty}^{\infty}|A_s(\Delta t,\Delta f)|^2 d\Delta t\,d\Delta f = |A_s(0,0)|^2$ known as the *radar uncertainty principle* [Wil91]). On the other hand, the area of the effective support of $R_{\mathbf{H}}(\Delta t,\Delta f)$ is roughly equal to the product of coherence time and coherence bandwidth $T_{\mathrm{c}}F_{\mathrm{c}} = 1/\sigma_{\mathbf{H}}$, which, due to the underspread property, is usually much larger than one. Consequently, the "equalization" with $1/A_s(\Delta t,\Delta f)$ performed in (1.83) involves divisions by values near zero, which result in numerical errors and noise enhancement.

An improved version of the estimator described above can be obtained by exploiting the underspread property[4] [AMH04]. For an underspread channel, the scattering function $C_{\mathbf{H}}(\tau,\nu)$ is effectively supported in a region $[0,\tau_{\max}]\times[-\nu_{\max},\nu_{\max}]$, with $\tau_{\max}\nu_{\max} \ll 1$. We can thus apply the sampling theorem to the 2-D Fourier transform of $C_{\mathbf{H}}(\tau,\nu)$, which is the TF correlation function $R_{\mathbf{H}}(\Delta t,\Delta f)$ (see (1.26)). Specifically, the samples $R_{\mathbf{H}}(i\Delta T, j\Delta F)$ completely determine $C_{\mathbf{H}}(\tau,\nu)$ provided that $\Delta T \le 1/(2\nu_{\max})$ and $\Delta F \le 1/\tau_{\max}$. Therefore, the TF correlation function needs to be estimated only at the lattice points $(i\Delta T, j\Delta F)$, i.e., (1.83) reduces to $\hat{R}_{\mathbf{H}}(i\Delta T, j\Delta F) = \hat{A}_r(i\Delta T, j\Delta F)/A_s(i\Delta T, j\Delta F)$.

[4]The development in [AMH04] is based on discretized signals and channel representations. We here describe the main ideas in a continuous-time setup.

Since the radar uncertainty principle does not prevent us from achieving $|A_s(i\Delta T, j\Delta F)| \approx |A_s(0,0)|$ by an appropriate design of the sounding signal $s(t)$, divisions by near-zero numbers can be avoided.

Regarding the design of $s(t)$, it is interesting to note that the ambiguity function of the impulse train $\Delta(t) = \sum_{k=-\infty}^{\infty} \delta(t-kT)$ in (1.72) equals $A_\Delta(\Delta t, \Delta f) = \sum_{k=-\infty}^{\infty} \sum_{l=-\infty}^{\infty} \delta(\Delta t - kT, \Delta f - l/T)$. While $\Delta(t)$ is impractical as an actual sounding signal, we can approximate it by means of the correlative channel sounding principle explained in Section 1.7.1, i.e., by using a sounding signal of the form $s(t) = \sum_{k=-\infty}^{\infty} g(t-kT)$ and a receive filter $\gamma(t)$. If $g(t)$ and $\gamma(t)$ are appropriately designed, then, according to Section 1.7.1, the output of the receive filter can be approximated as

$$y(t) \approx (\mathbf{H}\tilde{\Delta})(t)\,,$$

where $\tilde{\Delta}(t) = \sum_{k=-\infty}^{\infty} (g * \gamma)(t-kT)$ is a reasonable approximation to $\Delta(t)$. Based on this approximation, an estimate of the sampled TF correlation function can be obtained by evaluating (1.83) at the lattice points $(iT, j/T)$, with $A_s(iT, j/T)$ replaced by $A_{\tilde{\Delta}}(iT, j/T)$ and $\hat{A}_r(iT, j/T)$ replaced by $\hat{A}_y(iT, j/T)$:

$$\hat{R}_{\mathbf{H}}\Big(iT, \frac{j}{T}\Big) = \frac{\hat{A}_y\big(iT, \frac{j}{T}\big)}{A_{\tilde{\Delta}}\big(iT, \frac{j}{T}\big)}\,. \tag{1.84}$$

The main advantage over (1.83) is that we can achieve $A_{\tilde{\Delta}}(iT, j/T) \approx$ const., and thus avoid divisions by near-zero numbers in (1.84), by a suitable design of $g(t)$ and $\gamma(t)$. A 2-D Fourier transform of $\hat{R}_{\mathbf{H}}(iT, j/T)$ finally gives an estimate of $C_{\mathbf{H}}(\tau, \nu)$ within the delay-Doppler region $[0,T] \times [-1/(2T), 1/(2T)]$ of area 1. In the underspread case considered, this region contains the effective support of $C_{\mathbf{H}}(\tau, \nu)$, provided T is suitably chosen. A detailed bias-variance analysis of this estimator is provided in [AMH04], along with modifications that use a regularized division or allow for data-driven operation during an ongoing data transmission.

It is interesting to observe that for an idealized impulse-train sounding signal, the discrete-time version of the scattering function estimator described above can be equivalently obtained by first measuring the TF transfer function (cf. (1.78)) and then computing the 2-D periodogram (i.e., magnitude-squared 2-D Fourier transform) of the measured TF transfer function [AMH04]. This is not surprising since, as discussed in Section 1.4.1, the scattering function is the 2-D power spectral density of the TF transfer function (which is 2-D stationary in the WSSUS case). More generally, we can obtain a scattering function estimate by applying any 2-D spectrum estimator to a measured TF transfer function. A parametric 2-D spectrum estimator will be considered next.

Parametric estimation

Parametric estimation of the scattering function of a WSSUS channel can be based on the discrete-time ARMA model described in Section 1.6. For simplicity, we will here consider only the special case of the AR model [KD03]. This model is given by (1.67)

with $N_{\mathrm{MA}} = 1$, i.e., the channel impulse response is represented as

$$h[n,m] \;=\; -\sum_{\Delta n=1}^{N_{\mathrm{AR}}} a_m[\Delta n]\, h[n-\Delta n,m] \;+\; b_m[0]\, e_m[n]\,, \qquad m = 0,\ldots,M-1\,, \tag{1.85}$$

where $e_m[n]$ is normalized stationary white noise. According to (1.68), the (discrete-time) scattering function is given by

$$C_{\mathbf{H}}(m,\xi) = \frac{|b_m[0]|^2}{\left|\sum_{\Delta n=0}^{N_{\mathrm{AR}}} a_m[\Delta n]\, e^{-j2\pi\xi\Delta n}\right|^2}\,, \qquad m = 0,\ldots,M-1\,, \tag{1.86}$$

with $a_m[0] = 1$. Estimating $C_{\mathbf{H}}(m,\xi)$ thus reduces to estimating the MN_{AR} AR parameters $a_m[\Delta n]$ (where $m = 0,\ldots,M-1$ and $\Delta n = 1,\ldots,N_{\mathrm{AR}}$) and the M innovations variances $|b_m[0]|^2$ and, possibly, the AR model order N_{AR}.

The classical approach to estimating the AR parameters [Kay88, Sch91, SM97] capitalizes on the fact that the recursive structure (1.85) of the channel tap process $h[n,m]$ is inherited by the correlation function $r_h[\Delta n,m] = \mathsf{E}\{h[n,m]\, h^*[n-\Delta n,m]\}$ (see (1.71)), i.e.,

$$r_h[\Delta n,m] = -\sum_{\Delta n'=1}^{N_{\mathrm{AR}}} a_m[\Delta n']\, r_h[\Delta n-\Delta n',m]\,, \qquad \text{for } \Delta n > 0\,. \tag{1.87}$$

For m fixed and $\Delta n = 1,\ldots,N_{\mathrm{AR}}$, (1.87) constitutes a system of N_{AR} linear equations in the N_{AR} AR parameters $a_m[\Delta n]$. These equations are known as the *Yule-Walker equations*. Since the convolution structure of (1.87) entails a Toeplitz structure of the system matrix, the Yule-Walker equations can be solved efficiently by means of the Levinson algorithm [Kay88, Sch91, SM97]. For a practical estimator of the $a_m[\Delta n]$, the correlation $r_h[\Delta n,m]$ is replaced by the sample estimate $\hat{r}_h[\Delta n,m] = \sum_n \hat{h}[n,m]\, \hat{h}^*[n-\Delta n,m]$, where $\hat{h}[n,m]$ is a measured impulse response obtained via channel sounding (see Sections 1.7.1 and 1.7.2) and the summation with respect to n is over the measurement interval. The innovations variances $|b_m[0]|^2$ can be estimated as

$$\widehat{|b_m[0]|^2} = \hat{r}_h[0,m] + \sum_{\Delta n=1}^{N_{\mathrm{AR}}} \hat{a}_m[\Delta n]\, \hat{r}_h[-\Delta n,m]\,.$$

Finally, inserting the parameter estimates $\hat{a}_m[\Delta n]$ and $\widehat{|b_m[0]|^2}$ into (1.86) yields an estimate of the scattering function.

Non-WSSUS case

The estimation of the LSF of a non-WSSUS channel (see Section 1.4.3) can be viewed as a nonstationary spectral estimation problem. Accordingly, a nonparametric LSF estimator proposed in [Mat03] computes local multiwindow periodograms (cf. [Tho82]) of a measured channel transfer function $\hat{L}_{\mathbf{H}}(t,f)$, i.e.,

$$\hat{\mathscr{C}}_{\mathbf{H}}(t,f;\tau,\nu) = \sum_{i=1}^{I} \left| \int_{-\infty}^{\infty}\int_{-\infty}^{\infty} \hat{L}_{\mathbf{H}}(t',f')\, u_i(t'-t)\, v_i(f'-f)\, e^{-j2\pi(\nu t'-\tau f')}\, dt'\, df' \right|^2.$$

Here, $u_i(t)$ and $v_i(f)$, $i = 1,\ldots,I$, are suitably chosen window functions (e.g., prolate spheroidal wave functions). The number of individual periodograms, I, affects the bias and variance of the estimator; a larger I yields increased bias and reduced variance. A more detailed discussion of this estimator is provided in [Mat03].

A parametric LSF estimator can be based on the time-varying ARMA model (1.69) [JM05]. We will consider only the AR part with $\mathbf{B}[n,0] = \mathbf{I}$ for simplicity. It is convenient to represent the time-varying AR coefficient matrices $\mathbf{A}[n,\Delta n]$ over a block of duration N in terms of a $(2K_{\mathrm{AR}}+1)$-dimensional exponential basis, i.e., $\mathbf{A}[n,\Delta n] = \sum_{\Delta k=-K_{\mathrm{AR}}}^{K_{\mathrm{AR}}} \tilde{\mathbf{A}}[\Delta n,\Delta k] e^{j2\pi\frac{n\Delta k}{N}}$, $n = 0,\ldots,N-1$, with $2K_{\mathrm{AR}}+1 \ll N$ [JM05, JMH09]. We then obtain from (1.69) the following noisy recursion for the channel vector $\mathbf{h}[n] = (h[n,0]\cdots h[n,M-1])^T$:

$$\mathbf{h}[n] \;=\; -\sum_{\Delta n=1}^{N_{\mathrm{AR}}} \sum_{\Delta k=-K_{\mathrm{AR}}}^{K_{\mathrm{AR}}} \tilde{\mathbf{A}}[\Delta n,\Delta k]\mathbf{h}[n-\Delta n] e^{j2\pi\frac{n\Delta k}{N}} + \mathbf{e}[n]\,, \quad n = 0,\ldots,N-1\,.$$

This is autoregressive not only in time (time-delayed copies of $\mathbf{h}[n]$) but also in frequency (frequency-shifted copies of $\mathbf{h}[n]$). This *time-frequency AR* (TFAR) structure is inherited by the second-order statistics of $\mathbf{h}[n]$. Specifically, the expected matrix-valued ambiguity function of $\mathbf{h}[n]$,

$$\bar{\mathbf{A}}[\Delta n,\Delta k] \;\triangleq\; \mathsf{E}\left\{\sum_{n=0}^{N-1} \mathbf{h}[n]\mathbf{h}^H[n-\Delta n]\, e^{-j2\pi\frac{n\Delta k}{N}}\right\}, \tag{1.88}$$

can be shown to satisfy the recursion [JM05, JMH09]

$$\bar{\mathbf{A}}[\Delta n,\Delta k] \;=\; -\sum_{\Delta n'=1}^{N_{\mathrm{AR}}} \sum_{\Delta k'=-K_{\mathrm{AR}}}^{K_{\mathrm{AR}}} \tilde{\mathbf{A}}[\Delta n',\Delta k']\,\bar{\mathbf{A}}[\Delta n-\Delta n',\Delta k-\Delta k'] e^{j2\pi\frac{\Delta n'(\Delta k'-\Delta k)}{N}}, \tag{1.89}$$

for $\Delta n = 1,\ldots,N_{\mathrm{AR}}$ and $\Delta k = -K_{\mathrm{AR}},\ldots,K_{\mathrm{AR}}$. These "TF Yule-Walker equations" constitute a system of $N_{\mathrm{AR}}\,(2K_{\mathrm{AR}}+1)$ linear equations in the $N_{\mathrm{AR}}\,(2K_{\mathrm{AR}}+1)$ TFAR parameter matrices $\tilde{\mathbf{A}}[\Delta n,\Delta k]$. For a correlation-underspread channel (see Section 1.5.2), the phase factor $e^{j2\pi\Delta n'(\Delta k'-\Delta k)/N}$ in (1.89) can be approximated by 1. With this approximation, the TF Yule-Walker equations exhibit a two-level block-Toeplitz structure and can hence be solved efficiently by means of a vector version of the Wax-Kailath algorithm [WK83] (see [JM05, JMH09] for algorithmic details).

For a practical estimator of the TFAR parameter matrices $\tilde{\mathbf{A}}[\Delta n,\Delta k]$, the expected matrix ambiguity function $\bar{\mathbf{A}}[\Delta n,\Delta k]$ is replaced by a sample estimate that is obtained by dropping the expectation in (1.88) and substituting an estimate $\hat{\mathbf{h}}[n]$ for $\mathbf{h}[n]$. The resulting TFAR parameter estimates $\hat{\tilde{\mathbf{A}}}[\Delta n,\Delta k]$ can finally be used to compute an estimate of the LSF, based on an LSF expression that is similar in spirit to (1.86) [JM05, JMH09].

1.8 Conclusion

In this chapter, we provided a survey of many of the concepts and tools that have been developed during the past six decades for characterizing, modeling, and measuring time-

frequency dispersive channels. Our treatment was motivated by the twofold goal of presenting some fundamentals that may be helpful for understanding the subsequent chapters of this book and, more generally, of providing a convenient entry point into the rich literature on rapidly time-varying wireless channels.

Based on considerations of the physical propagation mechanisms, we discussed various deterministic and stochastic channel descriptions. Regarding the latter, both WSSUS and non-WSSUS channels were treated. Some emphasis was placed on the practically most relevant class of underspread channels and on important consequences of the underspread property. We reviewed parsimonious channel models, concentrating on the particularly useful basis expansion and ARMA-type models. Finally, we briefly discussed several techniques for measuring time-varying channels and their statistics. For some of these topics, extensions to multiantenna (MIMO) channels were presented. We note that while our discussion focused on terrestrial wireless channels, much of it applies to other channels as well (underwater, satellite, etc.).

Acknowledgment

This work was supported by the FWF under Grant S10603-N13 (Statistical Inference) and Grant S10606-N13 (Information Networks) within the National Research Network SISE, and by the WWTF under Grant MA 44 (MOHAWI).

References

[ABB+07] P. Almers, E. Bonek, A. Burr, N. Czink, M. Debbah, V. Degli-Esposti, H. Hofstetter, P. Kyösti, D. Laurenson, G. Matz, A. F. Molisch, C. Oestges, and H. Özcelik. Survey of channel and radio propagation models for wireless MIMO systems. *EURASIP J. Wireless Commun. Networking*, Vol. 2007, Article ID 19070, 2007.

[AMH04] H. Artés, G. Matz, and F. Hlawatsch. Unbiased scattering function estimators for underspread channels and extension to data-driven operation. *IEEE Trans. Signal Process.*, 52(5):1387–1402, May 2004.

[AS65] M. Abramowitz and I. Stegun. *Handbook of Mathematical Functions*. Dover, New York, NY, 1965.

[BB] D. Baum and H. Bölcksei. Information-theoretic analysis of MIMO channel sounding. Submitted to *Trans. Inf. Theory*.

[BB01] K. E. Baddour and N. C. Beaulieu. Autoregressive models for fading channel simulation. In *Proc. IEEE GLOBECOM-2001*, pages 1187–1192, San Antonio, TX, Nov. 2001.

[Bel63] P. A. Bello. Characterization of randomly time-variant linear channels. *IEEE Trans. Comm. Syst.*, 11:360–393, 1963.

[BGPvdV06] H. Bölcskei, D. Gesbert, C. B. Papadias, and A.-J. van der Veen, editors. *Space-Time Wireless Systems: From Array Processing to MIMO Communications*. Cambridge University Press, New York, NY, 2006.

[BH99] D. K. Borah and B. D. Hart. Frequency-selective fading channel estimation with a polynomial time-varying channel model. *IEEE Trans. Commun.*, 47:862–873, June 1999.

[Bin90] J. A. C. Bingham. Multicarrier modulation for data transmission: An idea whose time has come. *IEEE Commun. Mag.*, 28(5):5–14, May 1990.

[BPRV04] R. Balan, H. V. Poor, S. Rickard, and S. Verdu. Time-frequency and time-scale canonical representations of doubly spread channels. In *Proc. EUSIPCO–04*, pages 445–448, Vienna, Austria, Sept. 2004.

[BPS98] E. Biglieri, J. Proakis, and S. Shamai (Shitz). Fading channels: Information-theoretic and communications aspects. *IEEE Trans. Inf. Theory*, 44(6):2619–2692, Oct. 1998.

[CFM93] P. J. Cullen, P. C. Fannin, and A. Molina. Wide-band measurement and analysis techniques for the mobile radio channel. *IEEE Trans. Veh. Technol.*, 42(4):589–603, Nov. 1993.

[Cox72] D. Cox. Delay Doppler characteristics of multipath propagation in a suburban mobile radio environment. *IEEE Trans. Antennas Propag.*, 20:625–635, 1972.

[CV74] S.-K. Chow and A. N. Venetsanopoulos. Optimal on-off signaling over linear time-varying stochastic channels. *IEEE Trans. Inf. Theory*, 20(5):602–609, Sept. 1974.

[dCK+07] R. de Lacerda, L. S. Cardoso, R. Knopp, D. Gesbert, and M. Debbah. EMOS platform: Real-time capacity estimation of MIMO channels in the UMTS-TDD band. In *Proc. Int. Symp. Wireless Communication Systems (IWCS)*, Trondheim, Norway, Oct. 2007.

[Fla99] P. Flandrin. *Time-Frequency/Time-Scale Analysis*. Academic Press, San Diego, CA, 1999.

[Fla03] P. Flandrin. Ambiguity function. In B. Boashash, editor, *Time-Frequency Signal Analysis and Processing: A Comprehensive Reference*, chapter 5.1, pages 160–167. Elsevier, Oxford, UK, 2003.

[FMSC91] P. C. Fannin, A. Molina, S. S. Swords, and P. J. Cullen. Digital signal processing techniques applied to mobile radio channel sounding. *Proc. IEE-F*, 138(5):502–508, Oct. 1991.

[Gaa68] N. T. Gaarder. Scattering function estimation. *IEEE Trans. Inf. Theory*, 14(5):684–693, 1968.

[Gal64] R. G. Gallager. Characterization and measurement of time- and frequency-spread channels. Technical Report 352, M.I.T. Lincoln Lab, Cambridge, MA, April 1964.

[Gal68] R. G. Gallager. *Information Theory and Reliable Communication*. Wiley, New York, NY, 1968.

[Ger63] A. Gersho. Characterization of time-varying linear systems. *Proc. IEEE*, 51(1):238, Jan. 1963.

[Grö01] K. Gröchenig. *Foundations of Time-Frequency Analysis*. Birkhäuser, Boston, MA, 2001.

[GT98] G. B. Giannakis and C. Tepedelenlioğlu. Basis expansion models and diversity techniques for blind identification and equalization of time-varying channels. *Proc. IEEE*, 86(10):1969–1986, Oct. 1998.

[HBB92] F. Hlawatsch and G. F. Boudreaux-Bartels. Linear and quadratic time-frequency signal representations. *IEEE Signal Process. Mag.*, 9(2):21–67, April 1992.

[Jak74] W. C. Jakes. *Microwave Mobile Communications*. Wiley, New York, NY, 1974.

[JM05] M. Jachan and G. Matz. Nonstationary vector AR modeling of wireless channels. In *Proc. IEEE SPAWC-05*, pages 648–652, New York, NY, June 2005.

[JMH09] M. Jachan, G. Matz, and F. Hlawatsch. Vector time-frequency AR models for nonstationary multivariate random processes. *IEEE Trans. Signal Process.*, 57(12):4646–4659, Dec. 2009.

[Kai59] T. Kailath. Sampling models for linear time-variant filters. Technical Report 352, M.I.T. Research Lab. of Electronics, Cambridge, MA, May 1959.

[Kai62] T. Kailath. Measurements on time-variant communication channels. *IEEE Trans. Inf. Theory*, 8(5):229–236, Sept. 1962.

[Kay88] S. M. Kay. *Modern Spectral Estimation*. Prentice Hall, Englewood Cliffs, NJ, 1988.

[KD03] S. M. Kay and S. B. Doyle. Rapid estimation of the range-Doppler scattering function. *IEEE Trans. Signal Process.*, 51(1):255–268, Jan. 2003.

[Ken69] R. S. Kennedy. *Fading Dispersive Communication Channels*. Wiley, New York, NY, 1969.

[KSP+02] J. P. Kermoal, L. Schumacher, K. I. Pedersen, P. E. Mogensen, and F. Frederiksen. A stochastic MIMO radio channel model with experimental validation. *IEEE J. Sel. Areas Commun*, 20(6):1211–1226, Aug. 2002.

[LCS98] Y. Li, L. Cimini, and N. Sollenberger. Robust channel estimation for OFDM systems with rapid dispersive fading channels. *IEEE Trans. Commun.*, 46(7):902–915, July 1998.

[Leu04] G. Leus. On the estimation of rapidly time-varying channels. In *Proc. EUSIPCO 2004*, pages 2227–2230, Vienna, Austria, Sept. 2004.

[Mat03] G. Matz. Doubly underspread non-WSSUS channels: Analysis and estimation of channel statistics. In *Proc. IEEE SPAWC-03*, pages 190–194, Rome, Italy, June 2003.

[Mat05] G. Matz. On non-WSSUS wireless fading channels. *IEEE Trans. Wireless Commun*, 4(5):2465–2478, Sept. 2005.

[Mat06] G. Matz. Characterization and analysis of doubly dispersive MIMO channels. In *Proc. 40th Asilomar Conf. Signals, Systems, Computers*, pages 946–950, Pacific Grove, CA, Oct./Nov. 2006.

[MH98] G. Matz and F. Hlawatsch. Time-frequency transfer function calculus (symbolic calculus) of linear time-varying systems (linear operators) based on a generalized underspread theory. *J. Math. Phys., Special Issue on Wavelet and Time-Frequency Analysis*, 39(8):4041–4071, Aug. 1998.

[MH03] G. Matz and F. Hlawatsch. Time-frequency characterization of random time-varying channels. In B. Boashash, editor, *Time-Frequency Signal Analysis and Processing: A Comprehensive Reference*, chapter 9.5, pages 410–419. Elsevier, Oxford, UK, 2003.

[MH06] G. Matz and F. Hlawatsch. Nonstationary spectral analysis based on time-frequency operator symbols and underspread approximations. *IEEE Trans. Inf. Theory*, 52(3):1067–1086, March 2006.

[MMH+02] G. Matz, A. F. Molisch, F. Hlawatsch, M. Steinbauer, and I. Gaspard. On the systematic measurement errors of correlative mobile radio channel sounders. *IEEE Trans. Commun.*, 50(5):808–821, May 2002.

[MMS+99] G. Matz, A. F. Molisch, M. Steinbauer, F. Hlawatsch, I. Gaspard, and H. Artés. Bounds on the systematic measurement errors of channel sounders for time-varying mobile radio channels. In *Proc. IEEE VTC-99 Fall*, pages 1465–1470, Amsterdam, The Netherlands, Sept. 1999.

[Mol05] A. F. Molisch. *Wireless Communications*. Wiley, Chichester, UK, 2005.

[MSG+07] G. Matz, D. Schafhuber, K. Gröchenig, M. Hartmann, and F. Hlawatsch. Analysis, optimization, and implementation of low-interference wireless multicarrier systems. *IEEE Trans. Wireless Commun*, 6(5):1921–1931, May 2007.

[MSS07] A. R. Margetts, P. Schniter, and A. Swami. Joint scale-lag diversity in wideband mobile direct sequence spread spectrum systems. *IEEE Trans. Wireless Commun*, 6(12):4308–4319, Dec. 2007.

[NQ88] S. H. Nawab and T. F. Quatieri. Short-time Fourier transform. In J. S. Lim and A. V. Oppenheim, editors, *Advanced Topics in Signal Processing*, chapter 6, pages 289–337. Prentice Hall, Englewood Cliffs, NJ, 1988.

[NS82] A. W. Naylor and G. R. Sell. *Linear Operator Theory in Engineering and Science*. Springer, New York, NY, 2nd edition, 1982.

[Par92] J. D. Parsons. *The Mobile Radio Propagation Channel*. Pentech Press, London, UK, 1992.

[PDT91] J. D. Parsons, D. A. Demery, and A. M. D. Turkmani. Sounding techniques for wideband mobile radio channels: A review. *Proc. IEE-I*, 138(5):437–446, Oct. 1991.

[PKC+09] A. Paier, J. Karedal, N. Czink, C. Dumard, T. Zemen, F. Tufvesson, A. Molisch, and C. Mecklenbräuker. Characterization of vehicle-to-vehicle radio channels from measurements at 5.2 GHz. *Wireless Pers. Commun.*, 50:19–32, June 2009.

[PNG03] A. Paulraj, R. U. Nabar, and D. Gore. *Introduction to Space-Time Wireless Communications*. Cambridge University Press, Cambridge, UK, 2003.

[Pro95] J. G. Proakis. *Digital Communications*. McGraw-Hill, New York, NY, 3rd edition, 1995.

[Rap96] T. S. Rappaport. *Wireless Communications: Principles & Practice*. Prentice Hall, Upper Saddle River, NJ, 1996.

[Say02] A. M. Sayeed. Deconstructing multiantenna fading channels. *IEEE Trans. Signal Process.*, 50(10):2563–2579, Oct. 2002.

[Sch91] L. L. Scharf. *Statistical Signal Processing*. Addison Wesley, Reading, MA, 1991.

[Sch04] P. Schniter. Low-complexity equalization of OFDM in doubly-selective channels. *IEEE Trans. Signal Process.*, 52(4):1002–1011, April 2004.

[Sko84] M. Skolnik. *Radar Handbook*. McGraw-Hill, New York, NY, 1984.

[Sle78] D. Slepian. Prolate spheroidal wave functions, Fourier analysis, and uncertainty—V: The discrete case. *Bell Syst. Tech. J.*, 57(5):1371–1430, 1978.

[SM97] P. Stoica and R. Moses. *Introduction to Spectral Analysis*. Prentice Hall, Englewood Cliffs, NJ, 1997.

[SMH01] D. Schafhuber, G. Matz, and F. Hlawatsch. Simulation of wideband mobile radio channels using subsampled ARMA models and multistage interpolation. In *Proc. 11th IEEE Workshop on Statistical Signal Processing*, pages 571–574, Singapore, Aug. 2001.

[SMS93] K. Schwarz, U. Martin, and H. W. Schüßler. Devices for propagation measurements in mobile radio channels. In *Proc. IEEE PIMRC-93*, pages 387–391, Yokohama, Japan, 1993.

[SNB98] S. Salous, N. Nikandrou, and N. F. Bajj. Digital techniques for mobile radio chirp sounders. *IEE Proc. Commun.*, 145(3):191–196, June 1998.

[STC07] H. Suzuki, Thi Van Anh Tran, and I. B. Collings. Characteristics of MIMO-OFDM channels in indoor environments. *EURASIP J. Wireless Commun. Networking*, Vol. 2007, Article ID 19728, 2007.

[TG96] M. K. Tsatsanis and G. B. Giannakis. Modeling and equalization of rapidly fading channels. *Int. J. Adapt. Control Signal Process.*, 10:159–176, March 1996.

[TG97] M. K. Tsatsanis and G. B. Giannakis. Subspace methods for blind estimation of time-varying FIR channels. *IEEE Trans. Signal Process.*, 45(12):3084–3093, Dec. 1997.

[TGYL05] S. Tomasin, A. Gorokhov, H. Yang, and J. P. Linnartz. Iterative interference cancellation and channel estimation for mobile OFDM. *IEEE Trans. Wireless Comm.*, 4(1):238–245, Jan. 2005.

[TGZ96] M. K. Tsatsanis, G. B. Giannakis, and G. Zhou. Estimation and equalization of fading channels with random coefficients. *Signal Processing*, 53(2–3):211–229, Sept. 1996.

[Tho82] D. J. Thomson. Spectrum estimation and harmonic analysis. *Proc. IEEE*, 70(9):1055–1096, 1982.

[THR+00] R. Thomä, D. Hampicke, A. Richter, G. Sommerkorn, A. Schneider, U. Trautwein, and W. Wirnitzer. Identification of time-variant directional mobile radio channels. *IEEE Trans. Instrum. Meas.*, 49(2):357–364, April 2000.

[Tre92] H. L. Van Trees. *Detection, Estimation, and Modulation Theory, Part III: Radar-Sonar Signal Processing and Gaussian Signals in Noise*. Krieger, Malabar, FL, 1992.

[TV00] T. A. Thomas and F. W. Vook. Multi-user frequency-domain channel identification, interference suppression, and equalization for time-varying broadband wireless communications. In *Proc. IEEE Workshop Sensor Array and Multichannel Signal Processing*, pages 444–448, Boston, MA, March 2000.

[TV05] D. Tse and P. Viswanath. *Fundamentals of Wireless Communication*. Cambridge University Press, New York, NY, 2005.

[VB03] R. Vaughan and J. Bach Andersen. *Channels, Propagation and Antennas for Mobile Communications*. IEE Press, London, UK, 2003.

[WHOB06] W. Weichselberger, M. Herdin, H. Özcelik, and E. Bonek. A stochastic MIMO channel model with joint correlation of both link ends. *IEEE Trans. Wireless Comm.*, 5(1):90–100, Jan. 2006.

[Wil91] C. H. Wilcox. The synthesis problem for radar ambiguity functions. In R. E. Blahut, W. Miller, Jr., and C. H. Wilcox, editors, *Radar and Sonar, Part I*, pages 229–260. Springer, New York, NY, 1991.

[WK83] M. Wax and T. Kailath. Efficient inversion of Toeplitz-block Toeplitz matrix. *IEEE Trans. Acoust., Speech, Signal Processing*, 31(5):1218–1221, Oct. 1983.

[Woo53] P. M. Woodward. *Probability and Information Theory with Application to Radar*. Pergamon Press, London, UK, 1953.

[YPS03] J. Ye and A. Papandreou-Suppappola. Wideband time-varying channels with time-scale diversity and estimation. In *Proc. IEEE SSP-03*, pages 50–53, St. Louis, MO, Sept. 2003.

[Zad50] L. A. Zadeh. Frequency analysis of variable networks. *Proc. IRE*, 38(3):291–299, March 1950.

[ZM05] T. Zemen and C. F. Mecklenbräuker. Time-variant channel estimation using discrete prolate spheroidal sequences. *IEEE Trans. Signal Process.*, 53(9):3597–3607, Sept. 2005.